

**ACOUSTIC PROPERTIES
OF
ULTRASOUND CONTRAST AGENTS**

CIP-GEGEVENS KONINKLIJKE BIBLIOTHEEK, DEN HAAG

Jong, N. de

Acoustic properties of ultrasound contrast agents / N. de

Jong. - [S.l. : s.n.]. III.

Proefschrift Rotterdam. - Met lit. opg.

ISBN 90-9006071-5

NUCI 743

Trefw.: cardiologie / ultrasound / contrastvloeistof.

ACOUSTIC PROPERTIES OF ULTRASOUND CONTRAST AGENTS

akoestische eigenschappen van ultrageluids contrastvloeistoffen

proefschrift

ter verkrijging van de graad van doctor
aan de Erasmus Universiteit Rotterdam
op gezag van de rector magnificus
prof. dr. C.J. Rijnvos
en volgens besluit van het college van dekanen

De openbare verdediging zal plaatsvinden op
24 juni 1993 om 15.00 uur

door

Nicolaas de Jong

geboren te Nieuwerkerk a/d IJssel

PROMOTIECOMMISSIE

promotor	prof. dr. ir. N. Bom
co-promotor	dr. F.J. ten Cate
overige leden	prof. dr. B.F. Lachmann prof. dr. K.K. Shung prof. dr. ir. J.A.E. Spaan

Financial support by the Netherlands Heart Foundation for the publication of this thesis is gratefully acknowledged.

Bij onze voorstellingen en beschouwingen omtrent de krachten der natuur maken wij voortdurend gebruik van symbolen die wij, indien zij voldoende representatief zijn, vereren met de naam theorieën. Zo schrijven wij op grond van bepaalde analogieën elektrische verschijnselen toe aan de werking van een eigenaardig fluïdum, dat nu eens vloeit en dan weer in rust is. Dergelijke voorstellingen hebben voor- en nadelen. Zij bieden de geest een tijd lang een vredig onderdak, maar begrenzen hem ook, en op den duur, als de geest deze woning ontgroeit is, is het dikwijls moeilijk de muren te doorbreken van wat een gevangenis is geworden in plaats van een tehuis.

John Tyndall (1877)

uit: *Keerpunten in de Fysica*

Printing: Zuidam & Zonen bv, Woerden

Table of contents

I	Background	1
	Introduction	2
	Historical technical aspects of cavitation	2
	Historical clinical aspects of contrast echocardiography	6
	Contrast agents	8
	Potential clinical applications of contrast agents	10
	Aim of the study	12
	References	13
II	Basic principles of ultrasound contrast agents	17
	Introduction	18
	Physical mechanism of contrast agents	18
	Characteristics of fluids containing small gas bubbles	24
	Discussion	33
	References	35
III	Absorption and scatter of encapsulated gas filled microspheres	37
	Introduction	38
	Theory	39
	Simulation studies	45
	Experimental procedure	48
	Results	53
	Discussion and conclusion	56
	References	59
IV	Ultrasound scattering properties of Albunex^R microspheres	61
	Introduction	62
	Theory	63
	Experimental procedure	67
	Results	69
	Discussion and conclusion	74
	References	78

V	Higher harmonics of vibrating gas filled microspheres	79
	Introduction	80
	Theory	82
	Simulation	84
	Measurements	92
	Results	94
	Discussion	99
	References	101
VI	Transpulmonary echocontrast effects	103
	Introduction	104
	Methods and materials	105
	Results	109
	Discussion	114
	Conclusion	116
	References	117
VII	Discussion and conclusions	119
	The 2D echographic contrast instrument	120
	Albunex ^R	124
	Ultravue ^R	125
	Echovist ^R and Levovist ^R	126
	Videodensitometry	127
	Final conclusion	130
	References	130
	Summary	133
	Samenvatting	135
	List of symbols	137
	Acknowledgements	141
	Publications of the author	143
	Curriculum vitae	149



BACKGROUND

Abstract

Historical aspects of cavitation are reviewed as these are important for describing and understanding the interaction of medical ultrasound and current echocontrast agents. The potential clinical applications of the contrast agents within echocardiology are also discussed. The determination of myocardial perfusion after intravenous injection promises to be the most important clinical application. A short description of some commercially available contrast agents together with a couple of home-made agents is presented.

Introduction

The field of contrast echocardiography traces its origin to the work of Gramiak¹ and colleagues at the University of Rochester, NY, USA, which was first published in 1968. While performing M-mode echocardiography, he observed the appearance of a cloud of echoes during intracardiac injection of indocyanine green dye, a frequently used substance for measuring blood flow. It was subsequently discovered that the injection of almost any liquid through a small bore needle or catheter would produce this contrast effect. The source of this effect was attributed to microbubbles generated during injection as a result of cavitation at the catheter tip². Cavitation and contrast echocardiography have thus turned out to be very closely related and some production methods of ultrasound contrast agents are based on this cavitation principle. Furthermore, theoretical expressions describing cavitation have proved very useful for understanding the mechanism of scattering of ultrasound of gas bubbles. Atchley³ has given an excellent overview of the historical background of the cavitation research. To place developments in contrast echocardiography in clear perspective this historical background is briefly summarised.

Historical technical aspects of cavitation

Perhaps the first type of cavitation ever observed was the formation of bubbles in liquids supersaturated with gas. This form of cavitation is familiar to anyone who has ever opened or poured a carbonated beverage. Tomlinson⁴ has described a series of experiments performed with sodawater and various solids. He contends that if the solids are "chemically clean" no bubbles will form. However, if the solid initially chemically clean, should come into contact with a dirty cloth, unclean air, or dust particles, copious bubbles form on it when it is immersed in soda water. As an explanation, Gernez⁵ proposes that the outgassing of supersaturated gaseous solutions, such as sodawater, is caused by gas pockets embedded in the fissures found on the surface of every solid, regardless of its degree of finish. This is a form of cavitation that requires gaseous diffusion to "pump up" gas containing nuclei until they grow large enough to rise to the surface of the liquid.

At about the same time when Tomlinson and Gernez were doing their work (1869), another type of cavitation was being investigated. This other form of cavitation has its origin with the conception and developments of hydrodynamics. Not until

Bernouilli⁶ set down the guidelines for this new branch of science in 1738 was it understood that a negative pressure could be produced within a liquid. In the following years Euler and d'Alembert debated the consequences of negative pressures⁷. Euler believed that the application of a negative pressure could result in a rupture of the liquid, while d'Alembert refused to accept this view. The rise of cavitation as a topic for science began with the development of high-powered, high-rpm steam turbines in the mid 1800's. With this advance came the means of moving an object (such a propeller) through a fluid rapidly enough so that the object lost contact with the fluid. In fact, the term "cavitation" was first used by Thornycroft⁸ in his observations of propeller inefficiency in torpedo boat destroyers. Not only the inefficiency, but of much greater concern was the propeller erosion. In fact, this problem was so critical that in 1915 the British Admiralty appointed a special committee to investigate this phenomenon, and in 1917, Lord Rayleigh⁹ became involved. His typically straightforward and ingenious solution of the equations governing vapour cavity dynamics remains useful to this day.

Cavitation can be split into 2 main categories. First, the hydraulic cavitation which occurs with ship propellers, pumps, turbines, etc. Second, the acoustic cavitation, which describes the conception, growth and collapse of gas or vapour bubbles in a liquid exposed to a dynamic pressure. Sound waves produce such negative dynamic pressures because of their sinusoidal nature. Here controlling of the driving pressure is an important parameter, which is absent in the hydraulic cavitation. The tensile strength of a homogeneous liquid is defined as the limiting negative pressure that the liquid can withstand before a new stable phase forms, e.g. cavitation occurs. Putting liquids under stress and considering the consequences and measuring the tensile stress in to a liquid started in the mid 1800's. These **static** measurements form the basis for the present-day acoustic cavitation, which are actually studies of the **dynamic** tensile strength. Acoustic cavitation was first observed during the period from 1915 to 1920 by Langevin and his co-workers while he was pioneering the field of ultrasonics¹⁰. Söllner¹¹ was one of the first to observe cavitation in degassed liquids at room temperature and atmospheric pressures. In the 1930's and 1940's a number of other researchers investigated various aspects of ultrasonic cavitation and at that time the fundamental problem of cavitation was well formulated. Numerous measurements of the cavitation threshold, i.e. the tensile strength of water, yielded results in the range of 1-25 bar and even a tensile strength as high as 300 bar has been reported¹². What could account for a discrepancy of this order of magnitude? Failure in solids under tension is usually attributed to an imperfection in the solid. The

same logic was applied to the failure of liquids and resulted in theoretical predictions for a cavitation threshold of water on the order of several thousand bar⁷. The presence of inhomogenities in liquids, i.e. nuclei, as a source of the inception of cavitation resulted in numerous models. The most important was proposed by Harvey¹³, who suggested that stable gas pockets located in crevices found on dirt particles accounted for the cavitation. A different type of nucleus was suggested in 1954 by Fox and Herzfield¹⁴, which consisted of a gas bubble surrounded by a rigid skin of organic molecules. Strasberg¹⁵ reported, however, that the crevice model offered the best explanation for his extensive set of measurements.

Interaction of acoustics and bubbles

The earliest reference to bubbles as sound sources was made by Bragg¹⁶ who attributed the murmuring of a brook and the plonk of droplets falling into water to entrained air bubbles. Minnaert¹⁷ has since shown that the sound generated by gas bubbles in liquids is associated with simple volume pulsation of the bubble without changing shape. The bubble behaves as a simple damped oscillating system with one degree of freedom. Therefore, the differential equation of motion is of the same form as the classical mass-spring system. He derived for this system the frequency at which resonance occurs, assuming an adiabatic equation of state for the gas in the bubble and neglecting surface tension and damping factors. At that time experiments showed that liquids containing gasses possess higher sound damping characteristics than those which are gas free. Sørensen¹⁸ concludes that just a few widely dispersed bubbles, which are so small as to be invisible, can have an appreciable acoustic effect. Fox¹⁹ also carried out attenuation measurements on bubbly liquids and came to a similar conclusion as Sørensen. The first theoretical description of the behaviour of gas bubbles exposed to an acoustic field together with some aspects of collapsing bubble was described in 1950 by Noltingk and Neppiras²⁰. During collapse the walls of the bubble rush inwards until the cushioning action of the gas within the bubble stops the radial motion. At the end of the collapse the contents of the bubble is highly compressed and high instantaneous temperatures may occur within the bubble, depending on the degree to which adiabatic conditions still apply. Assuming strictly adiabatic conditions they calculated, at room temperature and an ambient pressure of 1 atmosphere, that the internal temperature of a collapsed bubble would reach the order of 10^4 degrees Celsius. In 1951 Poritsky²¹ investigated the effect of several types of damping connected with the motion of cavitation bubbles and concluded that the viscous damping component dominates for very small bubbles.

Later, in 1959, Devin²² thoroughly surveyed the fundamental processes by which pulsating bubbles dissipate their energy. This included the portion of energy radiated in the form of spherical sound waves, that part which is transformed into heat energy during the polytropic compression and expansion of the enclosed gas, and that part of the energy lost in viscous dissipation. In 1954 Fox²³ concluded that the cavitation nuclei consist of very small gas bubbles stabilized by an organic skin, which mechanically prevents loss by diffusion. He also calculated the higher resonance frequency of such bubbles. In 1955 Strasberg²⁴ described gas bubbles in a liquid as sources of sound, referring to the experiments of Brag. He considered that the gas bubbles initiate volume pulsation when subjected to a force, e.g. gas bubbles entrained in a liquid passing a fixed body or bubbles formed at a nozzle when they separate. In 1964 Flynn developed a thorough description of the cavitation phenomena including aspects of transient and stable cavitation, tensile strength of fluids and the influence of nuclei in the fluid, equation of motion and possible non-linear effects, as well as results from several experimenters. In 1968 Tucker²⁵ suggested that the second harmonic, which is the result of the non-linear behaviour of bubbles, is a very sensitive indicator for the presence of bubbles. One year later, Welsby²⁶ developed an analytical method to describe the first as well as the second harmonic of the bubble motion. Lauterborn²⁷ performed numerical studies on the near resonance behaviour of gas bubbles in 1976 for which only the viscous damping was included in the sub- and superharmonics. In 1977 Medwin²⁸ described the scattering, absorption and extinction cross-section for the linear case including all the damping factors for all bubble sizes. Miller²⁹ described in 1981 the ultrasonic detection of resonant cavitation bubbles in a flow tube by their second harmonic emission. The experimentally determined values he measured on small bubbles of 4 μm diameter agreed well with theory, which was analytical and comparable with the derivation given by Welsby. Eatock³⁰ studied the magnitude of the non-linear effect in the scattering of ultrasound by nitrogen bubbles in water using a numerical approach, for ultrasonic frequencies and at amplitudes typical for diagnostic medical devices. He was interested in possible bubble detection in blood or tissue for application in decompression research. He included all the damping mechanisms, viscous, thermal and reradiation, as well as the polytropic exponent and concluded that the application of the non-linear effect to the detection of bubbles would be limited to bubbles smaller than 10 μm . Chapelon³¹ described in 1987 a system for detection and sizing of moving bubbles. He noted Doppler shifts on the sidebands generated at the sum and difference of two impinging frequencies. In 1988 Tamura³² described acoustic measurements on elastic microcapsules. He used the dependency

of the resonance frequency on the ambient pressure to calculate this ambient pressure, out of attenuation measurements, using a double frequency Doppler shift.

Historical clinical aspects of contrast echocardiography

While nautical engineers and physicists were developing the theoretical basis of bubble cavitation, applications in diagnostic medicine was non-existent until the work of Gramiak¹. They observed the appearance of echoes in the bloodstream on M-mode echocardiography during injection of indocyanine green dye. Shortly thereafter it was discovered that other fluids produced similar results. The generation of bubbles at the injection site was attributed to the effect of injecting a fluid-gas mixture through a small bore. Due to the very nature of the bubble generating method, the contrast effects discussed in those early days involved only free-gas bubbles with inherent shortcomings such as indeterminate size, short life-time and inability to transverse the lung circulation. Still this exciting new tool in echocardiology was explored by a large number of investigators. The common denominator of this research was to determine in what way this new method could enhance the diagnostic potentials of echocardiography. An excellent overview of the research activities on contrast-echocardiography in the period 1970-1980 can be found in "Contrast Echocardiography" edited by Meltzer and Roelandt³³.

The application of contrast agents in echocardiography included the following topics:

- identification of cardiac structures,
- detection of intracardiac shunts,
- visualization of blood flow in M-mode,
- detection of valvular regurgitation,
- analysis of complex congenital heart disease,
- cardiac output determination by indicator dilution curves.

Apart from the injection of the contrast material directly into the left side of the circulation by means of a catheter, left sided applications of contrast bubbles after intravenous injection were not possible because of the blocking action of the lungs. The first breakthrough in this area was the development of encapsulated microbubbles by Rasor Associates of Sunnyvale, CA, USA. Their use for indicator dilution measurements was first reported by Bommer³⁴. Also the possible application of encapsulated microbubbles for the remote sensing of local blood pressure looked

very promising³⁵. However, necessary improvements in the production process and official registration turned out to be a time consuming effort.

Towards the end of the period 1970-1980 there was still reason to doubt whether the lung barrier could be crossed by microbubbles surviving long enough in the circulation to reach the left heart. Illustrative for the somewhat wild ideas at that time is the following quotation from Meltzer³⁶ proposing several possible methods to achieve enhanced contrast of the left heart in spite of the lungs.

- " A very active surfactant might be able to stabilize bubbles small enough to pass pulmonary capillaries so they would survive until they reached the left heart before dissolving.
- " A solid coat might protect a 'mini-microbubble' so it can traverse the pulmonary capillary bed without dissolution due to diffusion or surface tension effects. There is preliminary work suggesting that such a method, using a saccharide coating, can be successful.
- " A liquid, such as diethyl ether, could be administered intravenously and pass through the pulmonary capillary bed in a liquid state, but then boil on the left side of the heart, yielding a gas phase and therefore ultrasonic contrast.
- " A liquid or combination of substances could be administered intravenously which would pass through the lungs and undergo a chemical reaction on the left side of the heart, yielding a gas. The most likely candidate would be carbon dioxide, because it is relatively nontoxic and many chemical reactions liberate large quantities of carbon dioxide.
- " Bubbles of gas can be forced through the capillary by the increased local pressure that could be applied by an injection through a catheter firmly in the pulmonary wedge position.
- " An inhaled gas might, due to its composition and pressure, sufficiently alter the local partial pressures in the alveoli and capillaries that intravenously injected microbubbles would grow rather than decay during their transit through the lungs.
- " High energy ultrasound can be focused on a point within the left heart to cause cavitation.
- " Lower energy ultrasound than that necessary to cause cavitation could be employed to cause growth rather than decay of peripherally injected microbubbles, using the mechanism of 'rectified diffusion'.
- " A liquid of sufficient acoustic impedance difference from blood to yield ultrasonic

contrast could pass through the pulmonary capillary bed without the difficulties faced by gas bubbles. It is possible that suspensions of specially treated collagen or gelatin may fit into this category.

" A combination of two or more of these methods."

In the period 1980 until now many clinical experiments have been carried out in order to make contrast echocardiography an established technique. In the beginning of the 80's investigators were forced to use home-made contrast agent out of necessity. Later in the decade some commercial products could be used, while in the registration phase. In the early 80's studies were focused on determining myocardial perfusion and it was shown that areas of normal and under perfusion could be visualised^{37,38}. By 1984 sufficient progress had been made that the American College of Cardiology organized a seminar dedicated to myocardial contrast echocardiography. Feinstein³⁹ reported sonication studies which produced small and stable microbubbles. Ten Cate⁴⁰ described a transpulmonary contrast effect but of limited usefulness for myocardial perfusion imaging. Also a videodensitometric method for quantifying myocardial perfusion studies was presented⁴¹, which initiated increased interest for computerised systems.

Safety of contrast agents is reported in the years after. Both the intracoronary use of sonicated Renografin^{42,43} as well as intravenous use of commercial product as Albunex and Lechovist has been investigated^{44,45}. Thereafter more pathophysiologic studies were performed. Ten Cate⁴⁶ described the possibilities to determine the stenosis of the left anterior descending coronary artery by the contrast outwash in the interventricular septum and Cornel⁴⁷ who incidentally reported the Thebesian vein outflow in humans visualised by echocontrast. Cheiriff⁴⁸ and his group described myocardial perfusion studies to determine coronary flow reserve before and after Percutaneous Transluminal coronary angioplasty (PTCA). Coronary collateral perfusion after myocardial infarction or PTCA can be assessed^{49,50}. Also, successful thrombolysis, resulting in a patent coronary artery, is often not accompanied by a return of normal perfusion or wall motion⁵¹.

Contrast agents

The key to further developing the above clinical diagnostic procedures, as well as discovering entirely new techniques, lies in the development of contrast agents meeting specific requirements. In 1989 Ophir and Parker⁵² reviewed the contrast

agents which have found application in diagnostic ultrasound over the last two decades. They distinguish five different types of agents: free gas bubbles, encapsulated gas bubbles, colloidal suspensions, emulsions and aqueous solutions. During this period a variety of materials, mostly home-made, have been tested for potential clinical application. A selected sample is reviewed below.

Home-made contrast agents

Carbondioxide. There is extensive experience with intravascular use of carbon dioxide in radiology, especially for the diagnosis of pericardial effusion⁵³. However, carbon dioxide does not pass the pulmonary capillaries⁵⁴ and has only limited prospects.

Hydrogen peroxide, in diluted form, has been used as a contrast agent in animal studies⁵⁵. When injected into blood, the molecule splits with the aid of the catalytic action from the peroxidase in leucocytes, resulting in the liberation of free oxygen in sufficient quantities to form local gas bubbles⁵⁶. Although low doses may be harmless, higher doses clearly can cause air embolism⁵⁷.

Lipid coated bubbles as described by Simon⁵⁸ increases the echogenity in tumors in the brain of rats after intravenous injection. The mean diameter of these microbubbles is 3 μm , with an upper limit of 6 μm .

Ultravue is a registered trade mark of Delta Biotechnology Ltd, Nottingham, England. The microparticles are formed from recombinant albumin and must be suspended in demi-water before use. The particles are smaller than 8 μm , the thickness of the shell is in the order of tenth of a μm and they are filled with gas. Animal studies have shown that they give a good opacification of the myocardium after injection in the left ventricular cavity.

A number of university based groups have also explored encapsulating air bubbles in order to improve their longevity. Examples include polymer-coated microbubbles⁵⁹ and elastic microcapsules⁶⁰, but the resulting spheres are larger than 10 μm , the critical dimension for passing the lung capillary bed.

Sonication products. Many reports have been published based on sonicated contrast agents, which have found application in specific clinical areas. These are mostly based on radiographic agents such as Renografin-76^R, sorbitol, dextrose or saline which are sonicated with a 20 kHz high intensity sonicator⁶¹ just prior to use. The reported microbubble size varies from 6 to 11 μm mean diameter for the different agents. The

persistence (half-life) varies from 10 to 30 seconds⁶². Not all of these agents are suitable for intravenous injection. Particularly those agents having a high viscosity and a high osmolarity can influence the coronary flow, left ventricular function and hemodynamics.

Commercial contrast agents

Contrast agents, which are now under evaluation in clinical trials and close to registration are:

Albunex is a tradename of Molecular Biosystems, San Diego, California, USA. The agent consists of encapsulated gas filled microspheres suspended in human serum albumin. The shell of the microsphere is formed during the production process and consists of denatured protein molecules. The mean diameter is 4 μm and 95% of the microspheres are smaller than 10 μm . After intravenous injection this product opacifies the echocardiographic image of the left ventricular cavity.

SHU 454 and SHU 508A are registered trademarks of Schering AG, Berlin, Germany. Both products are Saccharide based and the microbubbles are formed immediately after mixing specially manufactured microparticles and a water based galactose solution. SHU 454 has a mean diameter of 3 μm and is intended for the opacification of right heart. This product was registered in 1991 (in Germany) and was the first microbubble product to achieve this status. SHU 508A consists of bubbles ranging in diameter from 2 to 8 μm , with 95 % having a diameter of less than 6 μm . Clinical studies have confirmed that they pass through the pulmonary bed and produce opacification of the left side of the heart.

Potential clinical application of contrast agents

Cardiology:

Two main areas of application can be currently identified involving either intravenous or intracoronary injection of the agent. This distinction is made because of the observed difference in size distribution and concentration of the contrast agent when it enters the coronary system after intravenous injection. This is due to pressure stability, filtration of the pulmonary circulation, and longevity of the agent in blood. If these effects could be minimized, the distinction would no longer be necessary.

Intravenous applications:

- Detection of the endocardial border. The endocardial border definition can be improved resulting in better imaging of wall motion abnormalities.
- Left ventricle function. Cardiac output or LV ejection fraction can be determined from the washout characteristics of the contrast agent.
- Quantification of valvular regurgitation. Doppler color flow mapping is currently used to assess mitral and aortic regurgitation. This method is based on blood velocity, rather than volume flow, but it is conceivable that videodensitometry using contrast agents could provide a method of evaluating valvular regurgitation.
- Congenital heart diseases. Detection of atrial and ventricular septal defects, transpositions, etc.
- Left ventricle flow patterns. The visualization of streaming down the septum in early diastole, and along the lateral wall toward the LV outflow tract may be useful for assessing abnormal intraventricular flow patterns and diastolic function.
- Enhancement of Color Doppler signals. All the current applications of Color Doppler can be improved by adding a specific amount of contrast agent.

Intracoronary applications:

- Determination of perfusion area. Determination of the perfusion territory for a given coronary artery and examine of possible collateral perfusion.
- Regional perfusion and coronary flow reserve. Measurements of the contrast effect before and after angioplasty relates to the success of the procedure.
- Visualization of Thebesian vein outflow.
- Patency of CABG (coronary artery bypass grafts).
- Perfusion of coronary artery implants during surgery.
- Assessment of the results of surgery for VSD (ventricular septal defect).

Potential applications:

- Pressure measurements. Some acoustic properties of the contrast agent depend on the ambient pressure and provide a mechanism for deriving left ventricle pressure.
- Contrast imaging. The nonlinear vibration of the contrast agents provide a mechanism for better definition of intracardial images.

Outside Cardiology:

- Gynaecology. Determination of the tubal function, tubal flow, and perfusion of the placenta.
- Urology. Determination of urodynamics. Investigation of the Kidney.
- Surgery. Intraoperative liver perfusion for enhancement of tumors.
- Phleboccontrast sonography. Determination of venous hemodynamics. Vena Cava.
- Neurology. Determination of carotid flow.

Aim of the study

Ultrasound contrast agents have been used in the medical diagnostic field for a number of years and for very different purposes. These agents have been employed when echo images proved inadequate or when further information about the blood flow was required. Originally, contrast agents were home-made, being produced simply by passing saline through a three-way stopcock. Such bubbles were quite large and their use was limited, for example, to detect ventricular septal defects. Although Color Doppler has made it possible to visualize blood flow inside the heart's chambers, there has been a renewed interest in contrast agents in recent years. As a result, a number of firms have announced plans to extend their current product line, (Röntgen and/or magnetic resonance contrast agents) to the field of ultrasound imaging.

The most important properties of these products are safety (biodegradability, non-toxicity, etc.) and effectiveness. Although the principal effect is the enhanced backscatter, there are other properties which can be exploited, and in the long run these may prove to be of greater importance. This thesis investigates the basic ultrasonic properties of contrast agents, especially contrast agents consisting of gas bubbles, particularly encapsulated gas bubbles. The basic properties include not only an enhancement of the backscatter signal, but also a change in the acoustic velocity of a medium containing gas bubbles. Resonance phenomena and an increased nonlinear vibration as function of the applied acoustic pressure are important characteristics of contrast agents. These properties have been investigated by computer modelling and acoustic measurements for frequencies in the medical diagnostic range. Furthermore, phase 1 studies on healthy volunteers, using a commercial available echocontrast agent, have been conducted and the results are compared with a theoretical model.

The acoustic behaviour of gas bubbles and encapsulated gas bubbles are now generally well understood and the developed theory can be used for analysis of clinical contrast studies. This opens the prospect for entirely new applications of echographic contrast imaging.

References

1. Gramiak R. and Shah P.M. Echocardiography of the aortic root. *Invest Radiol* 3 356-366 1968
2. Kremkau F.W., Shah R., Kramer D.H. Ultrasound cardiography contrast studies in anatomy and function. *Radiology* 92 939-948 1969
3. Atchley A. and Crum A. Acoustic cavitation and bubble dynamics. In: *Ultrasound. Its chemical, physical and biological effects* (Suslick s. ed.). Verlagsgesellschaft Weinheim Germany 1988
4. Tomlinson C., *Phil. Mag.* 34, 136, 220 1867
5. Gernez M., *Phil. Mag.* 33, 379 1867
6. Bernoulli D., "hydrodynamica, sive de viribus et motibus fluidorum comentarii". Strasbourg 1738
7. Freed D., Walker W.F., Cavitation and multiphase flow forum (Hoyt J.W., (ed.)) American Society for mechanical Engineers. New York 1984 page 1.
8. Thornycroft J., Barnaby S. W., *Inst. Civ. Eng.* 122, 51 1895
9. Lord Raleigh, *Phil. Mag.* 34, 94 1917
10. Klein E., *J. Acoustics. Soc. Am.* 20, 601 1948
11. Blake F.G., The tensile strength of liquids: A review of the literature. Tech. Memo. No. 9, Harvard Acoustics Research Laboratory 1949
12. Strasberg M.J. *J. Acoust. Soc. Am.* 31, 163 1959
13. Harvey E.N., Barnes K.K., McElroy W.D., Whitely A.H., Pease D.C., Cooper K.W. *J. Cell. Comp. Physiol.* 21, 1 1944
14. Fox F., Herzfield K.J. Gas bubbles with organic skin as cavitation nuclei. *J. Acoust. Soc. Am.* 26, 984 1954
15. Strasberg M.J. *J. Acoust. Soc. Am.* 31, 163 1959
16. Bragg W. The world of sound G. bell and Sons Ltd. London 1920
17. Minnaert M. *Phil. Mag.* (26) 236 1933
18. Sørensen C., *Annual Physik* (26) 121 1936
19. Fox F.E., Curley S.R., Larson G.S. Phase velocity and absorption measurements in water containing air bubbles. *J. Acoust. Soc. Am.* (27) 534-539 1954
20. Noltingk, B.E. & Neppiras, E.A., Cavitation produced by ultrasonics, *Proc. Phys. Soc. B* 63 (1950), 674-685.
21. Poritsky, H., The collapse or growth of a spherical bubble or cavity in a viscous fluid, *Proc. of First U.S. Nat. Congress on Appl. Mech.*, E. Sternberg, New York (1952), 813-821.
22. Devin, C., Survey of thermal, radiation, and viscous damping of pulsating air bubbles in water, *J. Acoust. Soc. Am.* 31 (1959), 1654-1667.
23. Fox, F., Gas bubbles with organic skin as cavitation nuclei, *J. Acoust. Soc. Am.* 26 (1954), 984-989.

24. Strasberg M. Gas bubbles as sources of sound in liquids. *J. Acoust. Soc. Am.* (28) 1 1956
25. Tucker, D.G. & Welsby, V.G., Ultrasonic monitoring of decompression, *Lancet* I (1968), 1253.
26. Welsby, V.G. & Safar, M.H., Acoustic non-linearity due to micro-bubbles in water, *Acustica* 22 (1969), 177-182.
27. Lauterborn, W., Numerical investigation of nonlinear oscillations of gas bubbles in liquids, *J. Acoust. Soc. Am.* 59 (1976), 283-293.
28. Medwin, H., Counting bubbles acoustically: a review, *Ultrasonics* 15 (1977), 7-13.
29. Miller D.L. Ultrasonic detection of resonant cavitation bubbles in a flow tube by their second-harmonic emissions. *Ultrasonics* september 1981
30. Eatock, B.C., e.a., Numerical studies of the spectrum of low-intensity ultrasound scattered by bubbles, *J. Acoust. Soc. Am.* 77 (1985), 1692-1701.
31. Chapelon J.Y., Newhouse V.L., Cathignol D. and Shankar P.M. Bubble detection and sizing with a double frequency Doppler system. *Ultrasonics* 26 1988
32. Tamura T., Chihara K., Shirae K., Ishihara K., Nagakura T., Tanouchi J. and Kitabatake A. Dynamic pressure measurements using two-frequency ultrasound. *Japanese Journal of Applied Physics* 28 1989 supplement 28-1 211 -213
33. Contrast echocardiography. Meltzer R.S. and Roelandt J. Martinus Nijhoff Publishers. The Hague/Boston/London 1982
34. Bommer W.J. Neef J., Neumann A., Weinert L. Lee G., Mason ?T. and DeMaria AN. Indicator dilution curves obtained by photometric analysis of two-dimensional echo-contrast studies. *Am J Cardiol* 41:370,1978 (abstract).
35. Tickner G, Rasor N. Noninvasive assessment of pulmonary hypertension using the bubble ultrasonic resonance pressure (Burp) method. Annual report # HR-62917-1A, NHLBI, 1977.
36. Meltzer R.S. Lancée C.T. and Roelandt J. Transmission of echocardiographic contrast through the lungs. In: Contrast echocardiography. Meltzer R.S. and Roelandt J.(eds.) Martinus Nijhoff Publishers. The Hague/Boston/London 1982
37. Matsumoto Y.K., Maeda T, Fukushima M, Hori M, Shimazu I, Inoue M, Abe H, Sato H, Minamimo T. Estimation of intramyocardial blood flow distribution with contrast echocardiography. *Circulation* 1982;62:II-28
38. Tei C, Sakamaki T, Shah PM, Meerbaum S, Shimoura K, Kondo S, Corday E. Myocardial contrast echocardiography: A reproducible technique of myocardial opacification for identifying regional perfusion deficits. *Circulation* 1983;67:585-593
39. Feinstein S.B., Ten Cate F.J., Zwehl W, Ong K, Maurer G, Tei C, Shah P.M., Meerbaum S, Corday E. Two dimensional contrast echocardiography, I: in vivo development and quantitative analysis of echo contrast agents. *J Am Coll Cardiol* 1984;3:14-20
40. Ten Cate F.J., Feinstein S, Zwehl W, Meerbaum S, Fishbein M, Shah PM, Corday E. Two-dimensional contrast echocardiography, II: Transpulmonary studies. *J Am Coll Cardiol* 1984;3:21-27
41. Ong K, Maurer G, Feinstein S, Zwehl W, Meerbaum S, Corday E. Computer methods for myocardial contrast two-dimensional echocardiography. *J Am Coll Cardiol* 1984;3:1212-1218
42. Berwing K, Schlepper M, Kremer P, Bahawar H. Comparison of myocardial perfusion determined by contrast echocardiography with left ventricular regional function in patients. *Circulation* 1987;76:IV-506

43. Moore C.A., Smucker M.L., Kaul S. Myocardial contrast echocardiography in humans: I safety - A comparison with routine coronary arteriography. *J Am Coll Cardiol* 1986;8:1066-1072
44. Feinstein SB, Cheirif J, Ten Cate FJ, Silverman PR, Heidenreich P, Dick C, Desir RM, Armstrong WF, Quinones MA, Shah PM. Safety and efficacy of a new transpulmonary ultrasound contrast agent: Initial multicenter clinical results. *J Am Coll Cardiol* 1990;16:316-24
45. Schlieff R., Straks T., Mahler M., Rufer M., Fritsch T., Seifert w. Successful opacification of the left heart chambers on echocardiographic examination after intravenous injection of a new saccharide-based contrast agent. *Echocardiography* 1990 7 1-4
46. Ten Cate F.J., Serruys P.W., Huang H, de Jong N, Roelandt J. Is the rate of disappearance of echo contrast from the interventricular septum a measure of left anterior descending coronary artery stenosis? *European Heart Journal* 1988;9:728-833
47. Cornel J.H., Ten Cate F.J., Serruys P.W.. Myocardial contrast echocardiography shows Thebesian vein outflow in humans. *American Heart Journal* 1992;123:1373-1374
48. Cheiriff J, Zoghbi W.A., Raizner A.E., et al. Assessment of myocardial perfusion in humans by contrast echocardiography, I: Evaluation of regional coronary reserve by peak contrast intensity. *J Am Coll Cardiol* 1988;11:735-743
49. Grill H, Brinker J, Taube J.C., Walford G, Midel M, Flaherty J, Weiss J. Contrast echocardiography mapping of collateralized myocardium in humans before and after coronary angioplasty. *J Am Coll Cardiol* 1990;16:1594-1600
50. Kaul S, Villanueva F.S. Is the determination of myocardial perfusion necessary to evaluate the success of reperfusion when the infarct-related artery is open? *Circulation* 1992;85:1942-1944
51. Ito H, Tomooka T, Sakai N, Yu H, Higashino Y, Fujii K, Masuyama T, Kitabatake A, Minamino T. Lack of myocardial perfusion immediately after successful thrombolysis. A predictor of poor recovery of left ventricular function in anterior myocardial infarction. *Circulation* 1992;85:1557-1564
52. Ophir, J. and Parker, K.J. Contrast agents in diagnostic Ultrasound. *Ultrasound in Med. & Biol.* (1989) Vol. 15, No.4, p 319-333
53. Philips J.H. The use of intracardiac carbon dioxide in the diagnosis of pericardial disease. *Am. Heart J.* 61 748-755 1961
54. Meltzer, ea. Why do the lungs clear ultrasonic contrast? *Ultrasound in Med & Biol.* 263-269 1980
55. Kemper ea. Hydrogen peroxide contrast-enhanced two dimensional echocardiography: Real-time in vivo delineation of regional myocardial perfusion. *Circulation* 68 603-611 1983
56. Reisner S.A., Shapiro J.R., Amico A.F. and Meltzer R.S. Contrast agents for myocardial perfusion studies: Mechanisms, state of the art, and future prospects. In: *Myocardial contrast two-dimensional echocardiography* (Meerbaum S. and Meltzer R. eds.) Kluwer Academic Publishers Dordrecht-London-Boston 1989
57. Finney J.W., Jay B.E., Race G.J., Urschel H.C., Mallams J.T. and Balla G.A. Removal of cholesterol and other lipids from experimental animal and human atheromatous arteries by dilute hydrogen peroxide. *Angiology* (17) 1966 223-228
58. Simon R.H., Ho S., Perkins C.R. and D'Arrigo J.S. Quantitative assessment of tumor enhancement by ultrastable lipid-coated microbubbles as a sonographic contrast agent. *Investigative Radiology* 1992 (27) 29-34

59. Wheatley M.A., Schrope B. and Peng S. Contrast agents for diagnostic ultrasound: development and evaluation of polymer-coated microbubbles. *Biomaterials* (11) 1990 713-717
60. Ishihara K., Kitabatake A., Tanouchi J., Fujii K., Uematsu M., Yoshida Y., Kamada T., Tamura T., Chihara K. and Shirae K. New approach to noninvasive manometry based on pressure dependent resonant shift of elastic microcapsules in ultrasonic frequency characteristics. *Japanese Journal of Applied Physics*. (27) suppl 27-1 1988 125-127
61. Feinstein S.B., Ten Cate F.J., Zwehl W., Ong K., Maurer G., Tei C., Shah P.M., Meerbaum S. and Corday E. Two-dimensional contrast echocardiography, I: in vivo development and quantitative analysis of echo contrast agents. *J. Am. Cardiol.* (3) 1984 14-20
62. Bleeker H.J., Shung K.K. and Barnhart J.L. Ultrasonic characterization of Albunex^R, a new contrast agent. *J. Acoust. Soc. Am.* 87(4) 1990



BASIC PRINCIPLES OF ULTRASOUND CONTRAST AGENTS

Abstract

The behaviour of gas bubbles and gas encapsulated spheres as an echographic contrast agent is reviewed. Compared with rigid spheres, gas bubbles are superior scattering agents, and they offer a number of useful properties which can be exploited in a variety of ways. The analysis of their velocity of sound, backscatter intensity, second harmonic emission, and resonant frequency all open new perspectives for the development of contrast agents for echocardiographic research with potential clinical applications.

This chapter is based on a manuscript, which has been published:

Title : Principles and recent developments in ultrasound contrast agents
Authors : N. de Jong, F.J. Ten Cate, C.T. Lancée, J.R.T.C. Roelandt, N. Born
In : Ultrasonics 1991 29(4)

Introduction

The most important property of ultrasonic contrast agents remains their capacity to enhance the backscattered signal. This has been employed in combination with conventional two-dimensional imaging to create images of greater clarity. It is anticipated that this property will continue to play an important role in contrast echocardiography for the foreseeable future. Nevertheless, there are other properties of ultrasonic contrast agents which can provide additional information related to the physical properties and characteristics of the fluid carrier. Depending on the application (cardiology, abdominal studies, etc.) a variety of contrast agents are currently employed. These include free and encapsulated gas bubbles, colloidal suspensions, emulsions, and aqueous solutions as recently reviewed by Ophir and Parker¹. They also indicate that in terms of an enhanced backscatter signal the most promising contrast agents are free or encapsulated gas bubbles, which are superior to colloidal suspensions, emulsions, or aqueous solutions.

This report deals with contrast agents most commonly used in the field of cardiology, where free and encapsulated gas bubbles predominate. An analysis of the ultrasonic properties of liquids containing small gas bubbles is reported and this is compared with the properties of liquids containing rigid spheres. The persistence of gas bubbles in a liquid is of particular importance and is described in detail. Finally, some additional properties of a liquid containing gas bubbles, which have potential applications in ultrasonic studies, are considered.

Physical mechanism of contrast agents

Particles can be detected by ultrasound when they possess acoustical characteristics which differ from the surrounding medium. This means a difference in speed of propagation, density, or absorption. In general, the physical size of contrast agents is much smaller than the wavelength of the acoustic field (at 3 MHz the wavelength in water is 0.5 mm). An important property of such a particle is the scattering cross section (Σ_s), which is defined as "the amount of scattered power divided by the incident intensity". The Σ_s can be described for the long wavelength situation assuming the Born approximation²:

$$\Sigma_s = \frac{4}{9} \pi R^2 (kR)^4 \left[\left\{ \frac{\kappa_d - \kappa}{\kappa} \right\}^2 + \frac{1}{3} \left\{ \frac{3\rho_d - 3\rho}{2\rho_d + \rho} \right\}^2 \right]$$

or

[II-1]

$$\Sigma_s = A_R \left[\gamma_\kappa^2 + \frac{1}{3} \gamma_\rho^2 \right]$$

- Σ_s = scattering cross section
- R = radius of the scattering element
- k = wave number, ($= 2\pi/\lambda$, λ = wavelength)
- κ_d = compressibility of the scattering particle
- κ = compressibility of medium
- ρ_d = mass density of scattering particle
- ρ = mass density of medium
- A_R = amplitude term ($= 4/9 \pi k^4 R^6$)
- γ_κ = compressibility term
- γ_ρ = density term

This formula denoting the Σ_s for one particle with a size much smaller than the wavelength is of critical importance in evaluating different contrast agents. Let us first consider the amplitude term A_R . This shows that the Σ_s increases with the radius of the scattering particle to the sixth power, and with the frequency to the fourth power (wavelength is equal to the acoustic velocity divided by the frequency). Thus, given a particle of a specific radius, the Σ_s is strongly influenced by the applied frequency. However, at this stage in the formula this is equally true for all contrast agents and therefore irrelevant for comparing one agent with another.

The second term γ_κ of the formula describes the effect of the difference in compressibility of the scattering particle and the surrounding medium. The third term γ_ρ describes the influence of the density difference between the particle and the medium. Note that when the compressibility and the density of the particle are equal to those of the surrounding medium, Σ_s is zero. Likewise, the greater the difference in these two quantities the greater the magnitude of Σ_s .

Differences in compressibility and density determine the value of this part of the formula and therefore the total scattering cross section. In order to determine which parameter has the greater influence on Σ_s , consider two extremely different scattering particles: a rigid sphere and a gas sphere of the same radius (1 μm). At an applied frequency of 3 MHz, the wavelength is 0.5 mm in water (note that the scattering particle is much smaller than the wavelength). The density of water is well known (1000 kg m^{-3}) as is the compressibility (0.45 $10^{-9} \text{ m}^2 \text{ N}^{-1}$).

Table II-a Comparison of components in equation [II-1] for an air bubble and an iron particle with a radius of 1 μm .

	ρ (kgm^{-3})	κ (m^2N^{-1})	A_R (m^2)	γ_κ^2	$1/3 \gamma_\rho^2$	Σ_s (m^2)
Air	1.2	$7.6 \cdot 10^{-6}$	$3.5 \cdot 10^{-20}$	$2.9 \cdot 10^8$	3.0	10^{-11}
Iron	7800	$5.5 \cdot 10^{-12}$	$3.5 \cdot 10^{-20}$	0.976	0.5	$5 \cdot 10^{-20}$

By way of an example, suppose the rigid sphere consists of iron which has a very high density (7.8 times that of water) and a low compressibility. Suppose the gas sphere consists of air (density 1.2 kg m^{-3} , compressibility $7.65 \cdot 10^{-6} \text{ m}^2 \text{ N}^{-1}$). The constituents of the formula for Σ_s are shown in Table II-a. There is a remarkable difference in scattering cross-section. The air bubble of 1 μm has a scattering cross-section of more than 100 million times that of a rigid sphere of the same size. Although there is a large difference in density, the contribution of the density term γ_ρ to the total Σ_s is relatively low, while the compressibility term has a significant effect. The lower compressibility of iron compared to that of water results in a negligible contribution of this factor. Generally, all spheres composed of rigid materials have a low compressibility which results in a negligible contribution to Σ_s , while all gasses have a significant impact on Σ_s .

When using gas bubbles as a contrast medium, there is another important effect resulting from mechanical resonance of the bubble which involves its stiffness and inertia. This effect is important because a resonating bubble effectively yields an increase in Σ_s . The stiffness is that of the enclosed volume of gas which acts like a spring when the bubble is disturbed from its equilibrium radius. The inertia is principally due to the mass of the liquid surrounding the bubble which oscillates with it. The simplest approximation of the resonant frequency is given by Anderson³:

$$f_r = \frac{1}{2\pi R} \sqrt{\frac{3\gamma P}{\rho}} \quad \text{[II-2]}$$

f_r = resonant frequency

R = radius of the bubble

P = Pressure

γ = C_p/C_v (ratio of the heat capacity at constant pressure and constant volume)

ρ = density of surrounding medium

In the above formula the resonant frequency is inversely proportional to the radius. For an adiabatic process with the heat capacity ratio of 1.4, the resonant frequency for a bubble radius of $2\text{ }\mu\text{m}$ in water, under normal atmospheric pressure, is 1.6 MHz. More complicated expressions for the resonant frequency, which include viscous and thermal losses and the effect of surface tension, are described by Anderson³. The surface tension will increase the resonant frequency while the viscous and thermal losses will result in a lower frequency. This effect becomes important for bubbles with a radius of less than $10\text{ }\mu\text{m}$.

Generally, the pertinent physical properties of gas bubbles result in their natural resonant frequency being much lower than that at which interference phenomena occur inside the bubble. These effects become important only when the resonant frequency approaches the velocity of sound divided by the radius of the bubble (wave number times radius approaches one).

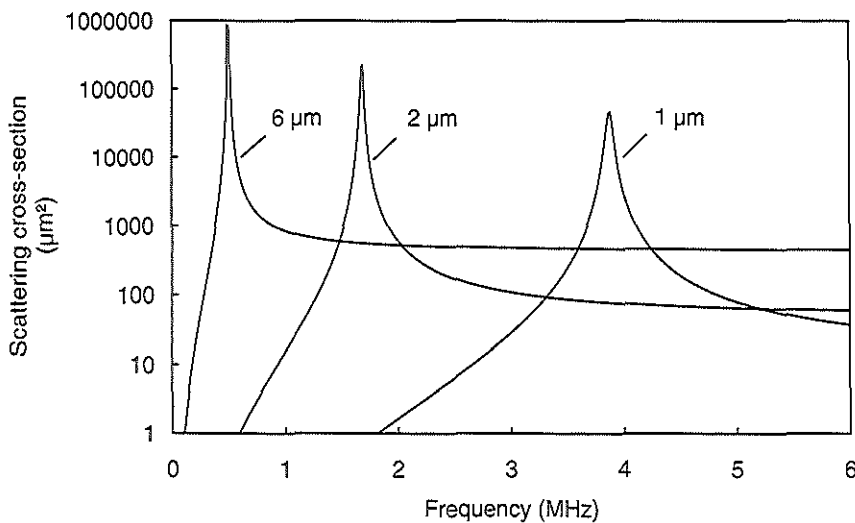


Figure 2-1 Scattering cross-section of a gas bubble as function of frequency for three radii; 1, 2 and $6\text{ }\mu\text{m}$.

The frequency dependence of the scattering cross-section is shown in Figure 2-1 computed for an ideal gas. It is assumed that the bubbles resonate in a lossless medium. The surface tension is included and equals 72 Nm^{-1} for an air-water transition. At frequencies below resonance the Σ_s increases with frequency to the fourth power as described previously. At frequencies above the resonant frequency

the normalized Σ_s has a constant value independent of frequency. Here the bubble has a Σ_s which is equal to the physical cross-section, and acts like a normal reflector. At intermediate frequencies the bubbles resonate and the Σ_s can reach peak values a thousand times higher than that predicted by formula [II-1].

Persistence of spheres containing gas

The reason that contrast agents containing bubbles of gas must have a radius larger than 5 μm , is based on the persistence of bubbles in relation to time required for the bubbles to pass from the site of injection to the site of detection⁴. Smaller bubbles tend to disappear before detection. On the other hand the bubbles must be small enough to traverse the lung circulation. Bubbles with radii larger than 5 μm are trapped in the lung microcirculation and do not appear in the left ventricle. Gas bubbles normally disappear rather quickly in a liquid, and a thorough analysis of this phenomenon has been carried out by Epstein and Plesset⁵. The differential equation describing the change in equilibrium radius with time, in a still liquid, is shown as equation [II-3].

$$\frac{dR}{dt} = \frac{D}{R} d_\tau \left[\frac{\frac{C_i}{C_0} - 1 - \frac{2\sigma}{R P_h}}{1 + \frac{4\sigma}{3R P_h}} \right] \left[1 + \frac{R}{\sqrt{\pi D t}} \right] \quad \text{[II-3]}$$

- R = radius of bubble
 D = diffusion constant (air-water)
 C_i/C_0 = ratio of the dissolved gas concentration to the saturation concentration
 σ = surface tension
 P_h = ambient pressure
 d_τ = $(R_g T C_0)/P_h$, R_g = universal gas constant
 T = temperature (Kelvin)
 C_0 = saturation concentration

The rate of decrease of bubble radius is a direct measure of the rate of disappearance of the bubble. This is determined by the diffusion constant which is dependent on both the gas and the fluid. The parameter d_τ is a constant for a given temperature and medium.

The first bracketed term in equation [II-3] relates to the amount of gas which has been already dissolved in the liquid. The bubble's surface tension is, in fact, the mechanism responsible for the bubble's disappearance as this generates an overpressure inside the bubble. The second bracketed component of equation [II-3]

is known in the field of thermodynamics as the "solution of the penetrations - theories" and denotes how far and how fast the gas saturates the liquid. This differential equation can be solved numerically (for example, by Runge-Kutta methods). The results of such computations are shown in Table II-b which lists disappearance times for several bubble sizes ranging from 1 to 1000 μm .

Table II-b Dissolution time (s) for air bubble in water (surface tension $70 \times 10^{-3} \text{ Nm}^{-1}$; $T = 300 \text{ K}$).

Sphere radius (μm)	Dissolved gas concentration	
	$C_1 / C_0 = 1$	$C_1 / C_0 = 0$
1000	$6 \cdot 10^6$	$1 \cdot 10^6$
100	600	100
10	6	1
1	< 1	< 1

Bubbles with radii larger than 100 μm disappear slowly in relation to the total circulation time, while bubbles less than 10 μm disappear too rapidly even in a saturated liquid to be of any practical use. The rate of disappearance depends on the dissolved gas concentration and in a saturated liquid the rate of disappearance is reduced by a factor of six.

In the event that the liquid becomes oversaturated with gas, it is possible for bubbles to grow depending on their size and surface tension. This is illustrated in Figure 2-2 which shows regions of stability/instability as a function of gas concentration and bubble radius. In the upper-right region the bubbles grow while in the lower-left they shrink. Figure 2-2 illustrates the point that bubbles with very small radii, less than 5 μm , can be made to grow to visible size with only modest dissolved gas concentration ratios, but it is virtually impossible for bubbles smaller than 1 μm to do so.

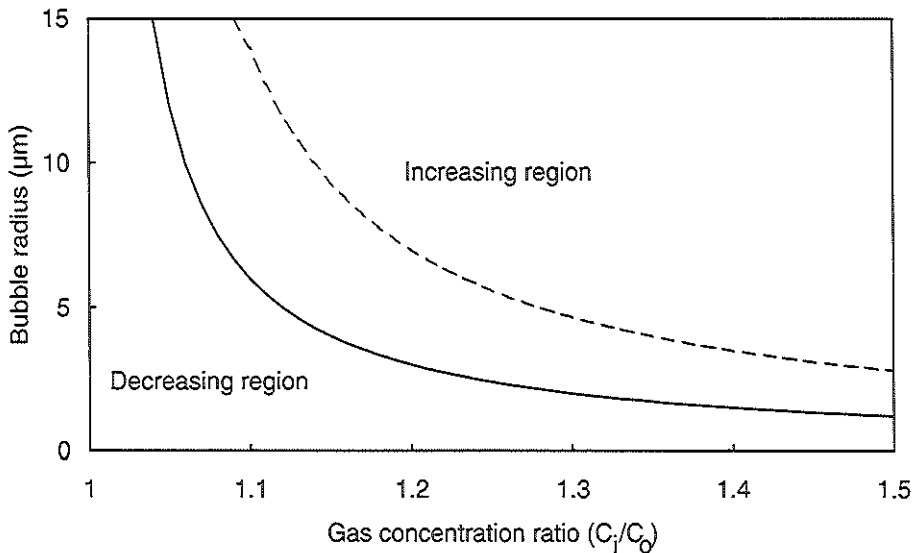


Figure 2-2 Stability curves for bubbles in a liquid for surface tension of 0.03 (—) and 0.07 (---) Nm^{-1} .

Characteristics of fluids containing small gas bubbles

As a contrast agent, gas bubbles are far superior to rigid spheres. In addition to an enhanced backscatter signal, there are other characteristics of the gas bubble-liquid system which characterise the system. The presence of small gas bubbles in a fluid change the acoustic properties of the media. Although the most well known is the enhanced backscatter, there are other characteristics which change and these can be observed by appropriate ultrasonic techniques. Some have definite potential for further development. They include:

1. acoustic velocity
2. backscatter intensity
3. second harmonic response
4. resonant frequency

1. Acoustic velocity

The velocity of (ultra)sound varies widely depending on the compressibility and density. For example, the velocity of sound in water is 1500 ms^{-1} , in dry air about 330 ms^{-1} , and for ceramic materials approaches 6000 ms^{-1} . Both compressibility and

density change in mixtures of these materials, and therefore the velocity of sound changes as well. Density and compressibility of mixtures are described by Twersky⁶. For small volume concentrations of the mixed component, density and compressibility are given by:

$$\rho = v_m \rho_m + (1 - v_m) \rho_w \quad [11-4]$$

$$\kappa = v_m \kappa_m + (1 - v_m) \kappa_w$$

ρ = density of suspension

ρ_m = density of the mixed component

ρ_w = density of the original component

κ = compressibility of the emulsion

κ_m = compressibility of the mixed component

κ_w = compressibility of the original component

v_m = partial volume concentration of the mixed component

The resulting velocity, c , is given by

$$c = \sqrt{\frac{1}{\rho \kappa}} \quad [11-5]$$

The density of any practical suspension of gas bubbles in water changes very little. However, due to the large compressibility difference, the compressibility of such a suspension increases greatly even for small volume concentrations. This results in a correspondingly large decrease in the velocity of sound.

An example of the extent to which velocity decreases in relation to the total gas content, as a summation of all bubble volumes, is illustrated in Figure 2-3. The velocity of sound is very nearly that of pure water up to a volume concentration of $10^{-4}\%$ at which point the velocity drops rapidly for gas volume concentrations above this level. Even volume concentrations as low as 0.1% significantly reduce the velocity of sound transmission. In the extreme situation the compressibility becomes that of air and the density difference becomes a significant factor, sufficient to cause an increase in the velocity of sound. The above explanation is valid for small bubbles and at low frequencies.

For example, for bubbles of 2 μm the relationship is valid for frequencies below 100

KHz. An extensive review of the velocity of sound in suspensions, covering the full frequency spectrum has shown that there is no change in acoustic velocity, as a function of the concentration, for frequencies above the resonant frequency⁷.

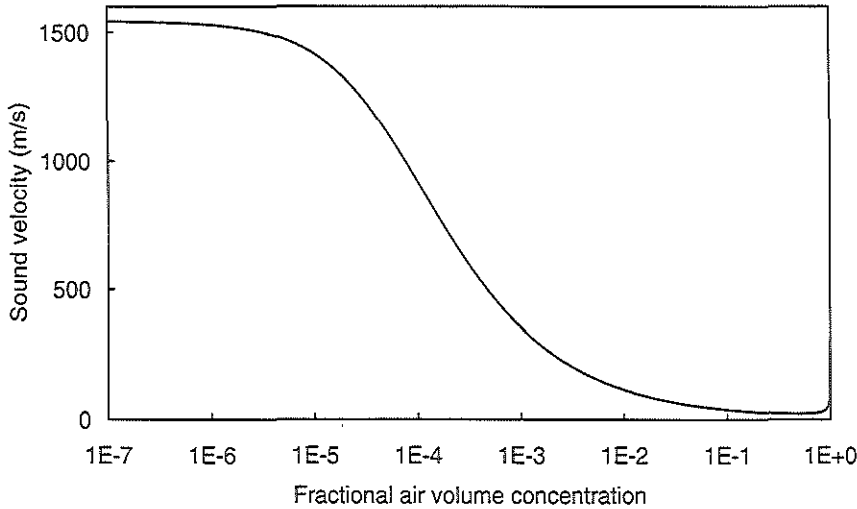


Figure 2-3 Emulsion sound velocity versus air volume concentration.

There are two ways to exploit the change in velocity of sound in a suspension. First, the gas concentration can be calculated from the velocity of sound. If the size distribution is known, the number of bubbles can be determined, which can be used for 'wash out' curves. This would provide information on the magnitude of flow and shunts. Second, the pressure in the liquid indirectly affects the velocity of sound. If the overpressure is not too large, the gas inside the bubble behaves as an ideal gas. Thus the compressibility is independent of the pressure. The fractional gas concentration, on the other hand, decreases with increases in pressure because the size of the bubbles depend on pressure. For low volume concentrations and a large difference in compressibility between gas and liquid, equation [II-4] can be simplified using $\rho = \rho_w$ and $\kappa = v_g \kappa_g$ where ρ_w is the density of the liquid, v_g the volume concentration of the gas and κ_g the compressibility of the gas. Equation [II-6] is derived by combining equations [II-4] and [II-5] together with the linear relationship between the pressure change and fractional volume concentrations.

$$\frac{P}{c} = \text{constant} \quad \text{[II-6]}$$

P = pressure

c = acoustic velocity

The above equation is valid for a fractional air concentration between 10^{-5} and 10^{-2} . Practical contrast agents undiluted contain about 2 % gas. After injection, assuming a dilution of 1:100, the gas volume concentration will be 2×10^{-4} . Therefore, it is possible to determine the pressure from the velocity of sound in the emulsion providing all the conditions required for deriving equation [II-6] are fulfilled.

2. Backscatter Intensity

When sound traverses a cloud of particles, each particle produces a scattered wave which reinforces/interferes with the incident wave. This interaction affects the shape of the scattered wave. This can result in coherent or incoherent scattering depending on whether the elements are regularly spaced. Considering a region where the scattering elements are much smaller than the wavelength and sparsely populated, then the relative incoherent backscattered intensity at a distance r is approximated by⁸:

$$\frac{I_s}{I_0} = \frac{1}{9} n V \frac{k^4 R^6 (\gamma_c + \gamma_p)^2}{r^2} \quad \text{[II-7]}$$

I_s = backscattered intensity

I_0 = incident intensity

n = number density of scattering particles

V = occupied volume

k = wave number

R = radius of the particle

γ_c = compressibility term

γ_p = density term

r = distance

Note that equation [II-7] indicates a linear relationship between the backscatter intensity and the number of scattering elements. A very important restriction is that the occupied volume be sparsely populated. In contrast echography the conditions of a sparse distribution of scattering particles is not necessarily fulfilled. The number of scattering particles per cubic wave length can be as high as a few thousand. In this case such effects as multiple scattering, attenuation, and interference must be taken

into account. Nevertheless, measurements on liquids with a low concentration of gas bubbles agree well with the theoretical analysis (Pownser⁹).

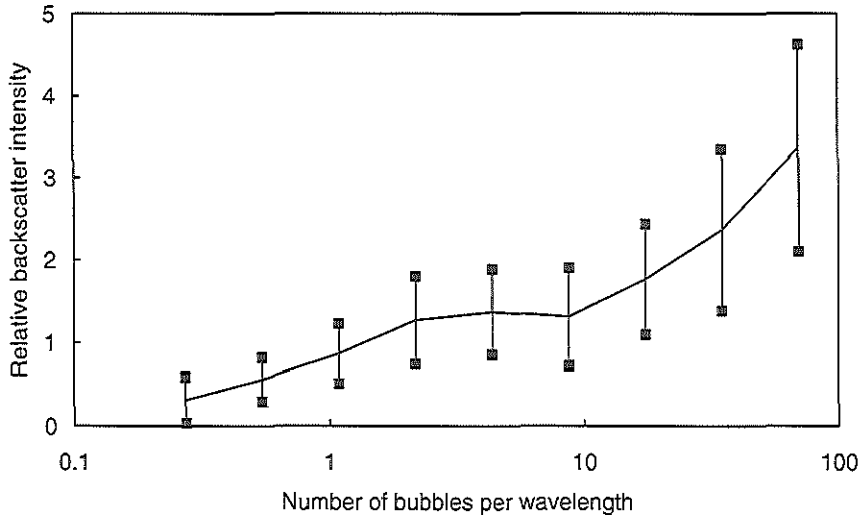


Figure 2-4 *Simulated backscatter intensity as function of concentration.*

For high concentrations the resulting backscattered signal is more difficult to evaluate as the individual contributions of each element to the amplitude and phase of the backscattered signal must be determined. The chaotic movement of the bubbles as a function of time alter the phase and the amplitude of the backscattered wave. Furthermore, multiple scattering should be taken into account. Although such a computation is theoretically possible, doing so in three dimensions for a few hundred million scattering particles, over a broad frequency spectrum, would require an inordinate amount of computer time. Therefore a one-dimensional model has been developed to simplify the computations.

In this one dimensional model the scattering particles are assumed to have a variable scattering cross-section and to occupy a random position in the ultrasound beam. The distribution of the scattering cross-section is assumed to be Gaussian. The position of the scattering particles is based on an equidistant grid where the deviation in position with respect to the grid is governed by a Gaussian distribution.

Some results of the expected backscatter signal as a function of the concentration of scattering particles (the bandwidth of the acoustic pulse impinging the particles is about 100%) is shown in Figure 2-4. The above mentioned distributions both have

a standard deviation of 0.5 times the mean value. The backscatter signal increases linearly with concentration for low concentration (as described previously), but for higher concentrations this is not the case due to phase interference. There are also rather large variations in the backscattered signal for any given concentration.

Of course, these results are very dependent on the assumed statistical properties. Given a very low standard deviation, the backscattered signal will even decrease for higher concentrations and eventually approach zero. Although this model does not represent reality, it does indicate a few important parameter dependencies which can be qualitatively projected to a three-dimensional model. The main conclusion which can be drawn from this computer simulation is that one can expect a backscatter decrease instead of an increase for higher contrast agent concentrations. Furthermore, acoustic measurements can vary considerably, and this indicates a need for appropriate signal averaging.

3. Second harmonic response of bubbles

The resonance phenomena described previously can be considered a first harmonic response. Bubbles can also respond to an acoustic field by radiating a second harmonic. This phenomena is dependent on the acoustic pressure of the wavefront and on the characteristics of the fluid.

The fundamental principle is illustrated in Figure 2-5. This shows the normal 'first harmonic' and 'second harmonic' scattering cross-section as a function of bubble size at a frequency of 1.64 MHz.

For a radius of less than 1 μm the 'first harmonic' Σ_s increases with the sixth power as described in equation [II-1]. Resonance occurs at a radius of 2 μm at which point the Σ_s is maximum. For values of radius greater than 2 μm Σ_s first decreases, then gradually increases again due to its own physical cross-section. The second harmonic (3.28 MHz) Σ_s curve is completely different. There is a very sharp peak at a bubble size of 2 μm which is only a few decibels lower than the first harmonic response. Furthermore, there is virtually no energy scattered for larger bubbles. For smaller bubbles there is a subharmonic present but the value of this is far below the peak value.

Miller¹⁰ has described the above phenomena in a theoretical analysis where only second order non-linear effects are taken into account. This assumption is valid only for a relatively low acoustic pressure. Furthermore, he reports an interesting experiment (described below) in which it is possible to distinguish between small and large bubbles by using this secondary emission. Two narrow-band transducers are

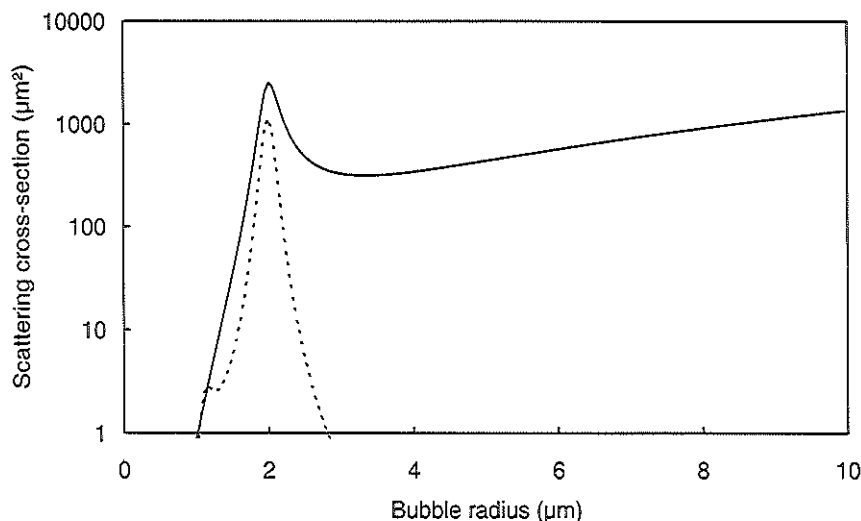


Figure 2-5 First (—) and second (---) harmonic response of a bubble in water.

used: one at 1.64 MHz for transmitting and receiving and the other at 3.28 MHz for receiving only. The two transducers are mounted in a tube containing bubbles of 500 μm and 4 μm . His uncorrected results are summarized in Table II-c. The first two columns contain the results for the 1.64 MHz transducer. The larger bubbles provide a greater response which is caused by the larger physical cross-section. Column 3 and 4 show the response for the 3.28 MHz transducer. The large difference in response between the 4 μm and the 500 μm bubble is clearly apparent. Therefore it should be possible to discriminate between small and large bubbles (or objects) by taking advantage of the second harmonic emissions.

Although such an approach is very promising, much more research is necessary to confirm and extend this approach. For example, the influence of the acoustic pressure should be linear, and is therefore easily checked. Also the influence of viscosity, as well as other damping mechanisms, must be considered.

Table II-c First and second harmonic response of bubbles¹⁰.

	First harmonic		Second harmonic	
	Small (4.2 μm)	Large (500 μm)	Small (4.2 μm)	Large (500 μm)
Response amplitude (mV)	0.64	28.8	0.51	0.012
Theoretical response	0.46	7.8	0.21	0.00026

4. The resonant frequency

The scattering cross-section of bubbles in water, as given in Figure 2-1, shows a clear frequency dependency. The computations given in this figure are carried out for a lossless medium. For bubbles in a lossless medium the decrease in power of an acoustic wave travelling through the medium is caused by the scattering of these bubbles. Neglecting also the forward scattering the attenuation is given by:

$$A_L(f) = \int_{R_{min}}^{R_{max}} n(R) \Sigma_s(R) dR \quad [II-8]$$

$A_L(f)$ = attenuation in a lossless medium

Σ_s = scattering cross-section

$n(R)$ = bubble concentration

R_{min} = minimum radius of the bubbles present

R_{max} = maximum radius of the bubbles present

Attenuation as function of the frequency is thus a measure of the number of bubbles, their radius, and distribution. By determining the attenuation the bubble size distribution can be estimated.

The transmission through a medium with bubbles, produced by sonication of a 5% solution of urografin, 2 minutes after sonication is shown in Figure 2-6. The solid line represents an experiment carried out by one broad-band measurement. The dotted line is the theoretical result, obtained by assuming a Gaussian size distribution of the bubbles. Attenuation is greatest at the resonant frequency, and remains constant at

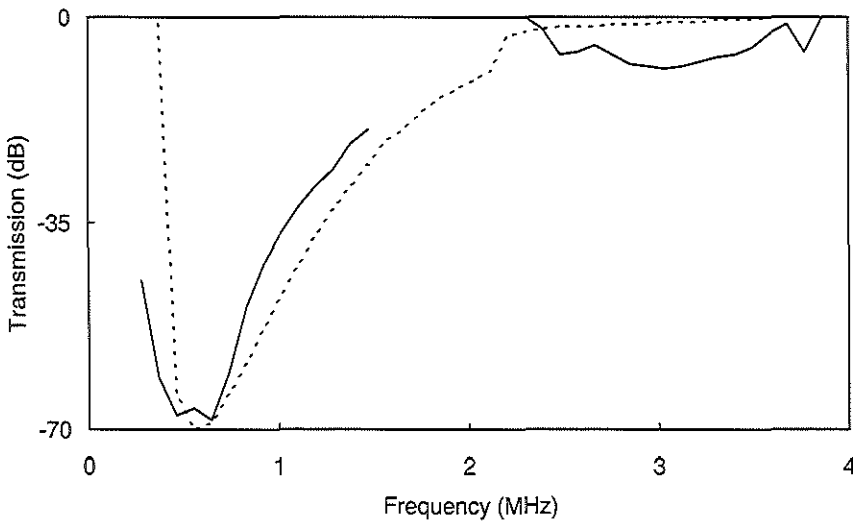


Figure 2-6 *Transmission through a medium with sonicated bubbles. —, measurements; --, simulations.*

much higher frequencies. The best fit is achieved for a mean radius of $4.5\ \mu\text{m}$ and a standard deviation of $1.5\ \mu\text{m}$. After four minutes two effects can be noticed: a shift towards a lower frequency of maximum attenuation and a decrease in the magnitude of the attenuation. This is caused by small bubbles disappearing by diffusion effects which results in fewer bubbles, but of relatively greater dimensions. After four minutes the best fit is achieved for a mean radius of $7\ \mu\text{m}$ and a standard deviation of $3\ \mu\text{m}$. The reproducibility of these measurements is about 15%.

This experiment shows a relationship between resonant frequency and bubble size. The theoretical calculations are based on a lossless medium according to [II-8] which is not realistic for bubbles in water. In chapter III the absorption occurring in a medium will be described.

There is yet another feature of the resonant frequency which may be useful. Equation [II-2] shows that the resonant frequency is dependent on pressure and diameter. Under atmospheric pressure and assuming that the bubble's content behaves like an 'ideal' gas, slow pressure and volume changes in the bubble are governed by equation [II-9].

$$\Delta V = - \frac{V}{P} \Delta P \quad \text{[II-9]}$$

ΔV = volume change
 V = volume of the bubble
 ΔP = pressure change
 P = pressure

Applying [II-2] to [II-9] yields an expression for the changes in the resonant frequency as function of the pressure:

$$\frac{\Delta f}{f_r} = \frac{5}{6} \frac{\Delta P}{P} \quad \text{[II-10]}$$

f_r = the original resonance frequency

From [II-10] can be seen that the proportional shift in the resonant frequency due to a (small) variation in pressure is linear related to the relative pressure change. It is therefore theoretically possible to determine the pressure from the change in the liquid measurements of the resonant frequency.

Based on the above approach Tamura¹¹ has confirmed this prediction using encapsulated bubbles. In these experiments two frequencies are used to eliminate attenuation effects, and it is possible to discriminate between pressure differences of at least 50 mm Hg (about 7×10^3 Pascal).

Discussion

Gas bubbles or gas encapsulated spheres are far superior echographic contrast agents compared with rigid scattering agents. This is due not only to the enhancement of the backscatter by a factor 10,000, but also to other useful properties of gas bubbles. There is one major disadvantage however. Under normal circumstances the bubbles disappear very quickly (within a few seconds for bubbles smaller than 10 μm in fluids with a normal value of surface tension, but greater longevity is obtained with reduced surface tension). Areas of clinical application will undoubtedly focus on the left ventricle and the coronary arteries. The delay for intravenously injected bubbles to appear in the heart is about 15 seconds (see Feinstein¹²), therefore the gas bubbles must be encapsulated to avoid bubble attrition due to gas diffusion. This

encapsulation however changes the properties of the bubble to that of one with a thin shell. Important properties such as shell elasticity, thickness, the Poisson ratio lower the resonant frequency and reduce the scattering cross-section. Nevertheless, it should be possible to determine a combination of applied frequency, bubble radius, shell thickness and elasticity which is optimum for medical diagnostic purposes. The exact difference between gas bubbles and gas encapsulated spheres remains a subject for further study.

The double resonance phenomenon promises to be one of the most important applications for bubble contrast agents. Assuming that it is possible to produce stable bubbles which can be detected in the left ventricle and myocardium, the capacity to discriminate between the contrast agent and tissue opens new perspectives for diagnostic ultrasound. Such a system would consist of two-dimensional transducers: one transducer to form conventional 2D images (at the bubble resonant frequency), the other for receiving second harmonic information. In this way two simultaneous images can be made. One provides a normal 2D image with all heart structures including the contrast agent; the other provides a image of only the contrast agent. Myocardial structures would not be visualised because they only reflect the original information.

Some cautionary remarks regarding this approach are necessary. The scattering of the second harmonic is pressure dependent, i.e. the pressure must be around 10^5 Nm^{-2} (= 760 mm Hg, Miller¹⁰). Such pressures can be expected to induce non-linear effects resulting in harmonic distortion. Such parameters would be detected by the high frequency transducer, and the ability to discriminate between components would depend on the properties of the medium, distance to the transducer, and the applied acoustic power.

The resonant phenomena of bubbles can be exploited in a number of ways. For example, it should be possible to measure the instantaneous pressure in the left ventricle due to the shift in resonant frequency as function of the ambient pressure according to equation [II-2] and equation [II-9]. In order to achieve a high sensitivity, the size of the bubbles which appear in the left ventricle should have a resonant frequency around the impinging frequency. Furthermore, the presence of bubbles in the coronary veins will certainly change the backscattered signal. Not only the amplitude will change, which may not be detectable, but more importantly the frequency content of the backscattered signal will also change because of the difference in scattering properties between bubbles and tissue. A knowledge of contrast agents together with tissue identification algorithm will be very useful.

Using the change in acoustic velocity caused by the presence of bubbles is difficult. This change is only apparent at a relatively low frequency (compared to the resonance frequency of the bubbles in the contrast agent). When using low frequency transducers the spatial resolution is rather poor and this limits the discrimination between different regions. One can only use frequencies employed nowadays for medical diagnostic purposes when the bubbles in the contrast agent are very small, but this limits their persistence.

For all the above mentioned applications the need for a stable well-defined gas-filled bubble is necessary. If one could develop such a contrast agent for which the physical properties could be controlled, all the above mentioned applications are within reach.

Conclusion

The use of gas bubbles or encapsulated gas bubbles offers new perspectives for echocardiographic research. This may allow the measurement of pressure within the heart and great vessels, estimation of flow by contrast dilution, and visualisation of structures heretofore of insufficient contrast to be detected by conventional techniques.

References

1. Ophir, J. and Parker, K.J. Contrast agents in diagnostic Ultrasound. *Ultrasound in Med. & Biol.* (1989) Vol. 15, No.4, p 319-333
2. Morse, P.M. and Ingard, K.U. *Theoretical acoustics*. McGraw Hill, New York (1968) p 418-427
3. Anderson, A.L. and Hampton, L.D. Acoustics of gas-bearing sediments 1. Background. *Journal of the Acoustical Society of America* (June 1980) Vol. 67, No. 6, p 1865-1889
4. Feinstein, S.B., Shah, P.M., Bing, R.J., Meerbaum, S., Corday, E., Chang, B.L., Santillan, G. and Fujibayashi, Y. Microbubble dynamics visualized in the intact capillary circulation. *J. Am. Coll. Card.* (1984) Vol. 4, p 595-601
5. Epstein, P.S. and Plesset, M.S. On the stability of gas bubbles in liquid-gas solutions. *The Journal of Chemical Physics* (November 1950) Vol. 18, No. 11, p 1505-1509
6. Twersky, V. Acoustic bulk parameters of random volume distributions of small scatterers. *J. Acoust Soc. Amer.* (1964) Vol. 36, p 1314
7. Medwin, H. Counting bubbles acoustically: a review. *Ultrasonics* (Jan. 1977) p 7-13
8. Morse, P.M. and Ingard, K.U. *Theoretical acoustics*. McGraw Hill, New York (1968) p 436-441

9. Pownser, S.M. and Feinstein, S.B. Quantitative radiofrequency analysis of sonicated echo contrast. *Digital Techniques in Echocardiography* Martinus Nijhoff Publishers, Dordrecht (1987) p 13-27
10. Miller, D.L. Ultrasonic detection of resonant cavitation bubbles in a flow tube by their second-harmonic emissions. *Ultrasonics* (Sept. 1981) p 217-224
11. Tamura, T., Chihara, K., Shirae, K., Ishihara, K., Nagakura, T., Tanouchi, J. and Kitabatake, A. Dynamic pressure measurement using two-frequency ultrasound. *Proceedings of 9th Symposium on Ultrasonic Electronics, Sendai 1988. Japanese Journal of Applied Physics* (1989) Vol. 28, Supplement 28-1, p 211-213



ABSORPTION AND SCATTER OF ENCAPSULATED GAS FILLED MICROSPHERES

Abstract

Albunex[®] is an ultrasound contrast agent for use in echocardiology and other areas. It is capable of passing through the lung circulation after intravenous injection. A theoretical model is developed for some acoustic properties, particularly the scatter and absorption, of this contrast agent, considering the individual microspheres as air bubbles surrounded by a thin shell. The attenuation, the sum of absorption and scatter, of this contrast medium is measured with 5 transducers to cover the frequency range from 700 kHz to 8.5 MHz. It is concluded that the model results in a good agreement with these acoustic measurements. When Albunex[®] is used intravenously the backscatter enhancement in the left ventricle is caused mainly by the microspheres with diameters between 5 and 8 μm .

This chapter is based on a manuscript, which has been published:

Title :Absorption and scatter of encapsulated gas filled microspheres:
theoretical considerations and some measurements
Authors :N. de Jong, L. Hoff, T. Skotland and N. Bom
In :Ultrasonics 1992 30(2)

Introduction

The ultrasonic properties of liquids containing gas bubbles have long been a subject of intensive investigation. Anderson¹ and Prosperitti² provide a thorough overview of the salient studies on such systems. The principal motivation, until recently, has involved underwater sonargraphy, e.g. naval applications, but lately the relatively new area of contrast echocardiography has received increased attention. There are some aspects of contrast echocardiography, however, which are quite different from that of underwater studies; in contrast echocardiography the bubbles are not so much a hindrance, but a tool to investigate the properties of the system. A crucial criterion for an echocardiographic contrast agent is that it is able to pass through the pulmonary microcirculation following intravenous injection and survive the maximum pressure developed in the left ventricle and myocardium. It can thus be used to study perfusion of the myocardium and other organs.

Not only must the bubbles be small enough to pass the lung capillary bed, they must also have a sufficiently long persistence to be detected³. These two conditions are mutually exclusive for naturally occurring bubbles in a gas saturated fluid. Small bubbles of diameters less than 10 μm tend to disappear within a few seconds^{4,5} and they will thus not reach the left ventricle after intravenous injection.

Contrast agents that overcome the size/persistence dilemma are now being evaluated in clinical trials. Albunex[®] (a registered trademark of Molecular Biosystem, San Diego, USA) is one such agent and is the subject of the study described in this report. This contrast agent consists of microspheres of encapsulated gas surrounded by a shell of human serum albumin. The shell is formed by sonication of an infusion solution of 5% human albumin⁶. The mean diameter of the microspheres is about 4 μm , whereas the shell thickness is in the range of 20 - 25 nm, i.e. less than 1% of the diameter. The building block of the shell is a protein, which in its native form has an ellipsoidal shape measuring about 4x4x14 nm. If it is assumed that the size of the albumin molecule does not change very much during the shell forming process, one can imagine this shell as consisting of a layer of up to 5-6 molecules.

Some of the ultrasonic properties of this contrast agent are described in this report. Theoretical considerations, based on a description of an ideal gas bubble, are extended to include a bubble with a shell. The unknown parameters of the shell are estimated by model studies where the measured response curves are compared to the theoretical model. It is shown that theory and measurement agree reasonably well and that the mathematical model may be useful for predicting and analyzing further applications of the Albunex[®] microspheres in echocardiography, e.g. by determining the size distribution for optimal backscatter at diagnostic frequencies.

Theory

Scattering cross-section

The scattering, absorption and the extinction cross-sections are important acoustic properties of gas encapsulated bubbles in echocardiographic applications. The scattering cross-section of a particle is defined as the quotient of the scattered power and the incident intensity. Medwin⁷ has shown that for an air bubble in a liquid this can be expressed as:

$$\Sigma_s = \frac{4\pi R^2}{\left(\frac{f_r^2}{f^2} - 1\right)^2 + \delta^2} \quad \text{[III-1]}$$

Σ_s = scattering cross-section

R = radius of the bubble

f_r = resonance frequency

f = frequency of applied ultrasound field

δ = total damping

The resonance frequency, f_r , and the total damping δ , in this expression are described in the following section. The resonance frequency of an air bubble in water can be determined assuming the following: 1) The wavelength of the acoustic field is much larger than the bubble diameter, 2) the radial displacement of the bubble is small compared to its radius and 3) the surrounding fluid is incompressible. These conditions are easily fulfilled for bubbles used as contrast agents in echocardiography. The diameter of the bubbles range from 1 to 10 μm , while the wavelength of the acoustic field used for medical diagnosis ranges from 0.2 to 0.75 mm (frequency between 7.5 and 2 MHz in water). The fluid (water, blood) is virtually incompressible. Also, the acoustic pressures used in the medical diagnostic field cause a radial displacement, which is small compared to the equilibrium diameter. According to Medwin⁷ the angular resonance frequency (ω_{Rg}) for an ideal gas bubble is given by:

$$\omega_{Rg}^2 = \frac{S_a}{m} b \beta \quad \text{[III-2]}$$

S_a = stiffness of the bubble-liquid system

m = effective mass of the system

b = $1/\Gamma$, Γ = polytropic exponent

β = surface tension coefficient

The equivalent mass m is given by Medwin⁷ together with the polytropic exponent

b^{-1} and the surface tension coefficient β . In a system consisting of a bubble surrounded by a shell, the shell causes an additional restoring force. Equation [III-2] thus becomes

$$\omega_r^2 = \omega_{rg}^2 + \frac{S_{shell}}{m} \quad [III-3]$$

where ω , is the angular resonance frequency of the system and S_{shell} the stiffness of the shell. The determination of S_{shell} is provided later in this article.

The damping coefficient (δ) is determined by the following mechanisms: 1) re-radiation, 2) damping due to the viscosity of the surrounding fluid, and 3) thermal damping as shown in the following expression:

$$\begin{aligned} \delta &= \delta_{rad} + \delta_{vis} + \delta_{th} \\ \delta_{rad} &= kR \\ \delta_{vis} &= 4 \frac{\eta}{\rho \omega R^2} \\ \delta_{th} &= B(\omega, R) \frac{\omega_r^2}{\omega^2} \end{aligned} \quad [III-4]$$

- δ_{rad} = damping due to re-radiation
- δ_{vis} = damping due to viscosity of the surrounding liquid
- δ_{th} = damping due to heat conduction
- k = wave number ($2\pi/\lambda$, λ = wavelength)
- η = viscosity of the surrounding liquid
- ρ = density of the surrounding liquid
- R = radius of the bubble
- ω_r = resonant angular frequency
- ω = applied angular frequency

The expression for $B(\omega, R)$ is given by Anderson¹ and Medwin⁷ (called d/b by Medwin). The polytropic exponent includes this factor B and evaluates to 1 for adiabatic conditions and γ for isothermic conditions (γ = ratio of heat capacity at constant pressure and constant volume, C_p/C_v). The resonance frequency can be determined within 5% of the exact value by taking the polytropic exponent equal to γ for bubbles with a radius smaller than 10 μm . Taking b equal to 1, the calculated resonance frequency remains within 5% of the exact values for bubbles with a radius larger than 100 μm . For the frequency range from 1-10 MHz, the adiabatic case is valid for bubbles with radii larger than 50 μm and the isothermic case for bubbles smaller than 1 μm . Thus, the full expression for b given by Medwin⁷ has to be used for bubble radii between these two values.

Absorption cross-section

The energy lost in an ultrasonic beam, i.e that portion which is converted into heat, is referred to as the absorption cross-section. Coackly⁹ derives the following expression for Σ_a

$$\Sigma_a = \Sigma_s \left(\frac{\delta}{\delta_{rad}} - 1 \right) \quad [III-5]$$

Extinction cross-section

The total energy loss for an acoustic beam travelling through a screen of bubbles is given by the sum of the absorption cross-section and the scattering cross-section. This sum is called extinction cross-section Σ_e :

$$\Sigma_e = \Sigma_s + \Sigma_a \quad [III-6]$$

Gas bubbles with an elastic shell

Bubbles surrounded by a thin elastic shell behave differently from bubbles without a shell. The restoring force can be dramatically increased by the stiffness of the shell (S_{shell}) (see also equation [III-2]).

Elasticity of the shell

The contribution of the thin shell to the acoustic cross-section can be calculated under the assumption that the shell is: 1) homogeneous, 2) of constant thickness, and 3) perfectly elastic, i.e. obeys Hooke's law. Assuming these conditions to be valid, Reismann⁸ has derived the relationship between the displacement u in bubble radius and the pressures inside and outside the bubble (see Figure 3-1).

$$u = R_0 \frac{P_a R_a^3 - P_b R_b^3}{3K(R_a^3 - R_b^3)} + R_a^3 R_b^3 \frac{P_a - P_b}{4GR_0^2(R_a^3 - R_b^3)} \quad [III-7]$$

u = radial displacement of the bubble

P_a = pressure inside the bubble

P_b = pressure outside the bubble

R_0 = equilibrium radius of the bubble

K = $E / 3(1-2\nu)$ [bulk modulus]

G = $E / 2(1+\nu)$ [shear modulus]

E = elasticity [Young's modulus]

ν = Poisson ratio

R_a = internal radius of bubble

R_b = external radius of bubble.

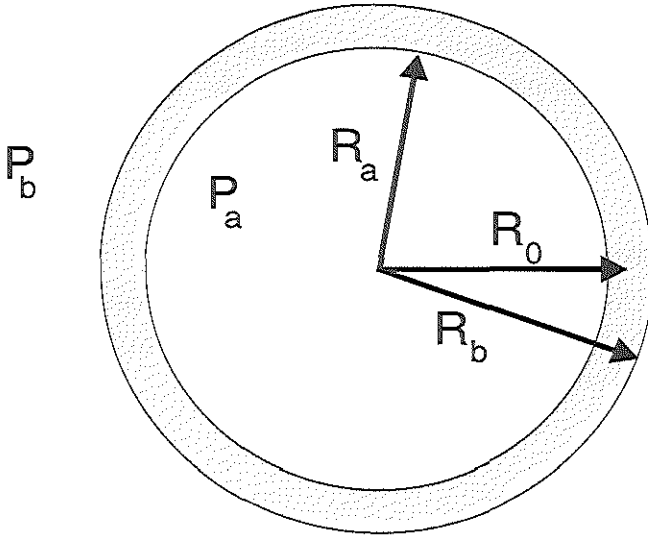


Figure 3-1 Spherical bubble surrounded by a thin shell. R_a , inner radius; R_b , outer radius; R_0 , radius; P_a , pressure inside the bubble; P_b , pressure outside the bubble.

When the shell thickness ($t_w = R_b - R_a$) is much smaller than the bubble radius, a series expansion in t_w can be made and the higher order terms neglected. Equation [III-7] then simplifies to:

$$u = (P_a - P_b) R_0^2 \frac{1-\nu}{2Et_w} \quad [\text{III-8}]$$

The contribution of the shell to the bubble stiffness can then be calculated:

$$S_{\text{shell}} = \frac{8\pi Et_w}{1-\nu} \quad [\text{III-9}]$$

An interesting conclusion of this result is that the shell stiffness is independent of the radius. Although the shell elasticity (E), wall thickness (t_w) and Poisson ratio (ν) are all unknown, it is not necessary to determine all these parameters separately to compare experimental results with theory. Only the resulting shell stiffness is of interest. Fox¹⁰ also examined the possible influence of bubbles covered with an

organic skin to explain the consistently higher resonance frequencies which have been measured. Equation [III-9] differs by a factor 9/4 from that derived by Fox. The acoustical behaviour as function of the frequency of a bubble without a shell differs from bubbles with a shell. The shell increases the stiffness as indicated in equations [III-2] and [III-3]. As a first approximation it is assumed that the surface tension is negligible because in our model we are dealing with a gas-solid transition instead of a gas-fluid. Furthermore it is assumed that the viscous, thermal, and re-radiation losses are not influenced by the shell. The viscous losses occur in the fluid independent of the presence of the shell, i.e. only the velocity of bubble vibration determines its relative contribution. The same reasoning is valid for the re-radiation factor. The influence of the shell on thermal losses, however, is not entirely clear. The heat exchange between gas and fluid is assumed to be optimal in the theory developed by Devin¹¹, later described for the off-resonance case by Eller¹². Here the surrounding fluid is considered as a reservoir with a large heat capacity. The shell may insulate the gas from the fluid while itself having insufficient heat capacity to exchange the energy required during expansion and compression of the bubble, and thereby reduce the heat exchange between gas and liquid. An additional loss of energy may be due to friction within the shell itself. This would contribute to the overall loss of acoustic energy, but is not included in our model.

So in the presented model it is assumed that the damping parameters are the same as for an ideal bubble and that the surface tension is negligible and therefore set to zero. The stiffness is increased due to the shell as described in equation [III-9] where the shell is characterized by the shell elasticity parameter, S_p , defined as $E \cdot t_w / (1 - \nu)$ expressed in Nm^{-1} .

Energy loss through a screen of bubbles

The characteristics of the bubbles can be determined from either backscatter or from transmission experiments. A problem which occurs when measuring backscatter is that the bubbles scatter omnidirectional with the result that the received intensity at the transducer depends on transducer characteristics such as the aperture, the measuring distance, concentration of the bubbles and frequency. A more practical approach, and one easily performed in vitro, is to measure the transmission. The transmission can be normalized to a reference measurement and thus made independent of the transducer properties.

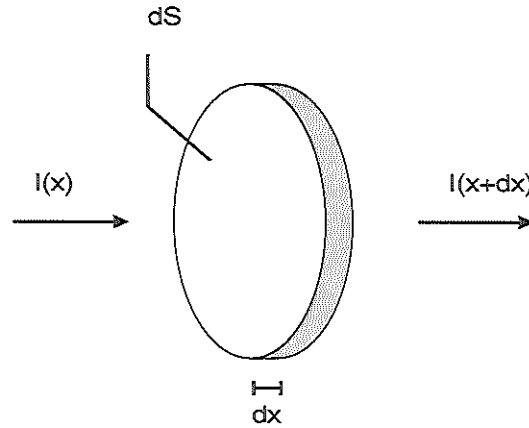


Figure 3-2 *Small volume element containing scatterers. dS , surface of element; dx , length of considered volume element in direction of wave propagation; $I(x)$, ultrasound intensity at position x ; $I(x+dx)$, ultrasound intensity at $x+dx$.*

Consider a cavity filled with bubbles and placed in the acoustic beam, and assume that the following conditions are met: 1) the beam width is smaller than the cavity, 2) the bubbles are homogeneously and uniformly distributed, 3) the number of bubbles in the sound beam is much greater than one, 4) the average distance between the bubbles is much greater than their size and 5) the forward scatter contribution is negligible. For a small volume element in the acoustic beam (Figure 3-2), the decrease in power, dP , over a distance dx on the surface dS is given by:

$$dP(x) = -dI(x)dS = -n\Sigma_e I(x)dSdx \quad [\text{III-10}]$$

Integrating the decrement in power over x from 0 to the thickness d of the cavity, results in:

$$\frac{I(d)}{I(0)} = \exp(-n\Sigma_e d) \quad [\text{III-11}]$$

- $I(d)$ = intensity of the acoustic field after the cavity
- $I(0)$ = incident intensity
- n = particle concentration
- Σ_e = extinction cross-section
- d = distance travelled through the bubble cavity

Note that for a given extinction cross-section, the ratio $I(d)/I(0)$ is determined by only the concentration and the thickness of the cavity. Two measurements need be carried out: a reference measurement without bubbles resulting in an intensity $I_1(d)/I(0)$, and a measurement with bubbles resulting in a measured intensity $I_2(d)/I(0)$. The quotient of these two is predicted by equation [III-11].

Simulation studies

The presence of a shell around a bubble results in an increase in the resonance frequency compared to that for an ideal bubble. This is caused by the stiffness of the shell which decreases the total compressibility. It is shown in equation [III-9] that $E \cdot t_w / (1 - \nu)$ is the determinant factor for this change in compressibility and is referred to in this article as the shell elasticity parameter. A value of zero for this parameter means that there is no contribution of the shell or that there is no shell present. Measurements, described later in this article, on Albunex[®] microspheres show that the value of this shell parameter is about 10 Nm^{-1} . In the simulation studies it is assumed that the damping parameters do not change by the addition of a shell. The exact damping coefficient as given in equation [III-4] and described by Anderson¹ and Medwin⁷ have been used. The surface tension is set to zero, except when calculations without the shell are performed. In this case the surface tension value of the water-gas transition is taken. The simulation studies are all carried out for a bubble in water. The resonance frequencies for several bubble diameters (range 1 to 20 μm) and shell parameters (range 0 to 20), are listed in Table III-a. The data in this table shows that an increase in bubble diameter results in a decrease in the resonance frequency and that the addition of the shell results in an increase in the calculated resonance frequency. Furthermore, it is shown that for diagnostic frequencies (2 - 7.5 MHz) and for bubbles without a shell the interesting bubble diameters range from ~1 to 5 μm , while this shifts clearly towards higher diameters for higher values of the shell parameter, i.e. for a shell parameter value of 10 the interesting bubble diameters range ~4 to 10 μm .

The predicted scattering cross-section as a function of frequency for a single bubble with a diameter of 6 μm , for several values of the shell parameter, is shown in Figure 3-3.

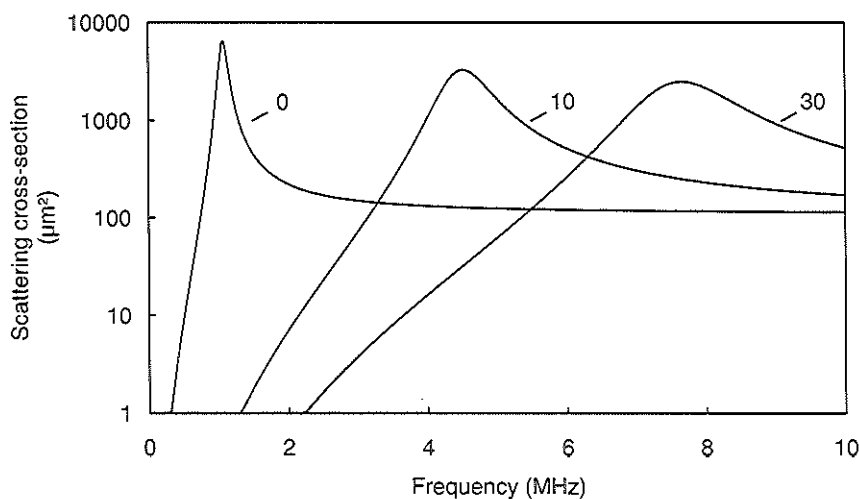


Figure 3-3 Theoretical scattering cross-section as a function of frequency for three different values of the shell parameter: 0; 10; 30. The simulations are performed assuming a bubble with a diameter of $6\ \mu\text{m}$ in water.

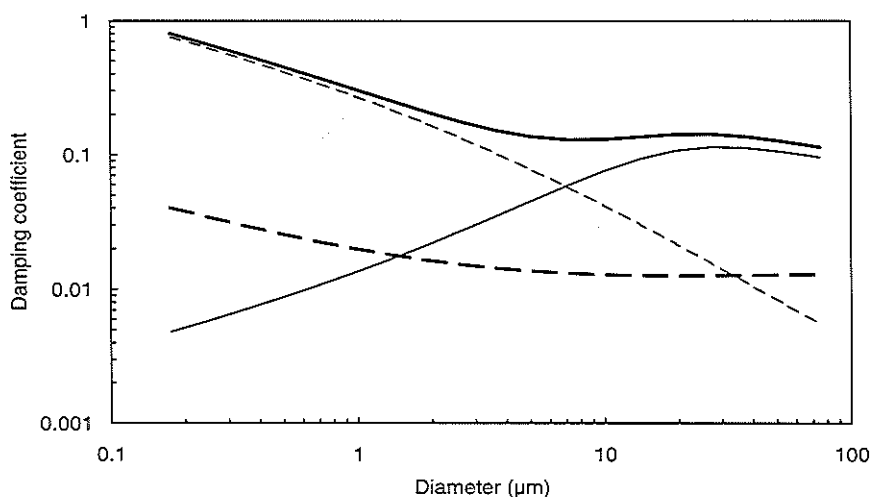


Figure 3-4 Damping coefficients for air bubbles in water as function of the diameter, calculated at their resonance frequency. \circ —, total damping; —, damping due to thermal conduction; — —, damping due to the viscosity of the surrounding liquid; \cdots , damping due to re-radiation.

Table III-a Resonance frequency in MHz for different values of the shell elasticity parameter, S_p , and bubble diameter.

bubble diameter (μm)	S_p			
	0	5	10	20
1	9.5	45.4	64.0	90.3
3	2.4	8.9	12.4	17.5
5	1.3	4.2	5.9	8.2
8	0.8	2.1	2.9	4.1
10	0.6	1.5	2.1	2.9
20	0.3	0.6	0.8	1.1

It is clear from this figure that the greater the shell parameter the higher the resonance frequency. All the curves demonstrate the well known fourth power relationship at low frequencies¹³, while at high frequencies the scattering cross-section is equal to the geometrical cross-section. The maximum value of the scattering cross-section decreases for higher values of the shell parameter.

The variation of the different damping parameters as a function of the diameter, calculated at the resonance frequency is shown in Figure 3-4. Several investigators have already examined this for the adiabatic case^{1,8,11}. Because of the implicit expression of the resonance frequency (equation [III-4]) and the different damping factors this must be solved numerically. Thermal damping clearly dominates for bubbles with a diameter larger than 10 μm , while for bubbles smaller than 5 μm diameter, damping due to fluid viscosity dominates. If surface tension is neglected, the re-radiation damping at resonance is constant with diameter and its magnitude is small compared to the thermal and viscous damping for bubbles in this size range. The minor increase for small values of diameter is due to the more important influence of the surface tension. The value of all these damping coefficients taken together is about 0.15, and there is little variation in this value for resonating bubbles with diameter between 4 and 50 μm .

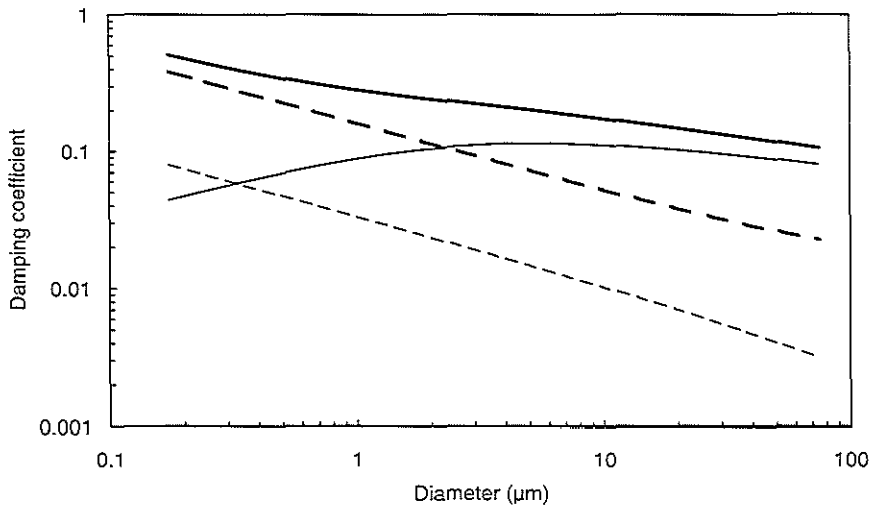


Figure 3-5 Damping coefficients for gas bubbles surrounded by an elastic shell in water with a shell parameter of 10, calculated at their resonance frequency as function of the radius. \blacksquare , total damping; —, damping due to thermal conduction; --, damping due to the viscosity of the surrounding liquid; \square , damping due to re-radiation

The relative contribution of the different damping coefficients at resonance as a function of bubble diameter for bubbles with a shell, where the shell parameter has a value of 10, is shown in Figure 3-5. The total damping for bubbles with a shell with a diameter between 1 and 15 μm is higher compared to those without a shell (compare to Figure 3-4). This is due principally to the higher resonance frequency for a given diameter. Re-radiation therefore becomes a more important factor together with the thermal damping for which the heat exchange approaches the adiabatic case at higher frequencies.

Experimental Procedure

Acoustic measurement set-up

The measurement set-up is illustrated in Figure 3-6. The transducer generates an acoustic field which traverses a bubble container with a beam width narrower than the bubble container. The acoustic beam is reflected at the back wall of the waterbath and is received by the same transducer. The bubble container measures 15 mm in length. The front and the backside consist of synthetic rubber to ensure a

minimal loss of acoustic energy, when the acoustic wave traverses.

Two measurements are carried out: first a reference measurement with the bubble container containing only the solution without microspheres, then a measurement with the bubble container filled with the microspheres to be investigated. A Fourier Transform is performed on the reflected pulses in order to obtain the frequency power spectrum. The transmission of the microspheres to be investigated is determined by normalizing the transmission spectrum with scatterers present to the transmission without scatterers. The final frequency spectrum is filtered using a moving window low-pass filter with a width of 200 kHz. The bubble container may be placed anywhere along the acoustic path. The bandwidth of the used transducers at the -20 dB level is about 100% of their central frequency. Using 5 transducers with different central frequencies it is possible to cover the frequency band from 700 kHz to 8.5 MHz. Such an array of transducers takes advantage of the very important fact that the measurement is not influenced by transducer characteristics such as focusing and aperture. In our study we used five transducers with the central frequencies of 1, 2.25, 3.5, 5, and 7.5 MHz.

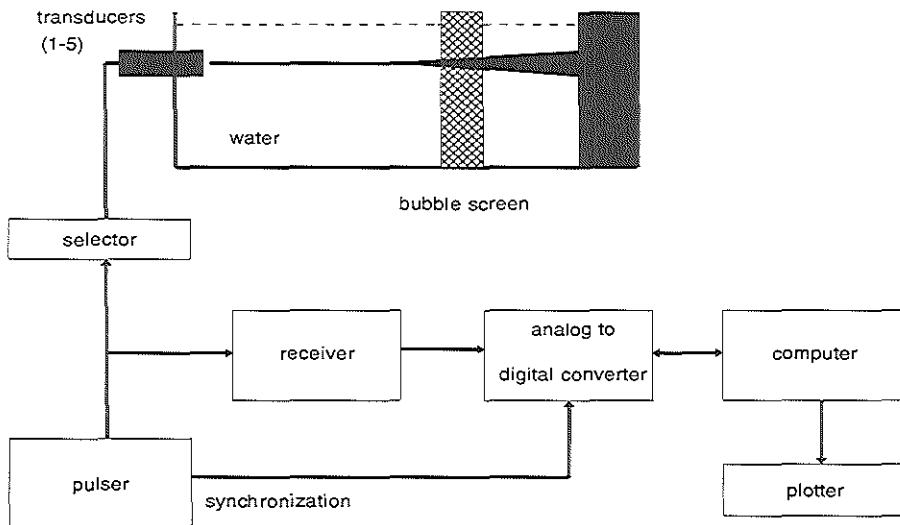


Figure 3-6 Schematic set-up for acoustic measurements.

The pulser (Avtech AVR-A-1-PW-C) generates a short pulse of a duration of 100 ns, which is transmitted to one of the five transducers (KB-Aerotech, Standard Medical Transducer). The reflected pulse from the back wall of the waterbath is received by

the same transducer, amplified by the receiver (Panametrics 5042 PR) and digitized by the analog to digital converter (LeCroy 9400 A). The digitized data are transferred to the computer (Compaq Deskpro 386/20e) for further analysis. Results can be plotted on the computer screen, a laser printer or a plotter.

Fractionation and determination of the size distribution

Albunex[®] has a rather wide size distribution. The size distribution of the batch (Nycomed AS, Oslo, Norway) used in this study is illustrated in Figure 3-7.

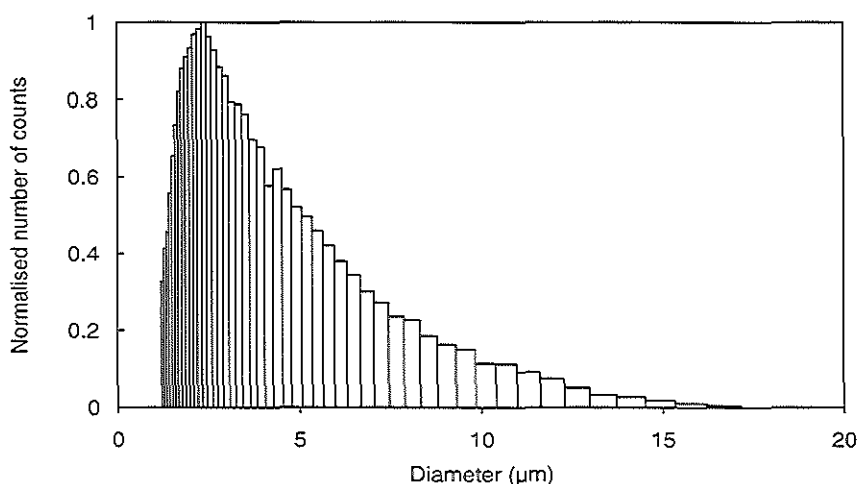


Figure 3-7 *Normalised size distribution of Albunex[®] as measured by the Coulter[®] Multisizer II.*

This distribution is measured with a Coulter Multisizer II (Coulter Electronics Ltd, Luton, England) with an aperture of 50 μm employing 64 channels with diameters ranging from 1 to 35 μm, and it is obtained after dilution of 20 μl Albunex[®] in 200 ml Isoton[®] (Isoton[®] is a particle free phosphate buffered saline with an added dispersant; Coulter Electronics Ltd, Luton, England). The mean diameter of this batch is 3.8 μm and the concentration before dilution $9 \cdot 10^8$ microspheres per ml. (In this study an experimental Albunex[®] production batch is used. This batch has a size distribution equal to that of the batches used for clinical trials, but with a somewhat higher concentration.) Less than 4% of the microspheres are larger than 10 μm, although there are microspheres present with a diameter greater than 15 μm.

Simulation studies show a large dependency in the scattering cross-section on the microsphere diameter. The scattering cross-section is also significantly dependent on the shell parameter. It is clear that precise and direct comparisons between experimental results and model studies are difficult without controlling some of these variables. Therefore, in order to estimate the resonance frequency and shell parameters from the measurements, multiple well-defined size distributions are required. One approach is to make multiple trial batches, each with a different size distribution, for which the variability in the shell parameter must be taken into account. Another possibility is to divide a single batch into specific size ranges and, as a first approximation, assume that the shell parameter is the same for all microspheres.

Several methods are available for generating a narrow size distribution. The flotation process takes advantage of the fact that the gas filled microspheres behave in a fluid according to Stoke's law. The velocity of the microspheres as they ascend the fluid column is a quadratic function of the radius of the microspheres. If the microspheres are released at the bottom of the tube, the distribution in size after a period of time will be a quadratic function of the height in the tube. The longer the time the sharper the border between the microspheres sizes. With this principle it should be possible to conduct the measurements at different levels, and to determine the acoustic response as a function of microsphere size.

It is also possible to fractionate the batch by using well defined mechanical filter which can provide a truncated size distribution. If the original Albunex[®] is filtered with such a mechanical filter, then the filtrate can be measured and compared with the acoustic results of other filtrates or with the whole distribution. In this way the acoustic contribution of the different microsphere sizes can be determined. Nuclepore[®] filters (Coster Corp., Cambridge, MA, USA) have been used in the present study as the pores in these polycarbonate membranes are strictly held to a tolerance range of 0% to - 20% of the rated pore size. The measured size distributions using filters of 3, 5, 8, and 10 μm is shown in Figure 3-8. It is remarkable that the number of microspheres for filtered and unfiltered samples below the rated pore size is practically identical. This means that very few microspheres are lost below the rated pore size and that there are hardly any microspheres present above it.

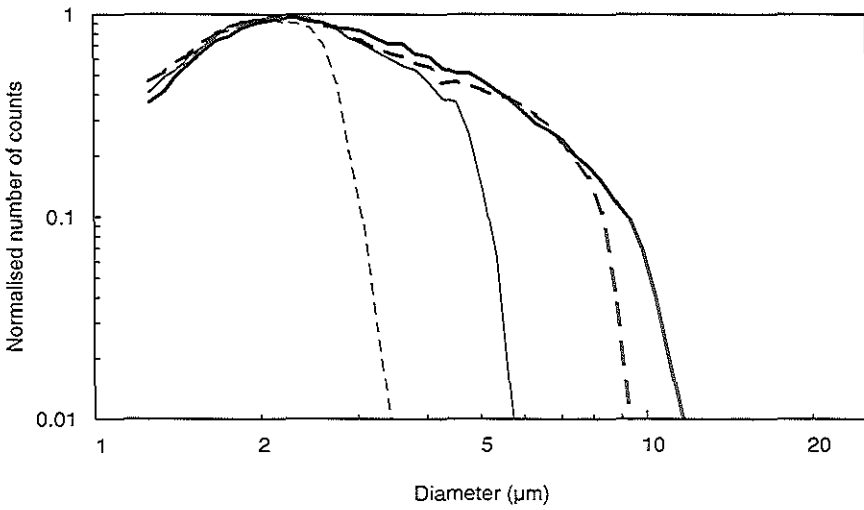

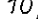
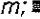



Figure 3-8 Size distribution of Albunex[®] passed through mechanical filters with the following pore sizes: , 10 µm; , 8 µm; , 5 µm and , 3 µm. The size distributions are measured by a Coulter[®] Multisizer II.

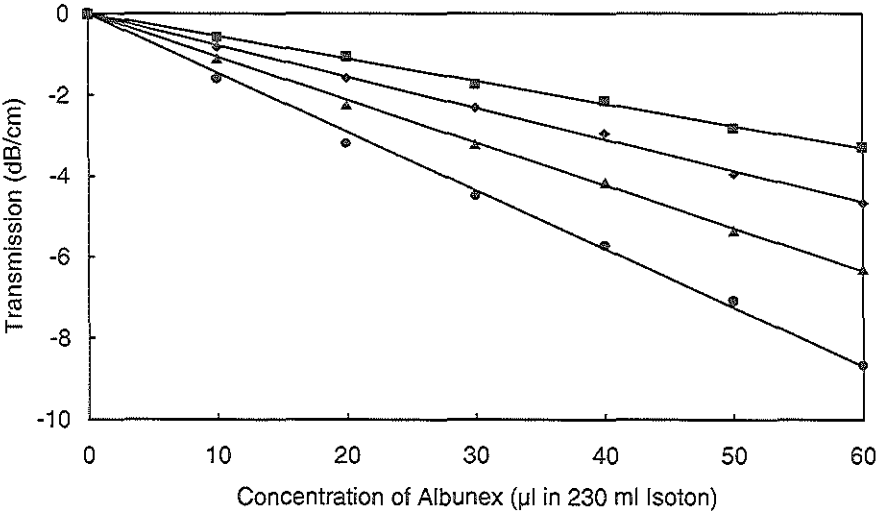


Figure 3-9 Transmission as function of Albunex[®] concentration at frequencies: (●) 2.3 MHz; (▲) 3.5 MHz; (◆) 5.0 MHz; (■) 7.5 MHz.

Results

Transmission as function of concentration

The acoustic transmission depends on the concentration of the Albunex[®] microspheres and the path length through the bubble container as shown in equation [III-11]. This equation also shows that the relationship between the transmission and concentration is linear when plotted on a logarithmic scale. The transmission as a function of the concentration, measured at the centre frequencies of the transducers used, 2.3, 3.5, 5.0 and 7.5 MHz, is shown in Figure 3-9. The transmission is expressed in dB cm⁻¹. The first measurement is performed with 10 µl of Albunex[®] diluted in 230 ml of Isoton[®]. The transmission at the above mentioned frequencies is then measured. Subsequently 10 µl of Albunex[®] is added and the transmission is determined again for the same frequencies. This procedure is repeated five times until the concentration is 60 µl Albunex[®] in 230 ml Isoton[®]. Linear regression is applied for each set of measurements. The slope relates to the extinction cross-section of Albunex[®]. The close fit to the straight lines indicates that virtually no microspheres disappeared during the measurements, and that the capacity to increase the Albunex[®] concentrations in this way is reproducible. The results show that the extinction cross-section is strongly frequency dependent. It is remarkable that higher frequencies are less attenuated than lower frequencies which is contrary to what is common in the diagnostic ultrasound field.

Transmission as function of frequency

Measurements of the transmission through a medium with microspheres as a function of frequency are shown in Figure 3-10 and Figure 3-11. These graphs depict the results of 5 transducers covering the band from 0.7 - 8.5 MHz. In Figure 3-10 a measurement is shown carried out with 55 µl unfiltered Albunex[®] diluted in 230 ml Isoton[®]. The agreement in the transmission at the overlapping frequencies of the different transducers confirms the independency on the transducer characteristics. The curve shows a minimum at 2.1 MHz. At lower frequencies a Rayleigh response appears, above 2.1 MHz the transmission increases and eventually seems to approach a constant value. The calculated theoretical curve is shown together with the measurements. The simulation is calculated from the size distribution as measured with the Coulter counter and according to equations [III-11] and [III-1]-[III-6]. Acoustic measurements and the measurement of the size distribution are performed on the same sample. Optimizing with respect to the frequency at which the minimal transmission occurs gives a shell parameter value of 9.5 ± 0.5 .

Results of acoustic measurements on filtered Albunex[®] are shown in Figure 3-11. The filtrates are obtained after passing Albunex[®] (55 μ l in 230 ml Isoton[®]) through Nuclepore[®] filters with pore diameters of 3, 5, 8 and 10 μ m respectively. The data in Figure 3-10 and Figure 3-11 show that although the number of microspheres with a diameter larger than 10 μ m is relatively small, they contribute significantly to the attenuation at frequencies between 1 and 4 MHz. On the other hand, microspheres with a diameter below 3 μ m, which dominate in number, contribute little to the attenuation of the whole Albunex[®] sample. The frequency at which the minimum transmission occurs increases as the larger microspheres are eliminated from the filtrate.

The relative contributions to transmission for the different microsphere diameters are obtained from the measurements of the filtered Albunex[®]. These are shown in Figure 3-12. The transmission is plotted as a function of the frequency for microspheres with diameters between 8 and 10 μ m, 5 and 8 μ m, 3 and 5 μ m and smaller than 3 μ m. The average value is taken for the transmission value for the overlapping frequency of the "adjacent" transducers. A smoothing filter is applied on the data (moving window low-pass filter with a bandwidth of 200 kHz). The theoretical curves, also shown in Figure 3-12, are determined, using the size distribution measured by the Coulter counter. The acoustic measurements and the measurements of the size distribution of the filtrates are performed on the same sample using the same procedure as for non-filtered Albunex[®]. The size distributions of such filtered Albunex[®] are shown in Figure 3-8.

A value 9.5 for the shell parameter is taken in the simulations. The measured and computed transmission curves show a similar pattern for all size ranges. The discrepancy in the curves of the 3-5 μ m range at low frequencies may be explained by the presence of a number of microspheres with different shell properties. The contribution of microspheres smaller than 3 μ m is very small in this frequency range, which is in agreement with the simulations. In general the simulated curves predict

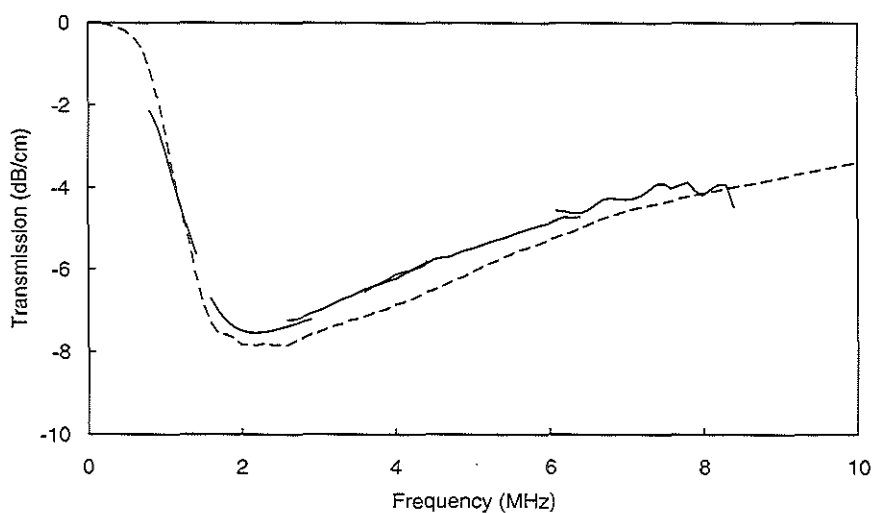


Figure 3-10 Transmission vs. frequency. —, measured spectrum obtained after dilution of 55 μ l in 230 ml. - -, simulated spectrum obtained with measured size distribution (Figure 3-7) and shell parameter value of 9.5.

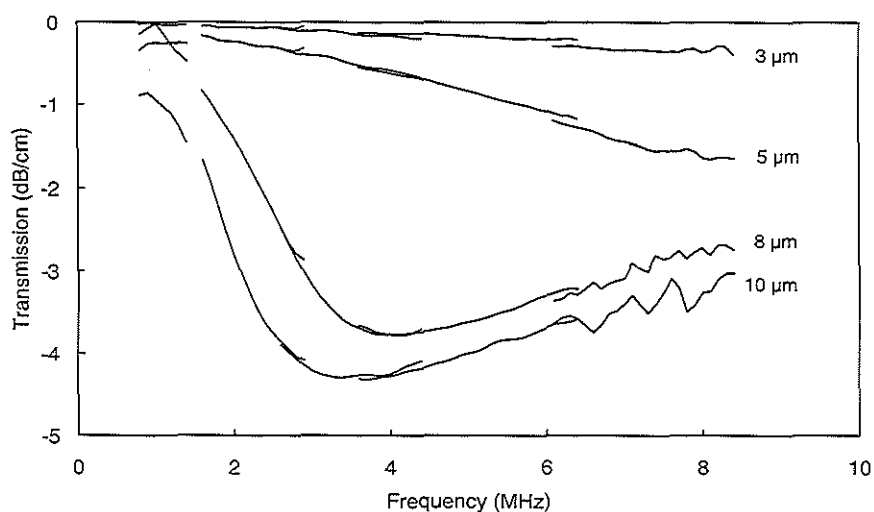


Figure 3-11 Transmission vs. frequency for samples containing filtered Alunex^R. 55 μ l Alunex^R is diluted in 230 ml Isoton^R. These dilutions are filtered through filters of 10, 8, 5 and 3 μ m.

at and around the resonant frequency a lower value of the transmission than measured. Furthermore, the simulated curves are somewhat narrower than the measured ones. This can have several explanations. First the assumption, made in the simulations, that the shell parameter is constant for all microspheres may not be entirely valid even for different microspheres with the same diameter. A distribution in the value of the shell parameter causes a broadening of the curve together with an increase in the value of the transmission. Second, no parameter has been included in the model to express the friction in the bubble shell. This missing factor should increase the total damping and thus give an increase in the transmission together with a broadening of the curve.

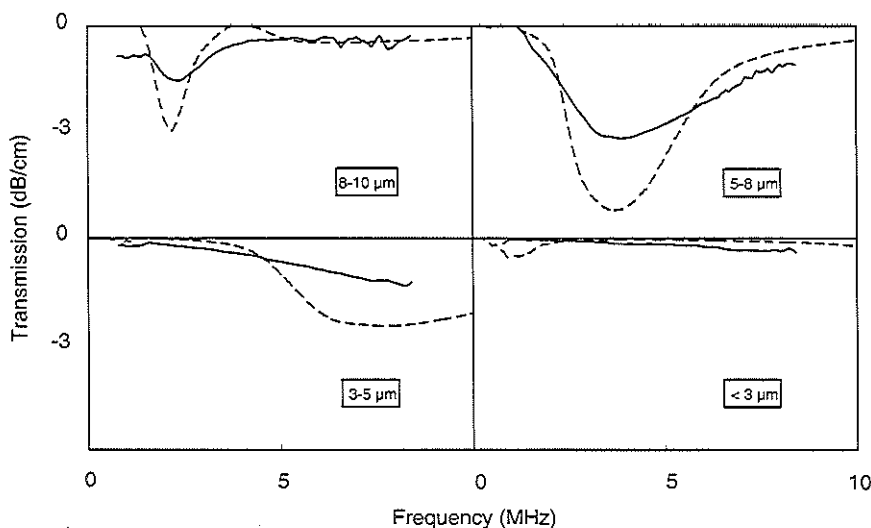


Figure 3-12 Simulation studies (---) and measurements (—) of the transmission vs. frequency for different bubble size ranges.

Discussion and Conclusion

The value of the shell parameter is the determinant factor for the behaviour of the shell. This parameter is determined by the physical parameters as mentioned in equation [III-9]. The optimal value of the shell parameter is found to be 9.5. Other studies have shown that the shell thickness is in the order of 20 - 25 nm. Assuming

that the Poisson ratio is 0.5, the elasticity of the shell works out to about $2 \times 10^8 \text{ Nm}^{-2}$. This is higher than the elasticity of a soft materials such as rubber ($0.01\text{--}1 \times 10^8 \text{ Nm}^{-2}$) and comparable with a synthetic material like Polyethylene¹⁴.

Although electron microscopic pictures taken with freeze edging techniques show a very homogenous inner surface of the Albunex[®] microspheres (H. Kryvi, University of Bergen, Norway, personal communication), one could not expect a shell configuration consisting of at most a layer of 6 molecules of a large protein to result in a completely homogenous shell with identical elastic properties for all microspheres. Hence the assumption of a homogeneous shell with simple elastic properties is very doubtful. It is clear that the model developed for the Albunex[®] microsphere is too simple to be completely correct. The results are nevertheless promising and show a reasonably good agreement between theory and measurements, as shown in the measurements and simulations on whole Albunex[®] in Figure 3-10.

The results shown in Figure 3-12 indicate that the optimal value for the shell parameter is almost independent of microsphere size for microspheres with a diameter larger than $5 \mu\text{m}$. Fine tuning of the shell parameter for the different size ranges, with the criterion of the minimum value of the transmission occurring at the same frequency, results in values which deviate no more than 20%. However, for microspheres with a diameter less than $3 \mu\text{m}$ this is not easily performed because of the low signal response. For the $3\text{--}5 \mu\text{m}$ range there is a tendency, for smaller values of the shell parameter to result in closer agreement with the measurements. These differences may be due to a variation in shell thickness and/or shell stiffness. Differences in shell properties with microsphere size could be a direct result of the production process.

It is evident from Table III-a that at frequencies used for medical diagnosis (2-7.5 MHz) and for a shell parameter value of 10, the most useful microsphere sizes range between 3 and $10 \mu\text{m}$. Figure 3-5 shows that the loss of acoustic energy in this range, calculated at the resonance frequency, is mainly caused by absorption, i.e. the extinction cross-section divided by the scattering cross-section, $\delta/\delta_{\text{rad}}$, is about 3. As thermal damping is the principal mechanism the loss of energy caused by microspheres, it is not greatly influenced by fluid parameters such as viscosity and density.

Table III-b Sum of backscatter and absorption contribution in dB cm⁻¹ for a dilution of 1:1000.

Frequency (MHz)	Diameter (μm)			
	0 - 3	3 - 5	5 - 8	8 - 10
1.0	0.1	1.0	1.0	3.8
2.5	0.3	1.0	8.3	6.2
3.5	0.5	1.6	13.1	2.8
5.0	0.7	2.8	11.6	1.6
7.5	1.5	5.0	5.5	1.7

The results with filtered microspheres show that only microspheres smaller than the filter pore size pass through the filter, and that hardly any microspheres are lost during this process. The clinical significance of these results depends on the area of application. Assuming that the filtering function performed by the lung capillaries is similar to mechanical filtration, the size of microspheres appearing in the left ventricle after intravenous injection are limited by the size of the lung capillaries. These capillaries have a mean diameter of around 7 μm which would not let pass the larger microspheres.

Although measurements of the transmission most directly relate to the extinction cross-section and the clinical use until now is based mainly on the backscatter properties of contrast agents, it is possible nevertheless to draw some conclusions from these measurements which are relevant to the clinical situation. The backscatter maximum should occur around the same frequency as the maximum of the extinction cross-section (equations [III-2],[III-5],[III-6]), although the backscatter will be far more influenced by the parameters of the surrounding fluid. In Table III-b the sum of backscatter and absorption is given for different frequencies and size ranges. The values in this table are expressed in dB/cm. The measurements are carried out for a concentration of 55 μl in 230 ml, in the table the values are recalculated for a dilution of 1:1000. The table shows that microspheres with diameter below 3 μm contribute little to the backscatter and absorption at frequencies used in medical diagnosis (2 - 7.5 MHz). The contribution from the microspheres with diameters in the range 3 to 5 μm is rather small as well, but their contribution increases for higher frequencies.

Microspheres in the diameter range 5 to 8 μm are the main source of backscatter and absorption in the frequency range 2 to 7 MHz, their spectra showing a maximum around 3.5 MHz, while microspheres with diameters between 8 and 10 μm give a strong contribution between 1 and 3 MHz, showing a maximum around 2.5 MHz. The fact that the microspheres with diameters between 5 and 8 μm give a higher contribution to the total backscatter and absorption than those with diameters between 8 and 10 can be explained from the size distribution of Albunex[®]. From the values given in the table, the conclusion can be drawn that for a 2.5 MHz diagnostic frequency the microspheres with a diameter between 5-10 μm provide a maximum in the sum of backscatter and absorption. At 3.5 and 5 MHz the main contribution comes from microspheres with a diameter between 5 and 8 μm , while the range shifts slowly towards 3-5 μm at 7.5 MHz. Microspheres with diameters larger than 8 μm may not be able to pass through the lung circulation when Albunex[®] is given intravenously. Thus, in this case the microspheres with diameters between 5 and 8 μm would be expected to be the main source of the backscatter and absorption in the left ventricle.

The acoustic response can be fairly accurately predicted from the measured size distribution of Albunex[®]. The simulation studies however show a consistently higher attenuation than measured. Improvements of the model of the Albunex[®] microspheres can be made by including the friction of the shell and by assuming a variable value of shell parameter as function of the diameter. These effects would lead to a broadening of the transmission curves as a function of the frequency and to an increase in the value of the transmission.

References

1. Anderson, A.L. and Hampton, L.D. Acoustics of gas-bearing sediments: 1. background. *Journal of the Acoustical Society of America* (1980) 67(6) 1865-1889
2. Prosperetti, A. Acoustic cavitation series part two: bubble phenomena: in sound fields: part one. *Ultrasonics* (1984) 22(2) 69-76
3. Meltzer, R.S. Tickner, E.G. Popp, R.L. and Roelandt, J. The source of echographic contrast in: *Contrast Echocardiography* (eds Meltzer, R.S. and Roelandt, J.) Martinus Nyhoff Publishers, The Hague, The Netherlands (1982) 7-16
4. Epstein, P.S. and Plesset, M.S. On the stability of gas bubbles in liquid- gas solution. *J. Chem. Phys.* 1950 18(11) 1505-1509
5. De Jong, N. Ten Cate, F.J. Lancée, C.T. Roelandt, J.R.C.T. and Bom, N. Principles and recent developments in ultrasound contrast agents. *Ultrasonics* (1991) 29(4) 324-330.

6. Feinstein, S.B. New developments in ultrasonic contrast techniques: Transpulmonary passage of contrast agent and diagnostic implications. *Echocardiography* (1989) 6(1) 27-33
7. Medwin, H. Counting bubbles acoustically: a review. *Ultrasonics* (1977) 15(1) 7-13
8. Reismann, H. and Pawlik, P.S. *Elasticity: Theory and Application*. John Wiley & Sons Inc., New York, USA (1980) Ch 5, 153-158
9. Coackly, W.T. and Nyborg, L.N. *Cavitation: Dynamics of gas bubbles: Applications in: Ultrasound: It's applications in medicine and biology: part one* (ed Frey, F.J.) Elsevier Scientific Publishing Company, New York-Oxford-Amsterdam (1978) Ch II 77-159
10. Fox, F.E. and Herzfeld, K.F. Gas bubbles with organic skin as cavitation nuclei. *Journal of the Acoustical Society of America* (1954) 26(6) 984-989
11. Devin, C. Survey of thermal, radiation, and viscous damping of pulsating air bubbles in water. *Journal of the Acoustical Society of America* (1959) 31(12) 1654-1667
12. Eller, A.I. Damping constants of pulsating bubbles. *Journal of the Acoustical Society of America* (1970) 47(5 part 2) 1469-1470
13. Morse, P.M. and Ingard, K.U. *Theoretical Acoustics*. McGraw Hill, New York, USA (1968) 418-441
14. Seachtling, H. *Kunststoff-Taschenbuch*. Carl Hanser Verlag, München-Wien (1979) 16 and 470-471

IV

ULTRASOUND SCATTERING PROPERTIES OF ALBUNEX^R MICROSPHERES

Abstract

The ultrasound scattering properties of Albunex^R as a function of frequency, microsphere diameter, and concentration are investigated. The simplified model of the Albunex^R microspheres developed in chapter III, where the individual microspheres are considered as air bubbles surrounded by a thin elastic shell is extended by including the internal friction in the shell when the microsphere vibrates. Acoustic scattering and transmission is measured in the frequency range from 700 kHz to 12.5 MHz. The measured transmission is used to estimate the two parameters in the theoretical model: the shell elasticity parameter, S_p and the shell friction, S_f . Introduction of the shell friction into the model improves the agreement between theory and measurements. For the scattered power, differences between measured and calculated values lie within 3 dB. It is concluded that for the frequencies 2.5 and 5 MHz the microspheres with a diameter between 5 and 12 μm are preferred as these microspheres deliver the most significant contribution to the total scattered power and cause relatively little attenuation.

This chapter is based on a manuscript, which has been published:

Title :Ultrasound Scattering of Albunex^R microspheres

Authors :N. de Jong and L. Hoff

In :Ultrasonics 1993 31(3)

Introduction

The scattering properties including frequency dependence of small solid particles and cardiac tissue has long been an area of active investigation^{1,2,3}. The fact that the orientation of cardiac tissue and blood cells can affect their scattering properties has also been described by several investigators^{4,5,6,7}. Morse and Ingard⁸ have developed a theoretical description of the scatter intensity as a function of angle and frequency for rigid spheres. Gas bubbles with diameters small compared to the wavelength of the acoustic field scatter in a spherically symmetric manner. Since the scattering cross-section of such gas bubbles is considerably larger than that of rigid spheres of the same size and as they scatter omnidirectionally, their backscatter properties are easier to measure. The major disadvantage, however, is the rapid disappearance of free gas bubbles⁹. Contrast agents which overcome this size-persistence dilemma are now under evaluation in clinical trials. Examples of such agents include Albunex[®] (a registered trade mark of Molecular Biosystems, San Diego, California, USA) and Lechovist[®] (Schering AG, Berlin, Germany). Albunex[®], which is the subject of this study, consists of gas filled microspheres with an adequate longevity. The acoustic attenuation of this contrast agent has been described in chapter III and in a paper by De Jong et al.¹⁰, where a theoretical model for the acoustic properties of Albunex[®] microspheres is developed, considering the microspheres as air-bubbles surrounded by an elastic shell. Comparison of transmission measurements with predictions based on the model proved to be promising. The loss of transmission energy is assumed to be caused by scattering of acoustic energy from the microspheres, viscosity in the surrounding fluid and thermal conduction within the microspheres. The current use of ultrasound contrast agents is generally limited to re-radiation effects, i.e. it relies on the backscatter properties of these agents. The overall attenuation, to which the scattering contributes, is considered useless and therefore should be minimized. The scattering properties of Albunex[®] are investigated in this report, and the previously described model is extended and compared with acoustic measurements. The scattered intensity from a cloud of Albunex[®] microspheres is derived for focused ultrasound transducers, assuming a low concentration of scatterers. Normalization to the response of an ideal flat plate allows for the elimination of system dependent parameters such as the characteristics of the transducer and electronic circuitry. The model of the Albunex[®] microsphere described in chapter III is improved by incorporating energy absorption due to frictional forces inside the shell. The two parameters in the model, the shell elasticity parameter S_p and the shell friction S_f are estimated by fitting the transmission measurements to the calculations. Acoustic

measurements are performed using 4 transducers, focused at 75 mm. Both the backscatter and the transmission are measured at this focal distance. The transducers cover a range from 700 KHz to 12.5 MHz. The Albunex[®] microspheres are filtered mechanically to determine the contribution of the different microsphere sizes.

Theory

Scattering

The scattering properties of a single bubble are described by its scattering cross-section, $\Sigma_s(R, \omega)$, defined as:

$$\Sigma_s(R, \omega) = \frac{P_s(R, \omega)}{I_0(\omega)} \quad \text{[IV-1]}$$

- ω = angular frequency
- $P_s(R, \omega)$ = scattered power
- $I_0(\omega)$ = intensity of the incident acoustic field
- R = radius of the bubble
- ω = angular frequency

When the concentration of the scatterers is low, the scattered power is proportional to the number of scatterers⁸, N . The total scattering then becomes, according to equation [IV-1].

$$P_s(R, \omega) = N I_0(\omega) \Sigma_s(R, \omega) \quad \text{[IV-2]}$$

Consider a small volume element containing scatterers homogenously distributed with number concentration $n(R)$ and radii R , as shown in Figure 4-1. The scattered power from the volume element will be:

$$dP_{sv}(\omega) = I_0(\omega) dV \int_0^\infty n(R) \Sigma_s(R, \omega) dR \quad \text{[IV-3]}$$

which can be written as:

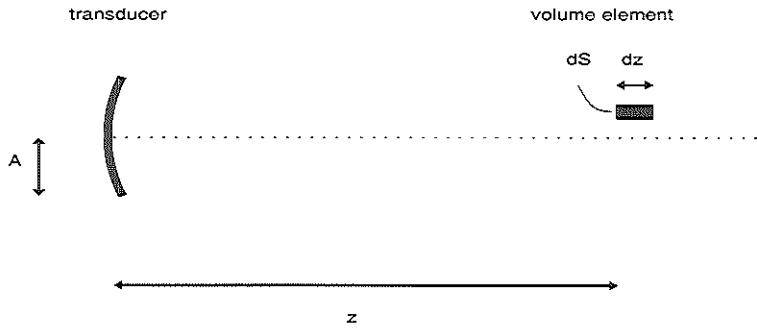


Figure 4-1 Transducer with small volume element with scatterers. A , radius of the transducer; z , focal distance of the transducer; dz , length of volume element; dS , area of volume element.

$$dP_{sv}(\omega) = I_0(\omega) dS dz \int_0^\infty n(R) \Sigma_s(R, \omega) dR \quad [\text{IV-4}]$$

- $dP_{sv}(\omega)$ = scattered power of the small volume element dV
 dS = cross-sectional area of volume element
 dz = length of volume element
 $I_0(\omega)$ = Incident intensity
 $n(R)$ = concentration of scatterers with radius R
 $\Sigma_s(R, \omega)$ = scattering cross-section of a scatterer with radius R
 R = radius of the scatterer
 ω = angular frequency.

Integrating over a surface normal to the acoustic beam delivers:

$$dP_s(\omega) = dz \iint_S I_0(\omega) dS \int_0^\infty n(R) \Sigma_s(R, \omega) dR \quad [\text{IV-5}]$$

The first integral of this equation denotes the total power, P_T , passing through surface S . The total scattered power then becomes:

$$\frac{dP_s(\omega)}{dz} = P_T \int_0^\infty n(R) \Sigma_s(R, \omega) dR \quad [\text{IV-6}]$$

For a focused transducer the total transmitted power, P_T , can be approximated by the reflected power of a perfect flat plate reflector in the focus of the transducer¹¹.

Scattered power measured with focused transducers

Equation [IV-6] gives the total scattered power over a small distance dz . As the microsphere diameters are much smaller than the wavelength of the acoustic field, their scatter is spherically symmetric. Having a low concentration, the scattered power from an ensemble of such scatterers, averaged over all configurations of scatterers within the volume-element, will also be spherically symmetric. The power received by the transducer with radius A at a distance z from the scattering volume in the far field is then:

$$P_R = \frac{A^2}{4z^2} P_s \quad [\text{IV-7}]$$

- P_R = power received by the transducer
- P_s = scattered power
- A = radius of the transducer
- z = distance from scattering volume to transducer.

For curved transducers equation [IV-7] holds for a scatter volume placed in focus, where the far field condition are valid.

The incident and the scattered power of the scatterers in the scatter volume, dV , are attenuated by the scatterers themselves. The amplitude of the time domain signal can be corrected for this attenuation according to:

$$A_{corr}(t) = A(t) 10^{\frac{\alpha(\omega)}{20} ct} \quad [\text{IV-8}]$$

- $A_{corr}(t)$ = corrected amplitude of the time domain signal
- $A(t)$ = measured amplitude of the time domain signal
- c = sound velocity
- t = time of flight in suspension with scatterers
- $\alpha(\omega)$ = attenuation at angular frequency ω , measured in dB per unit length.

Improving the Albunex[®] microsphere model

In chapter III a theoretical model is described for the acoustical properties of the Albunex[®] microsphere where the microsphere is considered as a gas bubble surrounded by a thin elastic shell. The increased restoring force due to the shell elasticity is taken into account by adding a shell elastic parameter. The shell elasticity parameter is defined in chapter III and its value is estimated 9.5 Nm^{-1} , delivering the best fit between measurements and calculations. This model provides a good prediction of the transmission through Albunex[®] although the agreement between theory and measurements was better for the larger microspheres than for the smaller ones. In the previously described model, the properties of the shell are considered independent of the microsphere diameter, and the internal friction, or viscosity, in the shell material is neglected. In order to further improve the agreement between theoretical calculations and measured acoustic properties, we now include the effect of internal friction in the microsphere shell. The properties of the shell are still considered uniform for all microspheres.

Internal friction, or viscosity, within the shell increases the damping of the microsphere oscillations. As shown in chapter III the restoring force due to the elasticity in the shell material can be written as: $F_s = k_1 \cdot dr$, where k_1 depends on the elastic properties of the shell material, but is independent of microsphere radius, and dr is the differential change in microsphere radius. Analogous to this, the damping force due to the friction within the shell will be of the form:

$$F_{fric} = -k_2 \frac{dr}{dt} \quad [\text{IV-9}]$$

F_{fric} = frictional force
 k_2 = parameter depending on viscous properties of the shell material, but independent of the microsphere radius
 dr/dt = radial velocity of the shell

According to Coackly¹² the damping coefficient can be derived from equation [IV-9] and results in:

$$\delta_f = \frac{S_f}{m\omega} \quad [\text{IV-10}]$$

δ_f = damping coefficient due the frictional damping within the shell
 S_f = shell friction parameter (is equal to k_2)

- ω = angular frequency of incident acoustic field
 m = effective mass of bubble-liquid system as defined by Coackley⁷². It is equal to $4\pi R^3 \rho$, where R is the radius of the bubble and ρ the density of the surrounding medium

The damping in the model as described in chapter III consists of three parts which are due to the thermal conduction within the bubble, the viscosity of the surrounding liquid and the re-radiation. In the improved model the frictional damping of equation [IV-10] is added to the total damping. The value of the shell friction, S_f must be determined from the measurements.

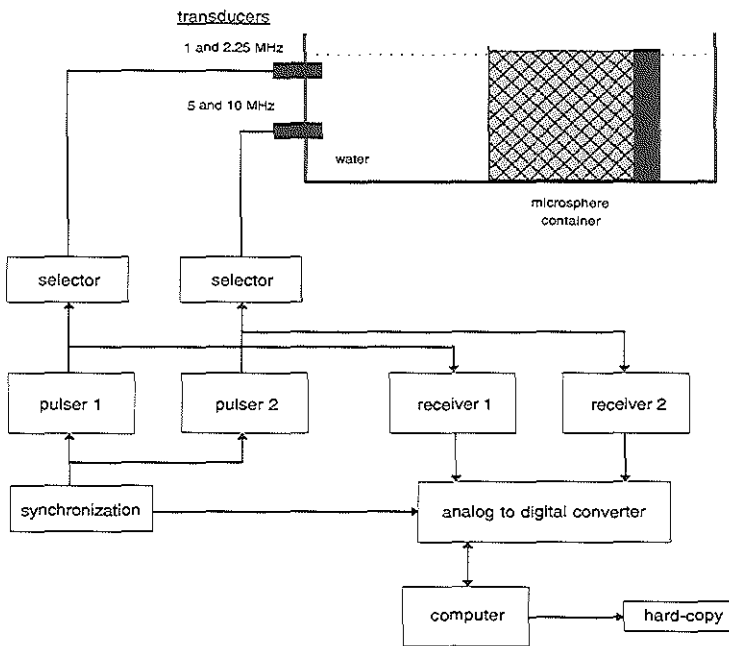


Figure 4-2 Schematic set-up of the apparatus for the acoustic measurements.

Experimental Procedure

Measurement set-up.

The measurement apparatus is illustrated in Figure 4-2. Four transducers with center frequencies of 1, 2.25, 5 and 10 MHz (Panametrics , videoscans) are mounted in a waterbath. The transducers are focused at a distance of 75 mm and their apertures

are 37, 25, 18 and 12 mm, respectively. The bandwidth of the transducers is about 100% of their central frequency at the -20 dB level. In this way it is possible to cover the frequency band from 750 kHz to 12.5 MHz. The electronic steering circuit consists of two sets; one for the 1 and 2.25 MHz and one for the 5 and 10 MHz transducers. Pulser 1 (Avtech avr-a-1-pw-c) generates a 125 ns pulse which is transmitted to the 1 or 2.25 MHz transducer. The signal received from either the back wall of the container or from the microspheres is amplified by receiver 1 (Panametrics 5052 PR). The amplified signal is then filtered with a low pass Chebychev filter, to remove noise and avoid aliasing, and digitized by the first channel of the A/D converter (digital oscilloscope, Lecroy 9400A). The 5 and 10 MHz transducers are directed by a pulser 2 (Avtech avl-2a-c-p), which generates a pulse of 35 ns width. The received signal from these transducers is amplified by receiver 2 (Panametrics 5052 PR). The amplified signal is low-pass filtered and digitized by the second channel of the analog to digital converter. The amplification of both receivers can be set between +40 dB to -40 dB in steps of 10 dB for an optimal signal amplitude. A separate function generator (Wavetek model 191) is used for controlling the repetition rate. Signals are recorded over a window length of 10 μ s, with a sample frequency of 50 MHz. The digitized signals are transferred to the computer (Compaq 386/20e) for further analysis.

The length of the microsphere container is 60 mm. The front of the container consists of 30 μ m thick synthetic material (TPX^R, Mitsui Petrochemical Industries, Ltd). The front has an angle of 15 degrees with the acoustic axis of the transducers to minimize multiple reflections. The back wall of the container is used as a reflector. For transmission measurements the container is placed such that the back wall is at the focal distance of the transducers, 75 mm. For backscatter measurements the container is located so that the front of the container is 70 mm from the transducers.

Measurement procedure

Albunex^R contains microspheres with a rather broad size distribution. To determine the influence of the different microsphere sizes, the microspheres are fractionated using the mechanical filtering method described in chapter III. The original Albunex^R microsphere suspension is filtered through Nuclepore^R filters (Coster Corp., Cambridge, MA, USA) with pore sizes 3, 5, 8 and 12 μ m. The size distribution of the sample after filtering is measured with a Coulter Multisizer II (Coulter Electronics Ltd, Luton, England) with an aperture of 50 μ m employing 64 channels with diameters ranging from 1 to 35 μ m. The mean diameter of the microspheres of the batch used in this study is 3.8 μ m and the concentration of 9×10^8 microspheres/ml before

dilution. (In this study an experimental Albunex[®] production batch is used. This batch has a size distribution equal to that of the batches used for clinical trials, but with a somewhat higher concentration).

First a reference measurement for all transducers is carried out with the microsphere container filled with pure Isoton[®] II and with the back wall of the container in focus of the transducers. After the reference measurements are recorded, either unfiltered or filtered Albunex[®] is introduced into the microsphere container and the transmission measurements are carried out with the back wall of the container positioned at focal distance. Then the container is repositioned and backscatter signals are recorded. The liquid is stirred immediately prior to measuring, so that it is circulating during the measurement sequence. Hence, problems with flotation are avoided, and the movement of the liquid ensures that the configuration of the microspheres in the liquid changes rapidly enough to achieve independent spectra from the time traces. The entire measurement procedure, for all transducers, takes about 2 minutes. After the acoustic measurements are finished, the microsphere container is placed in the Coulter Multisizer II to determine the microsphere concentration and size distribution. Fourier transformations are computed for all recorded time signals and averaged over 62 traces. The averaged power spectra of the measured backscatter or the transmission are normalized to the averaged power spectra of the reference measurement. The final result is smoothed using a moving window, with a width of 200 kHz, to remove rf noise.

Results

The magnitude of the measured backscatter signal depends on the radius of the transducer, the measuring distance, and the window length as expressed in equation [IV-6] and [IV-7]. The reference measurement, used for normalization is obtained with a PMMA (perspex) flat plate as reflector. The measured backscattered signal is normalized to the measured reference and corrected for the transducer aperture according to equation [IV-7], for the characteristics of the PMMA reflector and for the window length. The final result is expressed in dB cm⁻¹.

Scattered power vs. concentration

The measured scattered power as a function of the concentration is shown in Figure 4-3, for the 5 MHz transducer. The concentration of Albunex[®] is expressed as a volume (μl) of Albunex[®] diluted in 400 ml of Isoton[®]. The scattered power, averaged over the frequency range from 4 to 6 MHz, is expressed in dB cm⁻¹ and

measured over a distance of 3.75 mm in the Alburnex^R suspension. The measured values are shown together with the results corrected for the attenuation. The dotted line denotes a least square fit through these calculated values. The slope of this curve is 3.2 ± 0.2 dB cm⁻¹ per doubling in concentration. The theoretical value is a 3 dB increase for each doubling of the concentration. It is concluded that attenuation affects the results over the considered window length of 3.75 mm for concentration higher than 50 µl Alburnex^R in 400 ml Isoton^R, but when corrected the results do not differ much from the theoretical prediction even for concentrations as high as 1 ml Alburnex^R in 400 ml Isoton^R. This confirms the assumption that the scattered power is proportional to the concentration of microspheres.

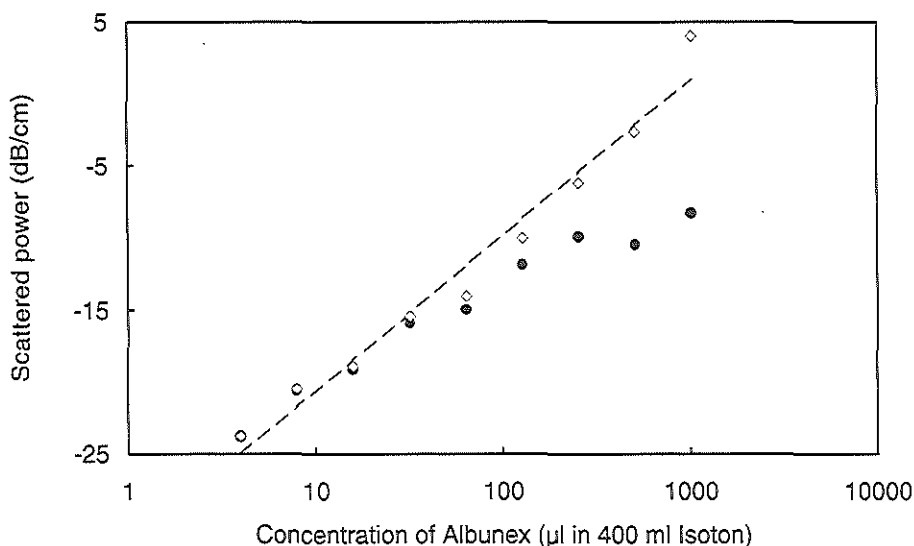


Figure 4-3 *Scattered power as a function of concentration of Alburnex^R microspheres measured with a 5 MHz. ●, measurement over a window length of 3.75 mm; ◊, corrected for attenuation; --, line fitted to the corrected values.*

Scattering and transmission as a function of frequency

Scattering and transmission are measured on samples of whole and of filtered Alburnex^R. The filters used have rated pore sizes of 12, 8, 5 and 3 µm. The concentration of each sample is chosen such that the attenuation occurring over the measuring length of 7.5 mm is lower than 2 dB cm⁻¹. The backscattered time signal is corrected according to equation [IV-8], using the measured attenuation. The used dilutions are: whole 1:20,000; 12 µm filter, 1:10,000; 8 µm filter, 1:10,000; 5 µm filter, 1:3500; 3 µm filter, 1:1400. After the acoustic measurements are performed,

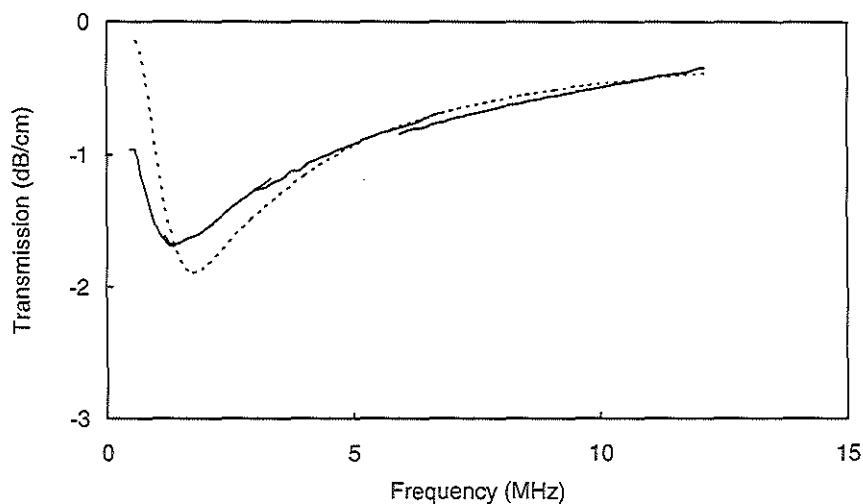


Figure 4-4 *Transmission vs. frequency. —, measured spectrum obtained after dilution of 35 μ l Albunex[®] in 700 ml Isoton[®]; - - -, simulated spectrum obtained with measured size distribution, a shell parameter of 8 Nm^{-1} and a shell friction of $4 \times 10^{-6} \text{ Nsm}^{-1}$.*

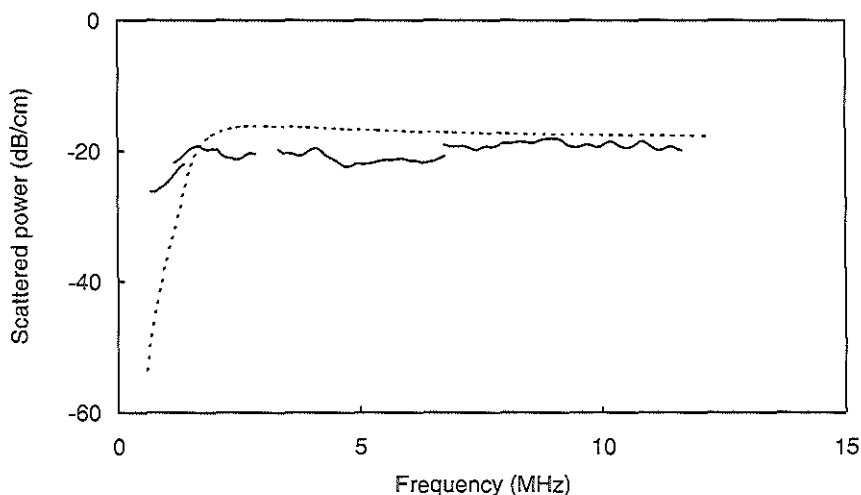


Figure 4-5 *Scattered power vs. frequency. —, measured spectrum obtained after dilution of 35 μ l Albunex[®] in 700 ml Isoton[®]; - - -, simulated spectrum obtained with measured size distribution, a shell parameter of 8 Nm^{-1} and a shell friction of $4 \times 10^{-6} \text{ Nsm}^{-1}$.*

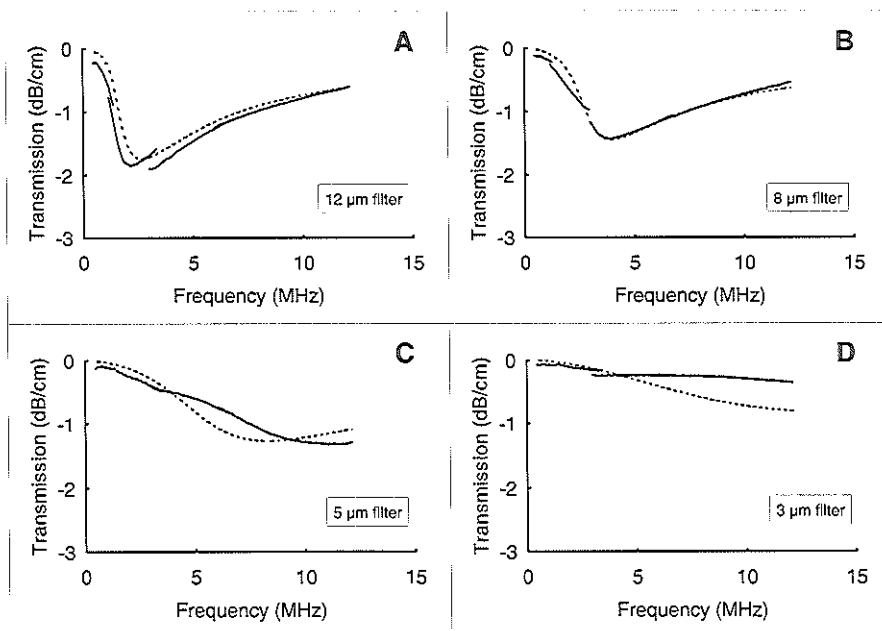


Figure 4-6 *Transmission vs. frequency for samples containing filtered Albumex^R. —, measured spectrum; - - -, simulated spectrum obtained with measured size distribution, a shell parameter value of 8 Nm^{-1} and a shell friction of $4 \times 10^{-6} \text{ Nsm}^{-1}$. A, $70 \mu\text{l}$ Albumex^R is diluted in 700 ml Isoton^R and filtered through a $12 \mu\text{m}$ filter; B, $70 \mu\text{l}$ Albumex^R is diluted in 700 ml Isoton^R and filtered through a $8 \mu\text{m}$ filter; C, $200 \mu\text{l}$ Albumex^R is diluted in 700 ml Isoton^R and filtered through a $5 \mu\text{m}$ filter; D, $500 \mu\text{l}$ Albumex^R is diluted in 700 ml Isoton^R and filtered through a $3 \mu\text{m}$ filter.*

the microsphere concentration and size distribution are measured on the same sample. This is used for calculating the theoretical values for both the transmission and the scattering, except for the transmission curve for whole Albumex^R, where the microsphere concentration and size distribution are determined separately. Two parameters have to be estimated in the model: the shell elasticity parameter, S_p and the shell friction S_f . These are estimated by fitting the theoretically calculated transmission results to the measurements, by minimizing the absolute difference between the two curves. This procedure results in an optimal value for the shell parameter, S_p , of 8 Nm^{-1} and an optimal value for the shell friction, S_f of $4 \times 10^{-6} \text{ Nsm}^{-1}$.

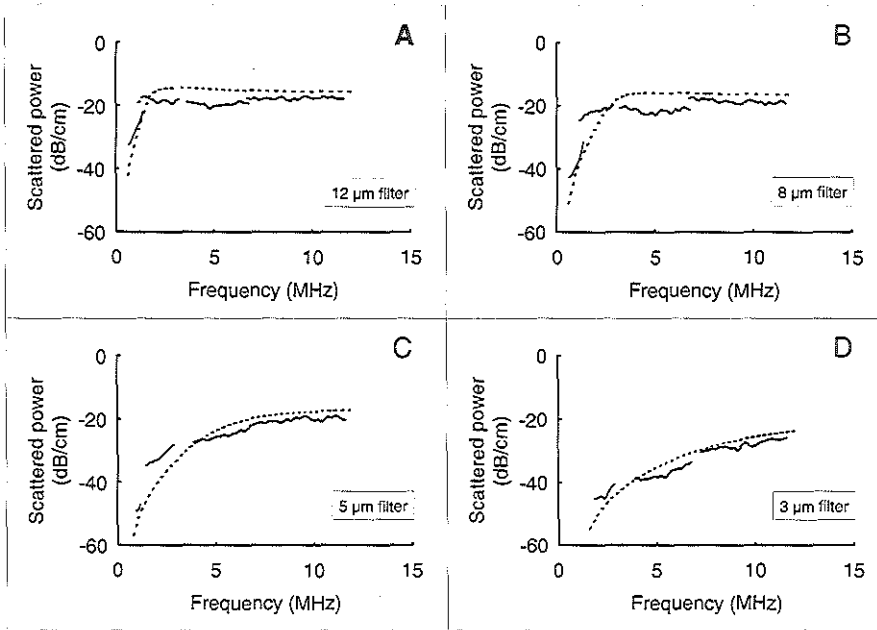


Figure 4-7 Transmission vs. frequency for samples containing filtered Alburnex[®]. —, measured spectrum; - - -, simulated spectrum obtained with measured size distribution, a shell parameter value of 8 Nm^{-1} and a shell friction of $4 \times 10^{-6} \text{ Nsm}^{-1}$; A, 70 μl Alburnex[®] is diluted in 700 ml Isoton[®] and filtered through a 12 μm filter; B, 70 μl Alburnex[®] is diluted in 700 ml Isoton[®] and filtered through a 8 μm filter; C, 200 μl Alburnex[®] is diluted in 700 ml Isoton[®] and filtered through a 5 μm filter; D, 500 μl Alburnex[®] is diluted in 700 ml Isoton[®] and filtered through a 3 μm filter.

The results of all the measurements and the simulations are shown in Figure 4-4, Figure 4-5, Figure 4-6 and Figure 4-7. In each figure the transmission or scattering as function of the frequency for the 4 transducers in their useful frequency range is shown, together with matching simulations.

The scattering and transmission results for whole Alburnex[®] are shown in Figure 4-4 and Figure 4-5. There is a clear minimum of the transmission at 1.5 MHz (Figure 4-4). The response calculated with the Alburnex[®] microsphere model, with a shell elasticity parameter of 8 Nm^{-1} and shell friction of $4 \times 10^{-6} \text{ Nsm}^{-1}$ shows the same pattern as the measurements. The total scattered power is virtually independent of the frequency in the range from 1.5 to 12.5 MHz (see Figure 4-5). For lower frequencies the scattered power increases with frequency. The calculated response

according to equation [IV-5] and [IV-6] is shown in Figure 4-5. The difference between the calculations and measurements is about 3 dB. The level of the scattered power is about -20 dB cm⁻¹ meaning that 1 % of the incident energy is scattered away.

The results obtained from filtered Alburnex[®] dilutions are shown in Figure 4-6 and Figure 4-7. Figure 4-6 contains all the transmission curves, while Figure 4-7 shows the scatter curves. The four panels in each figure denote the results for microspheres passing the Nuclepore[®] filters with pore sizes of 3, 5, 8 and 12 µm. A comparison of the panels in Figure 4-6 reveals that the frequency at which the minimum transmission occurs increases as the diameter decreases. No minimum could be detected in the frequency range from 750 kHz to 12.5 MHz for the microspheres smaller than 3 µm.

The measurements for scattered power, shown in Figure 4-7, indicate a constant response for the 12 µm microsphere at frequencies above 1.5 MHz. There is a clear decrease in scattered power for 8 µm microsphere at frequencies below 2 MHz, above this frequency the scattered power is independent of the frequency. For the curve of the 5 µm filtered microspheres there is a frequency dependency below 6 MHz, while for the 3 µm filtered microspheres there is a frequency dependency up to 12.5 MHz. The calculated curves shown in the figures are based on results from the size distribution measurement made after each set of recordings, using the model-parameters S_p equal to 8 Nm⁻¹ and S_f equal to 4x10⁻⁶ Nsm⁻¹. The agreement between measurements and theory is satisfactory.

Discussion and Conclusion

The model, reported in chapter III, for the acoustical behaviour of Alburnex[®] microspheres is far better at describing the behaviour of larger microspheres than smaller ones. Especially at higher frequencies, the predicted scattered power and attenuation are too high. By including the effect of a frictional loss in the shell into the model, it has been possible to improve the calculations of the acoustic scatter and attenuation of the smaller microspheres considerably. The values of the two parameters describing influences due to elastic and viscous properties of the shell are found by fitting the calculated acoustic transmission to the measurements, resulting in a shell elasticity parameter, S_p , equal to 8 Nm⁻¹ and a shell friction parameter, S_f , equal to 4x10⁻⁶ Nsm⁻¹. The same parameters result in a calculated scattered power, which is in good agreement with the scatter measurements.

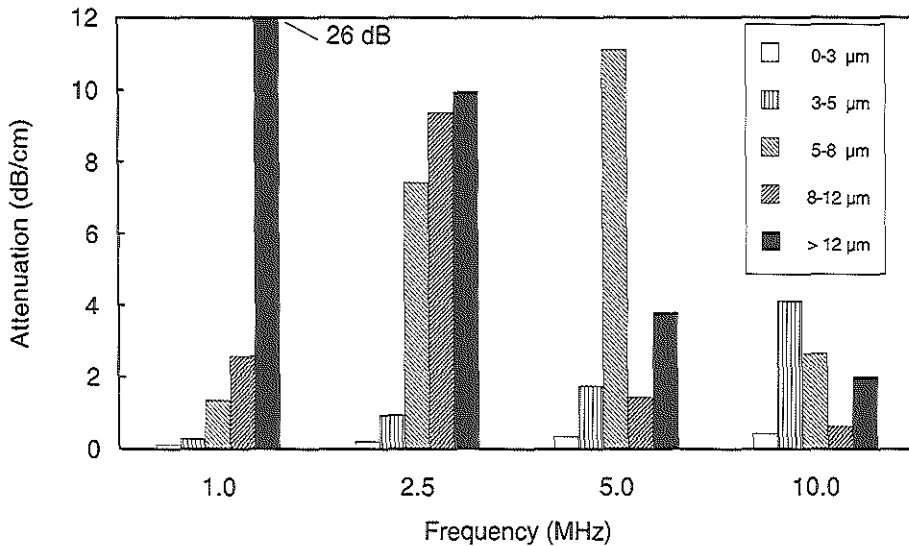


Figure 4-8 Attenuation for the frequencies of 1, 2.5, 5 and 10 MHz, Albunex[®] diluted 1:1000 and five microspheres size ranges.

The attenuation (the sum of scatter and absorbed power) is shown in the bar graph of Figure 4-8 for five size ranges, and at four frequencies (1, 2.5, 5.0, 10 MHz). The results are recalculated for a standardized dilution of 1:1000. At 1 MHz the larger microspheres dominate, especially the microspheres larger than 12 μm . For higher frequencies the relative contribution of the larger microspheres to the attenuation decreases. The figure indicates that microspheres smaller than 3 μm contribute relatively little to the attenuation for all frequencies studied.

In Figure 4-9 the scattered power normalised to the incident power is given for the same frequencies and for the same size ranges shown in Figure 4-8. The values are expressed for a standardised dilution of 1:1000, contributions smaller than -30 dB cm^{-1} are not shown. Microspheres with a diameter less than 3 μm only deliver a substantial scattered power for a frequency of 10 MHz. Microspheres with a diameter between 3-5 μm have a low contribution at a frequency of 2.5 MHz, but this increases for higher frequencies. The microspheres with diameters between 5-8 μm dominate for the frequencies 2.5, 5 and 10 MHz. Microspheres with a diameter larger than 8 μm deliver a substantial contribution at all frequencies.

The quotient of the scattered power and the attenuation is shown in Figure 4-10. When using the scattering properties of a contrast agent, it is desirable to keep the absorption as low as possible to avoid losing energy and shadowing biological structures. This means that one prefers a high value of the scatter to attenuation quotient. Microspheres smaller than 5 μm have a low quotient, and their scattered power is not high. For both 2.5 and 5 MHz and for both size ranges 5-8 μm and 8-12 μm the quotient is around 0.1, where for the lower frequency the smaller size range dominates and for the higher frequency the larger size range. For 10 MHz the values of the quotient increases to 0.4, but this still means that the absorption is 1.5 times the scattering. For frequencies between 2.5 and 5 MHz, which are often used in medical diagnosis, the absorption is around 10 times the scattering for microspheres with diameters between 5 and 8 μm .

The relatively large apertures of the transducers result in a significant phase difference between the edge and the centre of the transducer when receiving the backscattered signal. This can be as high as 90 degrees at the highest frequency and the largest apertures for a measuring depth of 7.5 mm. This effect results in differences of up to 2 dB in the received power. No corrections have been made to compensate for this effect. By using separate transducers for receiving and transmitting, phase differences can be reduced when receiving with a small aperture transducer, but this will influence the sensitivity of the system.

The theory for microsphere scattering demands a sparsely populated scatter volume. For a dilution of 1:10,000 the number of microspheres larger than 5 μm per mm^3 is about 20. For a frequency of 2.5 MHz this means 4, for 5 MHz 0.5 microspheres per cubic wavelength. The measurement of the integrated backscatter as a function of the concentrations shows that even for concentration at which an attenuation of 20-30 dB cm^{-1} occurs, the number of microspheres can be considered as low.

Frequencies between 2.5 and 5 MHz are frequently used for cardiac diagnosis. For these frequencies the scattered power divided by the attenuation is most optimal for microspheres with a diameter between 5 and 12 μm . Microspheres larger than 12 μm contribute relatively little to the total scattering, but they are responsible for a high attenuation. This can result in a shadowing of underlying heart structures. By removing these larger microspheres this shadowing can be reduced without weakening the scattering capabilities. The smaller microspheres (< 5 μm) do not contribute greatly to the backscatter either, but their attenuation is not a problem. Thus, from an acoustic standpoint there is little reason to remove these.

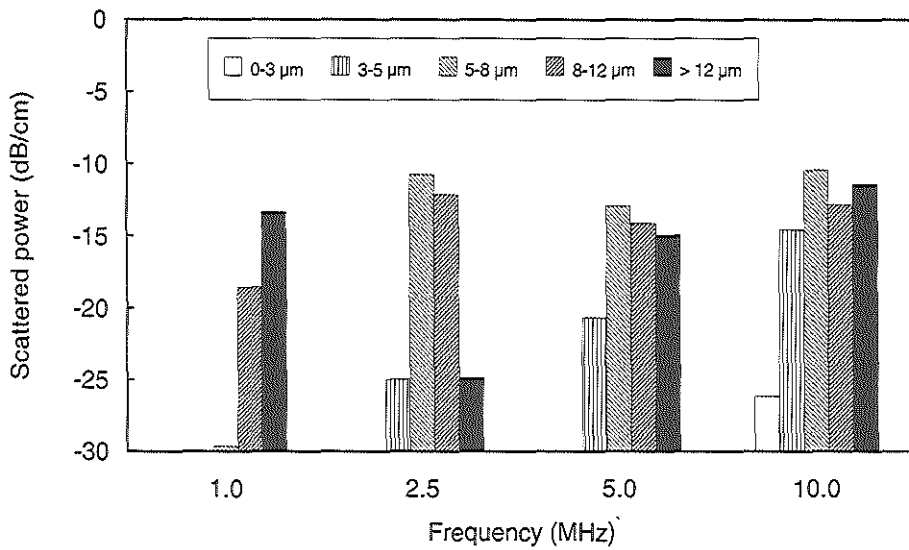


Figure 4-9 Scattered power normalized on the incident power for the frequencies 1, 2.5 5 and 10 MHz, Albunex[®] diluted 1:1000 and five microspheres size ranges.

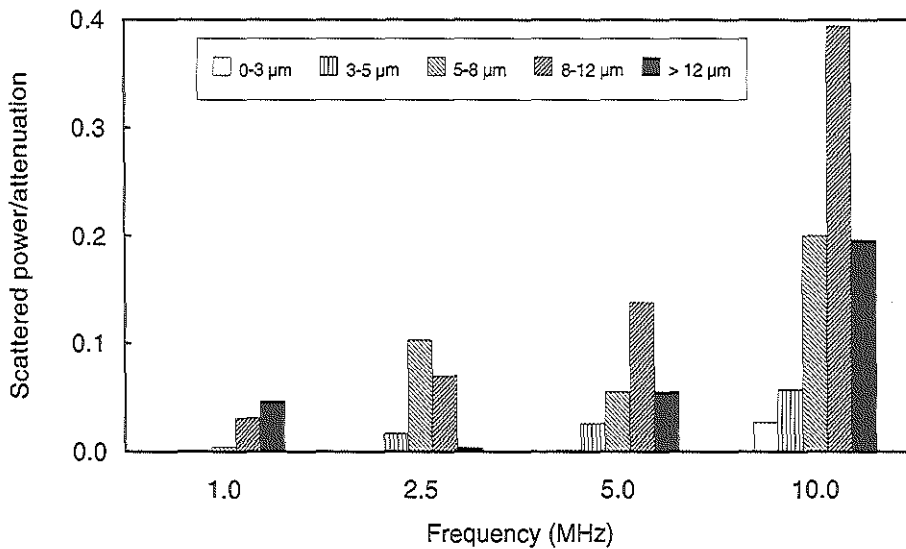


Figure 4-10 Scattered power of Albunex[®] divided by the attenuation for the frequencies 1, 2.5, 5 and 10 MHz, and five different microspheres size ranges.

When injecting Alburnex^R intravenously, it is assumed that all microspheres appear in the right ventricle, which will result in good scattering properties but also a high attenuation. The lung capillaries eliminate the microspheres with a diameter larger than about 8 μm . Therefore microspheres appearing in the left ventricle demonstrate ideal response properties, meaning good scattering properties and a low attenuation. When Alburnex^R is used as an intracoronary contrast agent, it is assumed that all the microspheres appear in the coronary system, which will deliver good scattering properties, but also a high attenuation.

References

1. Sleepe, G.E. and Lele, P.P. On estimating the number density of random scatterers from backscattered acoustic signals. *Ultrasound in Medicine and Biology* (1989) 14(8) 709-727
2. Shung, K.K., Sigelmann, R.A. and Reid, J.M. Scattering of Ultrasound by Blood. *IEEE transaction on biomedical engineering* (1976) 23(6) 460-467
3. Rijsterborgh, H., Mastik, F., Lancée, C.T., Sassen, L.M.A., Verdouw, P.D., Roelandt, J. and Bom, N. The relative contributions of myocardial wall thickness and ischemia to ultrasonic myocardial integrated backscatter during experimental ischemia. *Ultrasound in Medicine and Biology* (1991) 17(1) 41-48
4. Kroon de, M.G.M., Wal van der, L.F., Gussenhoven, W.J. and Bom, N. Angle dependent backscatter from the arterial wall. *Ultrasound in Medicine and Biology* (1991) 17(2) 121-126
5. Shung, K.K., Sigelmann, R.A. and Reid, J.M. Angular dependency of scattering of ultrasound by blood. *IEEE transaction on biomedical engineering* (1977) 24(4) 325-330
6. Campbell, J.A. and Waag, R.C. Ultrasonic scattering properties of three random media with implications for tissue characterization. *Journal of the Acoustical Society of America* (1984) 75(6) 1879-1886
7. Davros, W.J. and Madsen, E.L. Frequency-dependent angular scattering of ultrasound by tissue-mimicking materials and excised tissue. *Journal of the Acoustical Society of America* (1986) 80(1) 229-237
8. Morse, P.M. and Ingard, K.U. *Theoretical Acoustics*. McGraw Hill, New York, USA (1968) 418-441
9. Epstein, P.S. and Plesset, M.S. On the stability of gas bubbles in liquid- gas solution. *J Chem Phys* (1950) 18(11) 1505-1509
10. Jong de, N., Hoff, L., Skotland, T. and Bom, N. Absorption and scatter of encapsulated gas filled microspheres; Theoretical considerations and some measurements. *Ultrasonics* (1992) 15(2) 95-103
11. Lizzi, L., Greenebaum, M., Feleppa, E.J. and Elbaum, M. Theoretical framework for spectrum analysis in ultrasonic tissue characterization. *Journal of the Acoustical Society of America* (1983) 73(4) 1365-1373
12. Coackly, W.T. and Nyborg, L.N. *Cavitation: Dynamics of gas bubbles; Applications in: Ultrasound: It's applications in medicine and biology: part one* (ed Frey, F.J.) Elsevier Scientific Publishing Company, New York-Oxford-Amsterdam (1978) Ch II 77-159



Higher harmonics of vibrating gas filled microspheres

Abstract

The acoustic behaviour of an ideal gas bubble in water is considered and the equation of motion is extended to model an Albunex^R microsphere. Calculations reveal large differences in nonlinear behaviour between ideal gas bubbles and Albunex^R microspheres. Acoustic measurements on diluted Albunex^R at two driving frequencies (1 and 2 MHz) are reported which show that the level of the second harmonic response is about 20 decibels below the first harmonic at an acoustic pressure amplitude of 50 kPascal. It is demonstrated that, under controlled conditions, it is possible to discriminate between Albunex^R and other scattering/reflecting objects using the nonlinear behaviour of the microspheres.

This chapter is based on a manuscript, which has been submitted for publication:

Title : Higher harmonics of vibrating gas filled microspheres

Authors : N. de Jong, R. Cornet and C.T. Lancée

Introduction

The first theoretical description of the behaviour of bubbles exposed to an external pressure field was developed by Lord Rayleigh in 1917 and is still useful today although much has been done in the last forty years to extend this knowledge. In 1950 Noltingk and Neppiras³ developed a theoretical description of the behaviour of gas bubbles exposed to an acoustic field including some aspects of collapsing bubbles, while in 1959 Devin⁴ thoroughly surveyed the fundamental processes by which pulsating bubbles dissipate their energy. A linear approach describing the phenomenon of resonating bubbles in a sound field was provided by Medwin⁵ in 1977. Analysis of the nonlinear process however, is crucial to understanding the higher harmonic phenomena and this did not occur until 1968. Tucker⁶ suggested that the presence of second harmonic echoes, which is solely due to the nonlinear behaviour of bubbles, is very sensitive indicator for the presence of bubbles. One year later Welsby⁷ developed an analytical method for describing the first as well as the second harmonic of bubble vibration. As the mathematical solution to the nonlinear equation is virtually intractable over the entire frequency and bubble size range, Lauterborn⁸ in 1976, resorted to numerical techniques to describe the near resonance behaviour of gas bubbles. The analysis was limited to a simplified model taking into account only viscous damping.

Experimental work has paralleled the development of the analytical models. The ultrasonic detection of resonant cavitation bubbles in a flow tube by their second harmonic emission was reported by Miller⁹ in 1981. The experimental results obtained for bubbles of 4 μm diameter agreed well with the theory, which was similar to the analytical derivation given by Welsby. Eatock et al.¹⁰, using a numerical approach, studied the magnitude of the nonlinear effect in the scattering of ultrasound by nitrogen bubbles in water for ultrasonic frequencies and amplitudes typical for diagnostic medical devices. They were interested in possible bubble detection in blood or tissue for application in decompression research. This analysis included all the damping mechanisms (viscous, thermal and reradiation) as well as the polytropic exponent. They concluded that the application of the nonlinear effect to the detection of bubbles would be limited to bubbles with radii smaller than 10 μm .

Albunex[®] is a registered trademark of Molecular Biosystem, San Diego, USA and is used for this study. The second harmonic behaviour of another contrast agent, SHU 508 (a registered trade mark of Schering, Berlin, Germany) has been described by

Schrope¹¹. The equation of motion as given by Eatock¹⁰ is investigated for gas bubbles, and several examples in the medical diagnostic frequency range 1-10 MHz are demonstrated. The equation is extended for Albunex^R, which is considered as a suspension of encapsulated gas filled microspheres. Several simulations are presented which show that the nonlinear behaviour of Albunex^R is actually less than that of ideal gas bubbles. The influence of the size distribution of Albunex^R is also investigated. The theoretical computations are compared with acoustic measurements. Further it is demonstrated that it is possible to discriminate between Albunex^R and other scattering/reflecting objects using the nonlinear behaviour of the microspheres.

About Albunex^R

Albunex consists of microspheres of encapsulated gas surrounded by a shell of human serum albumin. The mean diameter of the microspheres is about 4 μm , whereas the shell thickness is in the range of 15 - 20 nm. The mechanical properties of the shell pertinent for the ultrasonic studies are described in chapter III and IV and by De Jong¹².

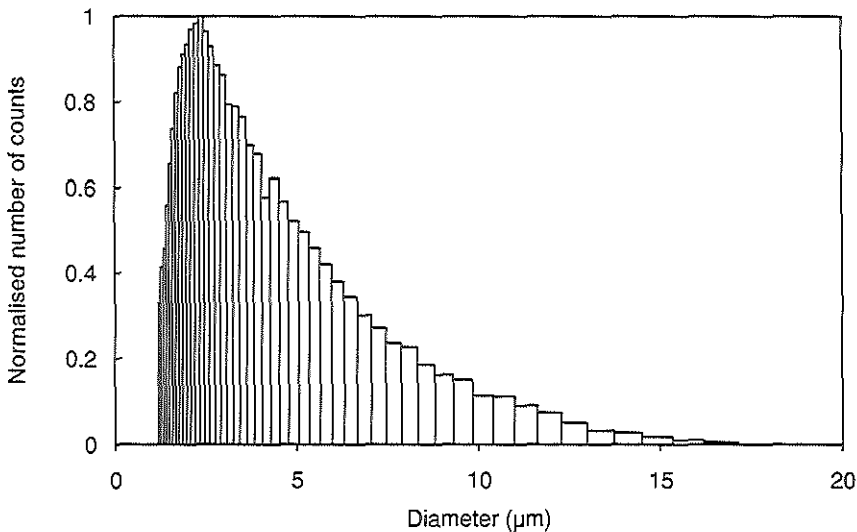


Figure 5-1 *The normalized size distribution of Albunex^R as measured with the Coulter counter.*

Essentially two parameters are involved: S_p , a shell elastic parameter with a estimated value of 8 Nm^{-1} and S_f , a shell friction factor with a estimated value of $4 \times 10^{-6} \text{ Nsm}^{-1}$. The presence of the shell surrounding the bubble causes an increase in stiffness of the overall bubble-liquid system and an increase in energy loss due to the internal friction inside the shell. The size distribution of Albunex[®] as measured with a Coulter counter is shown in Figure 5-1. The mean diameter of the microspheres of the batch used in this study is $3.8 \mu\text{m}$ and the concentration before dilution 9×10^8 microspheres/ml. (In this study an experimental Albunex[®] production batch is used. This batch has a size distribution equal to that of the batches used for clinical trials, but with a somewhat higher concentration.) About 95% of the microspheres are smaller than $10 \mu\text{m}$, while there are microspheres present larger than $15 \mu\text{m}$.

Theory

The bubble model developed by Rayleigh provides the theoretical basis: the bubble contains gas and vapour, is considered as spherical and is surrounded by an incompressible liquid of infinite extent. The volume is defined by a single variable, the radius, and the motion is assumed to be spherically symmetric. The wavelength of the ultrasound is much larger than the radius of the bubble and only the behaviour of the bubble surface is of interest. The liquid is Newtonian, so its viscosity is constant. It is assumed that the vapour pressure remains constant during the compression/expansion and that there is no rectified diffusion during the short period of exposure to the ultrasound. The gas in the bubble is compressed/expanded according to the gas law with the polytropic exponent Γ remaining constant during the vibration. It is necessary to solve the equations of the conservation of mass and momentum for the gas and the liquid phase to account adequately for the vibration of the bubble. The following expression is given by Eatock¹⁰ for an ideal gas bubble and is called the RPNNP equation named to its developers Rayleigh, Plesset, Noltingk, Neppiras & Poritsky.

$$\rho R \ddot{R} + \frac{3}{2} \rho \dot{R}^2 = p_{g0} \left(\frac{R_0}{R} \right)^{3\Gamma} + p_v - p_{l0} - \frac{2\sigma}{R} - \delta_t \omega \rho R \dot{R} - p_{ac}(t) \quad [\text{V-1}]$$

- R = instantaneous bubble radius
- \dot{R} = first time derivative of the radius
- \ddot{R} = second time derivative of the radius
- ρ = density of the surrounding medium
- R_0 = initial bubble radius

- p_{g0} = initial gas pressure inside the bubble
 Γ = polytropic exponent of the gas
 p_v = vapour pressure
 p_{i0} = hydrostatic pressure
 σ = surface tension coefficient
 δ_t = total damping coefficient
 ω = angular frequency of incident acoustic field
 $p_{ac}(t)$ = time varying acoustic pressure.

The initial gas pressure inside the bubble, p_{g0} , and the total damping coefficient, δ_t , are given by:

$$p_{g0} = \frac{2\sigma}{R_0} + p_{i0} - p_v \quad [V-2]$$

$$\delta_t = \delta_{rad} + \delta_{vis} + \delta_{th} + \delta_f \quad [V-3]$$

$$\delta_f = \frac{S_f}{m\omega} \quad [V-4]$$

- δ_{rad} = damping coefficient due to re-radiation
 δ_{vis} = damping coefficient due to viscosity of the surrounding liquid
 δ_{th} = damping coefficient due to heat conduction
 δ_f = damping coefficient due to the internal friction inside the shell
 S_f = shell friction parameter
 m = effective mass of bubble-liquid system.

Expressions for the thermal, reradiation and viscous damping coefficients together with the effective mass of the bubble-liquid system are given by Medwin⁵.

For an Albunex^R microsphere there is an additional loss term due to the internal friction inside the shell and an additional restoring force due to the shell stiffness. The internal friction can be expressed as in equation [V-4]¹², while the restoring force is equivalent to an additional pressure difference equal to $S_p(1/R - 1/R_0)$ ¹³ as described in chapter III and IV. Equation[V-1] becomes then:

$$\rho R \ddot{R} + \frac{3}{2} \rho \dot{R}^2 = p_{g0} \left(\frac{R_0}{R} \right)^{3\Gamma} + p_v - p_{i0} - \frac{2\sigma}{R} - S_p \left(\frac{1}{R_0} - \frac{1}{R} \right) - \delta_t \omega p R \dot{R} - p_{ac}(t) \quad [V-5]$$

The values of the shell elasticity parameters, S_p , and the shell friction S_f have been determined for Albunex[®] in chapter IV and their values are 8 Nm^{-1} and $4 \times 10^{-6} \text{ Nsm}^{-1}$ respectively¹². The damping coefficient appearing in equation [V-3] are derived from the linear theory and are therefore assumed to be independent of the applied pressure. For high pressures this may not hold, but the pressure is assumed to be within the limits associated with the linearized theory. In equation [V-5] all variables, except the radius and its time derivatives, are determined by their initial conditions and are considered as constant during the bubble vibration (the lumped constant approach).

Simulations

method

Calculations are performed for an air bubble and an Albunex[®] microsphere in water at 20 °C. Physical constants used are summarized in Table V-a. The list includes the constants, such as viscosity, acoustic velocity, specific heat and thermal conductivity which are used to calculate the damping coefficient.

Table V-a Physical constants used in simulations.

water	density	ρ	998	kg m^{-3}
	surface tension	σ	0.072	N m^{-1}
	viscosity	η	0.001	N s m^{-2}
	acoustic velocity	c	1500	m s^{-1}
	vapour pressure	p_v	2.33	N m^{-2}
air	ratio specific heat	γ	1.4	
	density	ρ_g	1.3	kg m^{-3}
	specific heat at constant pressure	C_{pg}	1000	$\text{J kg}^{-1} \text{K}^{-1}$
	thermal conductivity	C_g	0.024	$\text{W m}^{-1} \text{K}^{-1}$
Albunex	shell elasticity parameter	S_p	8	N m^{-1}
	shell friction parameter	S_f	$4 \cdot 10^{-6}$	kg s^{-1}
general	atmospheric pressure	p_{i0}	$1.01 \cdot 10^5$	N m^{-2}

The solution of equation [V-5] results in an instantaneous radius, velocity and acceleration of the bubble wall. The scattered sound pressure at the bubble surface, p_s , is defined in equation [V-6]¹⁴

$$|p_s(n\omega)| = |pn\omega R_0 \dot{R}(n\omega)| \quad [V-6]$$

- p_s = scattered pressure
 ρ = density of the surrounding liquid
 ω = angular frequency
 n = harmonic number (1, 2, 3, 1/2, 1/3)
 R_0 = initial radius
 \dot{R} = first derivative of the radius

The scattering cross-section, Σ_s^n , of the n-th harmonic of a scatterer, defined as the quotient of the scattered power and the incident acoustic intensity of the first harmonic, is used as the parameter defining the acoustic behaviour.

$$\Sigma_s^n = 4\pi R_0^2 \frac{|p_s(n\omega)|^2}{|p_{ac}(\omega)|^2} \quad [V-7]$$

$p_{ac}(\omega)$ = applied acoustic pressure

The second order differential equation [V-5] can be solved numerically using the fourth order Runge Kutta method. A sinusoidal wave is taken as driving acoustic pressure which starts at $t=0$ and is cosine windowed for the first five periods to quickly reach a steady state condition. The amplitude of the acoustic wave is 50 kPascal unless stated otherwise. The initial conditions at $t=0$ are those of a bubble at rest: $R=R_0$ and $\dot{R} = 0$. Values for the instantaneous radius, velocity and acceleration of the bubble are taken after a steady state is reached. The angular resonance frequency ω_0 is determined according to Eatock¹⁰.

Results

The simulations have been carried out with driving frequencies, bubble sizes and pressure amplitude which are realistic in the field of diagnostic ultrasound. The following categories are considered:

- The scattering cross-section of ideal gas bubbles, with diameters of 2, 3.4 and 6 μm , driven at a frequency of 2 MHz and a amplitude of 50 kPascal is calculated. The resonance frequency of 2 μm bubble is 4 MHz, for 3.4 μm 2 MHz and for 6 μm 1.1 MHz. So the bubbles are driven at half resonance, resonance and above their resonance frequencies.
- The scattering cross-section of Alburnex^R microspheres, with diameters of 6, 9.6

and 20 μm , driven at a frequency of 2 MHz and a amplitude of 50 kPascal is calculated. The resonance frequency of 6 μm microsphere is 4 MHz, for 9.6 μm 2 MHz and for 20 μm 700 kHz. So the microspheres are driven at half resonance, resonance and above their resonance frequencies.

- c) The scattering cross-section of an ideal gas bubble with a diameter of 3.4 μm and an Albunex[®] microsphere with a diameter of 9.6 μm are compared as a function of the driving frequency. For these diameters a maximum occur at a driving frequency of 2 MHz.
- d) For a typical Albunex[®] size distribution the scattered power as a function of the diameter is calculated at two driving frequencies, 2 and 3.5 MHz.
- e) The scattered power as a function of the driving frequency is calculated for two size distributions; a typical Albunex size distribution and a distribution where microspheres larger than 8 μm haven been removed.

a) Ideal gas bubble

The results of the simulation studies for ideal gas bubbles, with diameters of 2, 3.4 and 6 μm , driven at a fixed frequency of 2 MHz, and an acoustic pressure of 50 kPascal are shown in Figure 5-2. The left panels shows 3 periods of the relative diameter change of the bubble after 15 periods ($t=0$ in the figure), while the right panels present the corresponding Fourier transforms expressed in the scattering cross-section using equation [V-6] and [V-7]. The scattering cross-section of the bubble with a diameter of 6 μm at 2 MHz is 200 μm^2 which is about twice as high as its physical scattering cross-section, which is equal to $4\pi R^2$, due to fact that 2 MHz is not far above resonance. The vibration can be considered only slightly nonlinear as shown by the 20 dB drop in the 4 MHz component. The driving pressure and the change in diameter have a phase difference of approximately 180° , which is typical for a mass-spring system acting above its resonance frequency⁸. A bubble with a diameter of 3.4 μm driven at its resonance frequency shows a change in diameter which varies between 60% of its initial diameter in the expanding phase and about 40% in the compression phase. The driving pressure and the diameter are 100° out of phase for this amplitude of the driving pressure. For low amplitudes (linear case) the phase difference is 90° . The resulting scattering cross-section contains higher harmonics which even exceed that of the first harmonic, which has a value of 670 μm^2 . When such highly nonlinear behaviour occurs, the level of the first harmonic is no longer independent of the applied pressure, but actually decreases as pressure increases because energy flows into the higher harmonics. A bubble with a diameter

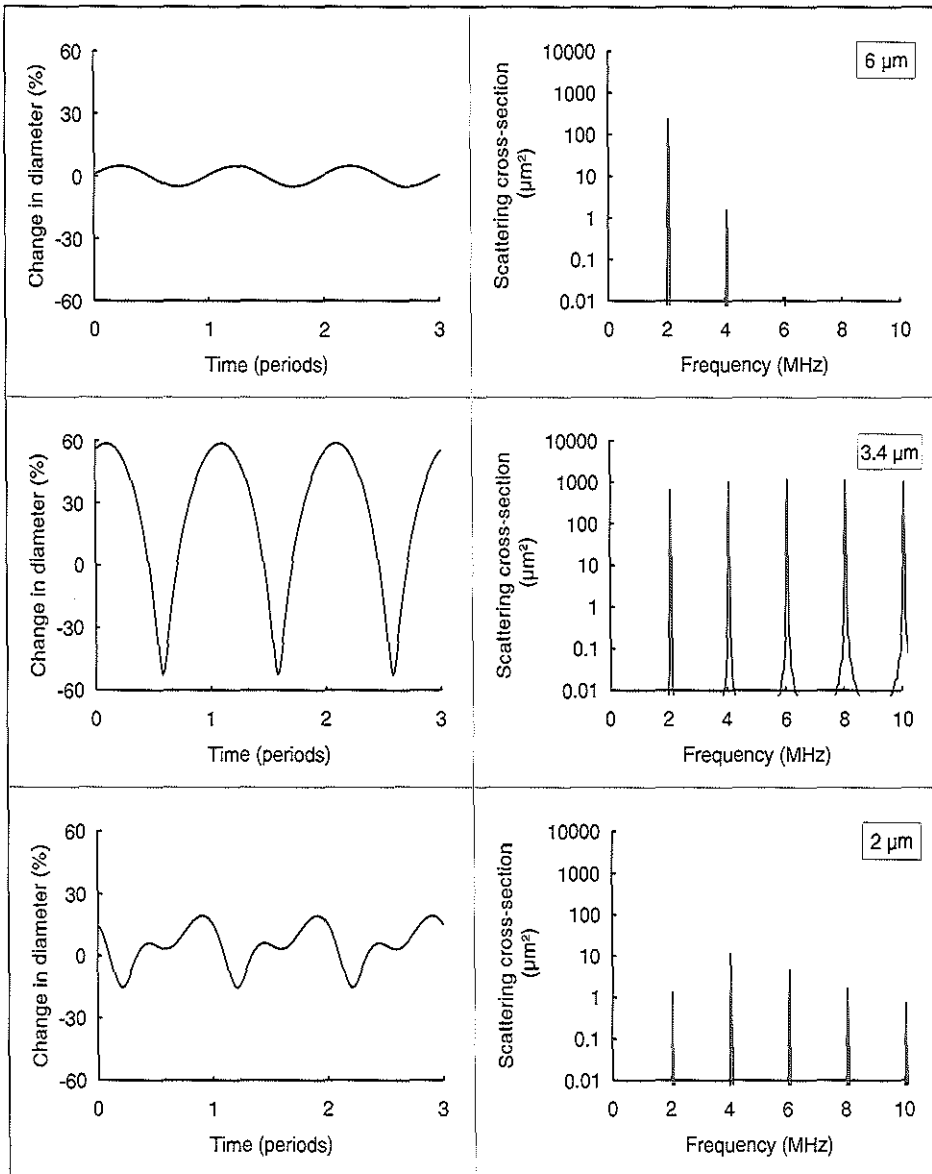


Figure 5-2 *Calculated behaviour of an ideal gas bubble in water for an acoustic driving frequency of 2 MHz at a pressure amplitude of 50 kPascal. Bubble diameters; 6 μm (above resonance); 3.4 μm (resonance) and 2 μm (half resonance). The left panels show the change in diameter as a function of time, the right panels the corresponding frequency domain components.*

of 2 μm exposed to an acoustic field of half its resonance frequency, generates higher harmonics with a magnitude which is 20 dB higher than the first harmonic.

b) Albunex^R microsphere

Simulation studies for Albunex^R microspheres, with diameters of 6, 9.6 and 20 μm , driven at a fixed frequency of 2 MHz, and an acoustic pressure of 50 kPascal are shown in Figure 5-3. Compared to an ideal air bubble these results are less spectacular. The shell surrounding the Albunex^R microsphere increases the stiffnesses. Therefore the diameter at which resonance occurs is larger than that for an air bubble. For the microsphere with a diameter of 20 μm , the relative change in diameter is very small. The scattering cross-section is 1200 μm^2 , which is close to its physical scattering cross-section. The second harmonic is more than 40 dB below the first harmonic. For the microsphere at resonance (9.6 μm diameter), the diameter and driving pressure are out of phase as shown in the middle panel of the figure. The scattering cross-section at 2 MHz is 1200 μm^2 , which is more than 4 times the physical scattering cross-section. The second harmonic at 4 MHz has a value which is about 20 dB below the first harmonic. The lower panel (6 μm diameter) shows the response for a microsphere driven at half its resonance frequency. The second harmonic is more than 20 dB below the first harmonic. The absolute value of the scattering cross-section at the first harmonic is 20 dB below the physical scattering cross-section due to the steep frequency dependency of the scattering cross-section below resonance. The absolute value of the second harmonic is of the same order of magnitude as that of the microsphere with a diameter of 20 μm .

c) Ideal gas bubble vs Albunex^R microsphere

The scattering cross-section of the first and second harmonic for an Albunex^R microsphere (diameter: 9.6 μm) and an ideal gas bubble (diameter: 3.4 μm) is shown in Figure 5-4. The driving frequency is denoted on the x-axis. The diameters have been chosen such that the first harmonic is maximum at a driving frequency of 2 MHz. Above this frequency the scattering cross-section becomes equal to the physical scattering cross-section. The overall level of the scattering cross-section for an ideal gas bubble is, of course, lower than this for the Albunex^R microsphere due to the difference in diameter. The second harmonic maximum occurs at a driving frequency of 2 MHz, which means that this second harmonic has a peak amplitude

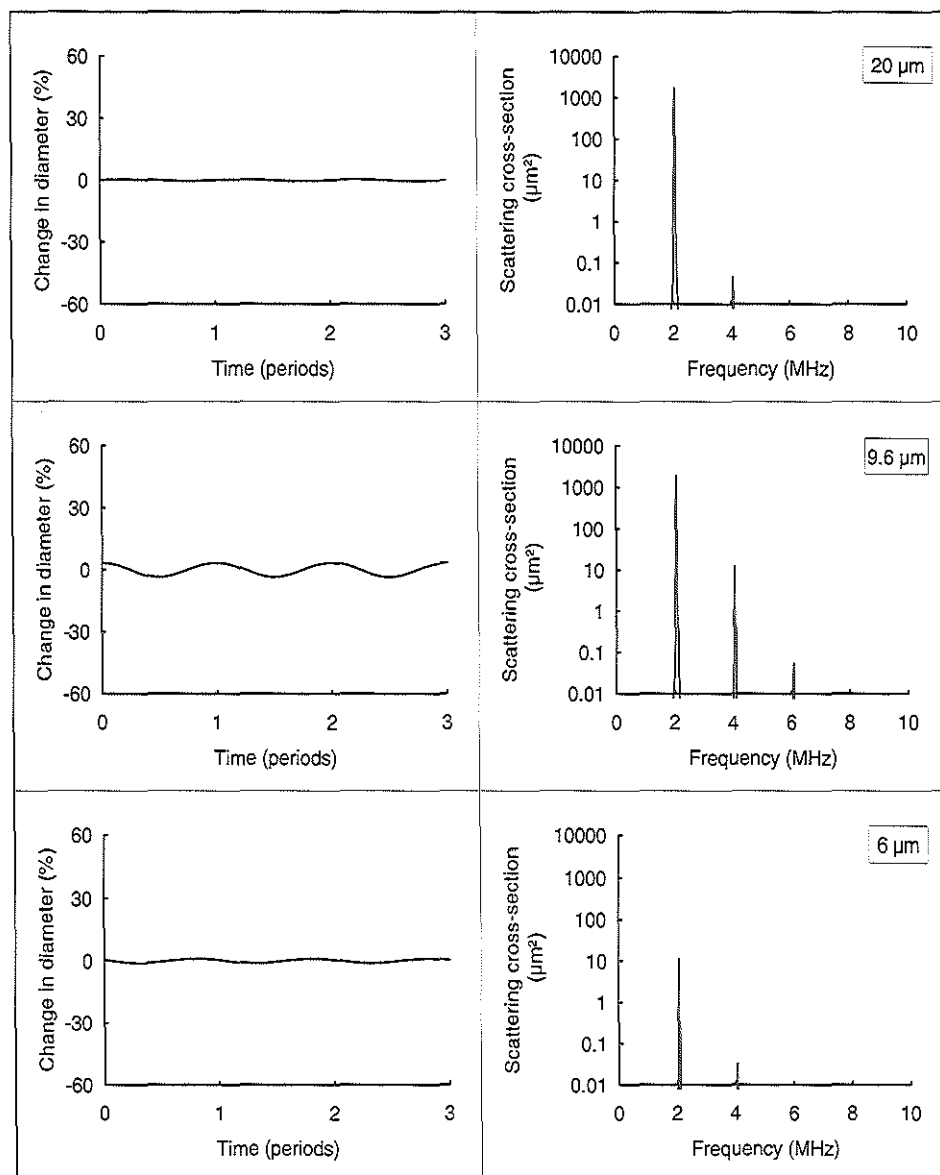


Figure 5-3 Calculated behaviour of an Albnex® microsphere in water for an acoustic driving frequency of 2 MHz at a pressure amplitude of 50 kPa. Microsphere diameters 20 μm (above resonance); 9.6 μm (at resonance) and 6 μm (half resonance). The left panels give the change in diameter as a function of time, the right panels the corresponding frequency components.

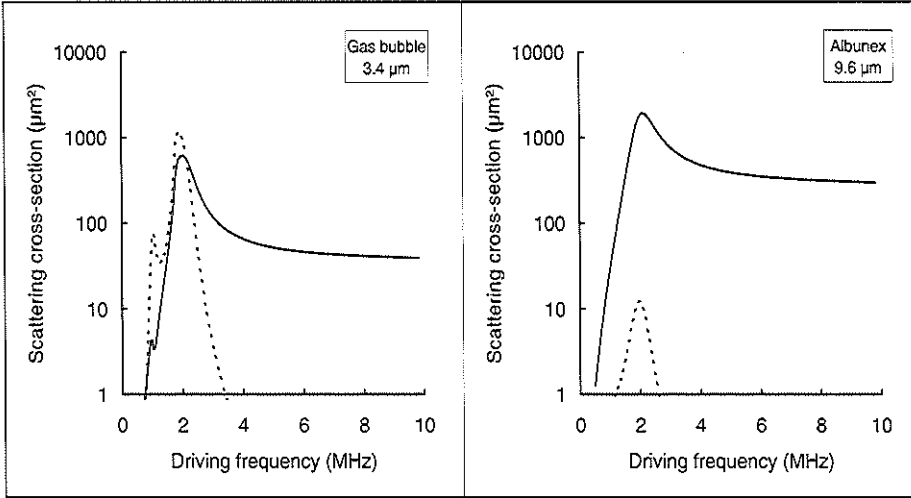


Figure 5-4 Calculated scattering cross-section as a function of the driving frequency at a pressure amplitude of 50 kPascal. Left panel: an ideal gas bubble with a diameter of 3.4 μm. Right panel: an Albunex[®] microsphere with a diameter of 9.6 μm. —, First harmonic; - - -, Second harmonic.

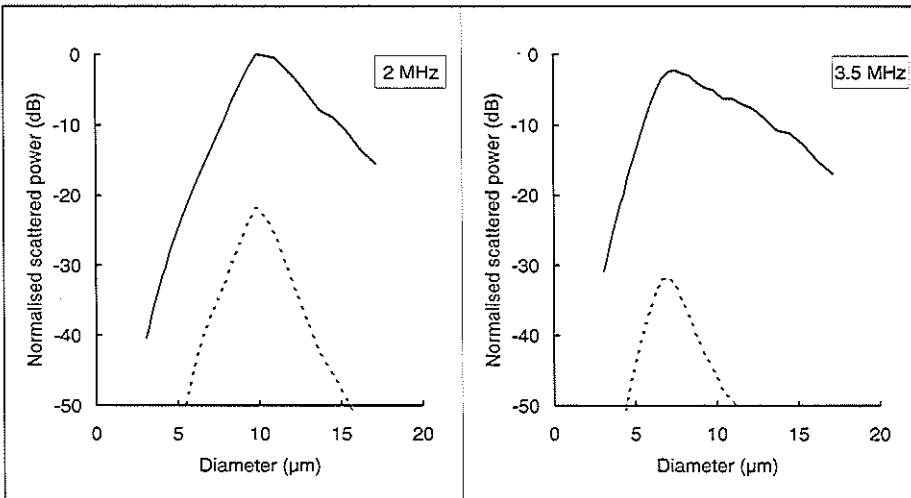


Figure 5-5 Calculated scattered power as a function of the diameter of the Albunex[®] microsphere corrected for the size distribution as shown in Figure 5-1. Left panel: driving frequency 2 MHz. Right panel: driving frequency 3.5 MHz. Pressure amplitude 50 kPascal. —, First harmonic; - - -, Second harmonic.

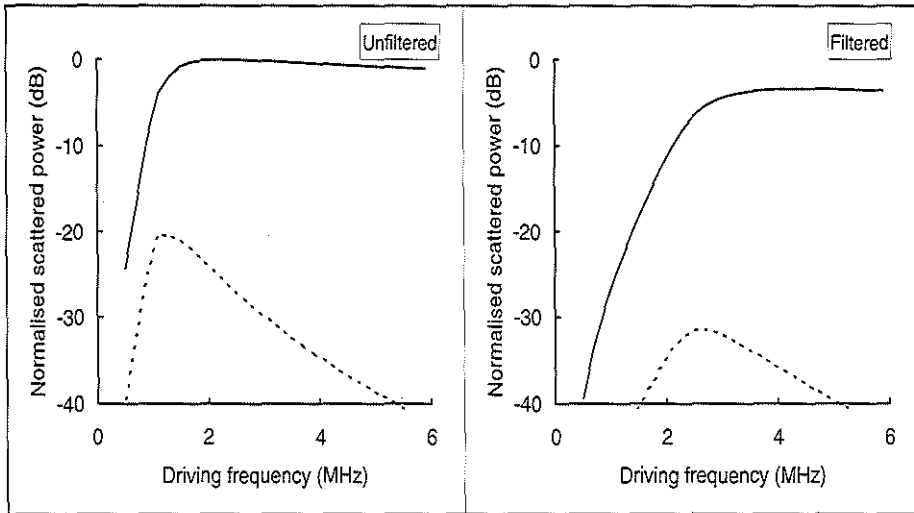


Figure 5-6 *Calculated scattered power as function of the driving frequency at a pressure amplitude of 50 kPascal. Left panel: unfiltered Alunex^R. Right panel: filtered Alunex^R, filter pore size 8 μm . —, First harmonic; - -, Second harmonic.*

at 4 MHz. Both panels demonstrate a steep drop in the magnitude of the second harmonic for lower and higher driving frequencies. There is a secondary maximum at half the resonance frequency for the ideal gas bubbles, but this is barely noticeable for the Alunex^R microsphere.

d) Alunex^R containing microspheres of different sizes

While the previous modelling is performed for only one specific diameter of the bubbles or microspheres, in practice these bubbles or microspheres will cover a certain size range. Alunex^R has a rather broad size distribution, as shown in Figure 5-1. The normalized scattered power is computed and presented in Figure 5-5. At 2 MHz Alunex^R microspheres with a diameter around 10 μm contribute most to the scattered power. At 3.5 MHz a maximum is found for a diameter of 6 μm , while the level of predicted scattered power is only a few decibels lower compared to that at 2 MHz. For the second harmonic the scattered power peaks at the same diameter as for the first harmonic.

e) Filtered Albunex^R

Finally, the first and the second harmonic of the scattered power, as a function of the frequency, for two different size distributions of Albunex^R is shown in Figure 5-6. The first one is the same size distribution as shown in Figure 5-1. The second one is based on the measured size distribution after filtering diluted Albunex^R through a Nuclepore^R filter with a rated pore size of 8 µm, resulting in a truncated distribution at 8 µm¹³ as shown in Chapter III. Unfiltered Albunex^R results in a calculated scattered power which is independent of frequency above 1.5 MHz. The second harmonic shows a maximum at 1 MHz, which is 10 dB lower than the first harmonic. The first harmonic for filtered Albunex^R is frequency independent above 3 MHz, while the second harmonic shows a maximum at 2.5 MHz, which is about 20 dB below the first harmonic.

Measurements

Set-up

Higher harmonics occur during the transmission of an ultrasonic wave through water as a result of nonlinear propagation effects. For a plane wave with an acoustic pressure p_{ac} the second harmonic, p_2 is given by¹⁵:

$$p_2 = \left(\frac{B}{A} + 2\right) \frac{\pi f}{2\rho c^3} l p_{ac}^2 \quad [\text{V-8}]$$

- B/A = nonlinear parameter of the medium
- f = frequency
- ρ = density of the medium
- c = acoustic velocity
- p_{ac} = applied acoustic pressure
- l = distance travelled from the source.

The nonlinearity parameter B/A has a value of 5.2 for water. For example, if we take an acoustic pressure of 100 kPascal at a frequency of 2 MHz, the second harmonic component for a plane wave has a value of -23 dB below the original component at a distance of 10 cm from the source. Therefore, in order to avoid any misinterpretation of the results the maximum travel distances used here are 4 cm which results in a maximum nonlinear component of -37 dB for acoustic pressures less than 50 kPascal.

Three kinds of measurements are carried out: 1) Nonlinearity parameter B/A , 2)

Scattering and 3) Imaging measurements. The measurement set-up is illustrated in Figure 5-7. The transducers are mounted in a rectangular waterbath which measures 40 mm square. The acoustic beams of the transducers lie in one plane. The transducers are driven by a sine wave generator and controlled with respect to amplitude, frequency and the burst length. The received signal is amplified and digitized by an analog to digital converter (Lecroy 9400) and sent to a personal computer (IBM compatible 486) for further signal processing. The transmitting transducers are calibrated with a Marconi PVDF Hydrophone (type Y-33-7603) with an aperture of 0.5 mm.

1) Nonlinearity parameter B/A.

Transducers with a center-frequency of 1 and 2.2 MHz, are used as transmitters at an applied frequency of 1 and 2 MHz respectively. The burst length is limited to 10 periods. The receiving transducers are placed opposite to the transmitters, and have a center-frequency of 3.5 and 5 MHz respectively. The sensitivity of the transducer with a center frequency of 3.5 MHz is -20 dB at 1 MHz and -10 dB at 2 MHz. The transducer with a center frequency of 5 MHz has a sensitivity of -10 dB at 2 MHz and -5 dB at 4 MHz. The applied acoustic pressures are 25 and 50 kPascal. Measurements are carried out with Albunex[®] diluted 1:40,000 in Isoton[®]

2) Scattering

The two transducers with center frequency 1 and 2.25 MHz are used as transmitters with an applied frequency of 1 and 2 MHz respectively. Burst length is 3 periods. The amplitude of the acoustic pressure is 25 and 50 kPascal. The two transducers have an aperture of 13 and 9 mm respectively, resulting in a focal length of 25 mm. The receiving transducer has a center-sensitivity at 3.5 MHz and a aperture of 10 mm. Albunex[®] diluted 1: 20,000, Albunex[®] filtered with a 8 μm Nuclepore[®] filter and Eccospheres[®] are measured. Eccospheres[®] are glass coated microspheres filled with gas. The coating of these spheres is about 1.5 μm thick and the sizes ranges from 2 to 50 μm . Twenty gram of this product is suspended in water and filtered with a 12 μm Nuclepore[®] filter to remove the larger spheres. These Eccospheres[®] are free of resonance phenomena in the frequency range 1-5 MHz, and it is therefore expected that they will not show any nonlinear behaviour.

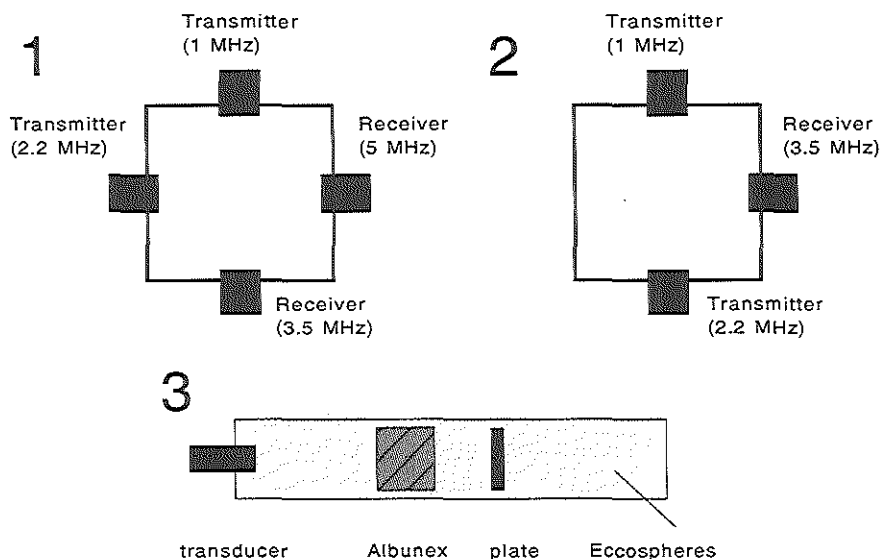


Figure 5-7 Measurement set-up. 1) set-up for measuring B/A parameter. 2) Scattering measurements. 3) "imaging" experiment.

3) Imaging

Current imaging in medical diagnostic ultrasound is performed using one transducer to generate the ultrasonic energy and to receive the backscattered signal. This situation is reproduced using only one transducer to act as both transmitter and receiver. The transducer has a center-frequency of 3.5 MHz and the transmitting signal consists of a burst of 2 periods at 2.2 MHz. The backscattered signal contains both 2.2 MHz as well as 4.4 MHz components. These components are extracted by digital processing. The medium consist of Eccospheres^R smaller than 12 μm , Albunex^R diluted 1:20.000 in another inner cavity, and a flat plate of TPX^R material. The duration of the captured signal is 50 μs corresponding to a travel distance of 37 mm.

Results

1) Nonlinearity parameter B/A

Nonlinear propagation can be expressed in terms of the ratio of the second harmonic and the first harmonic component. The results of the studies in pure Isoton^R and Albunex^R diluted 1:40,000 in Isoton^R at two different acoustic pressures and two driving frequencies are shown in Figure 5-8. The addition of Albunex^R results in a substantial increase in nonlinear propagation in all cases. For example, at a driving

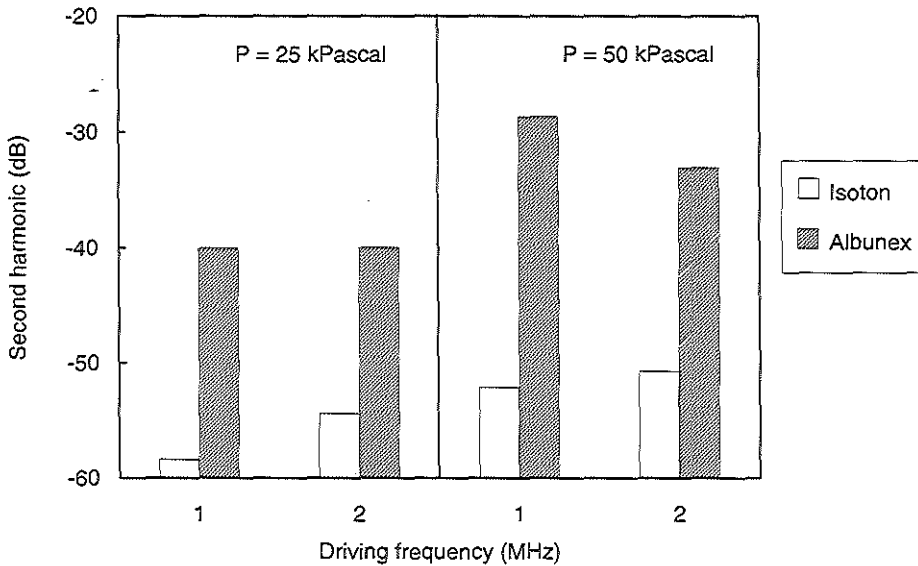


Figure 5-8 Measured second harmonic amplitude for driving frequencies 1 and 2 MHz and for an acoustic pressure amplitude of 25 and 50 kPascal for Isoton[®] and Alunex[®] diluted 1:40,000 in Isoton[®]. Acoustic path is 40 mm.

frequency of 1 MHz and an amplitude of 50 kPascal the second harmonic component increases from -52 dB in pure Isoton[®] to -28 dB for diluted Alunex[®].

A 6 dB increase is expected for Isoton[®] for a doubling in frequency or acoustic pressure. For a plane wave of a frequency of 1 MHz and a pressure of 50 kPascal the calculated value of the second harmonic is -43 dB, while only -52 dB is measured. These differences can be ascribed to the assumption in the theoretical model that there is an homogeneous acoustic field, whereas the near field condition prevails from 0 to 30 mm, resulting in pressure varying with distance from the transducer¹⁶.

2) Scattering

Ultrasonic scattering properties of diluted, unfiltered Alunex[®] is compared with the scattering of Eccospheres[®], with spheres smaller than 12 μm . The concentration of the Eccospheres[®] is chosen such that the scattered amplitude is of the same order of magnitude as the scattering of Alunex[®]. An example of a time trace, together with the frequency response averaged from 62 time traces, is shown in Figure 5-9. No correction has been made for the difference in the sensitivity at 1 and 2 MHz of the 3.5 MHz receiver. Alunex[®] shows a clear sensitivity at the second harmonic, which

is 8 dB (uncorrected) below the first harmonic. The level of the second harmonic for the Eccospheres[®] is more than 20 dB below the first harmonic.

The results for filtered and unfiltered Albunex[®] at two driving frequencies (1 and 2.2 MHz) is shown in Figure 5-10. A 3.5 MHz transducer is used as receiver and the received power at 1 and 2.2 MHz is corrected for the sensitivity of this transducer. The first harmonic is always higher than the second harmonic. For filtered Albunex[®] the difference is about 30 dB, for unfiltered 20 dB. It can be noticed that the effect of filtering on the magnitude of the second harmonic is considerable at a driving frequency of 1 MHz, while at 2.2 MHz the effect is minimal.

3) Imaging

An example of an A-mode recording from a medium containing Eccospheres[®], Albunex[®] and a flat plate reflector is shown in Figure 5-11. The driving frequency is 2.2 MHz as transmitted by the 3.5 MHz transducer. The time trace as received by the same transducer is shown in the top panel. The flat plate response can be clearly recognised, while the Albunex[®] and the Eccospheres[®] scatter more or less equally for this specially chosen concentration. The received signal, filtered with a Gaussian bandpass filter (center-frequency 2.2 MHz, bandwidth 0.5 MHz), extracts the first harmonic and is shown in the middle panel. The second harmonic, obtained by filtering the original signal with a bandpass filter (center frequency 4.4 MHz, bandwidth 0.5 MHz), is shown in the bottom panel. The scale of the y-axis is different from the other panels in order to magnify the effect. The Albunex[®] response at 4.4 MHz (second harmonic) is much higher than that of the Eccospheres[®] and the flat plate, clearly demonstrating the nonlinear behaviour of Albunex[®].

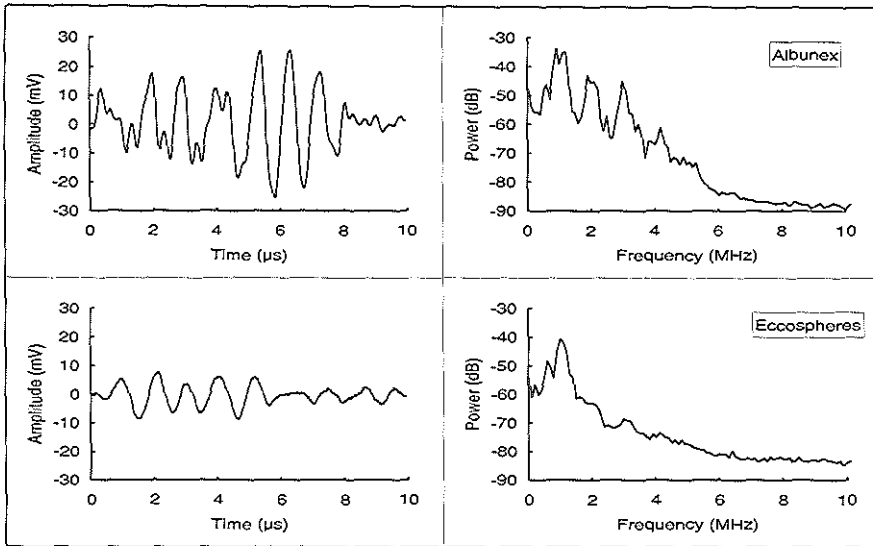


Figure 5-9 Measured response with the 3.5 MHz transducer as receiver and the 1 MHz transducer as transmitter for Albunex® and Eccospheres®. Left panels: time traces. Right panels: corresponding frequency components after Fourier transformations and averaging.

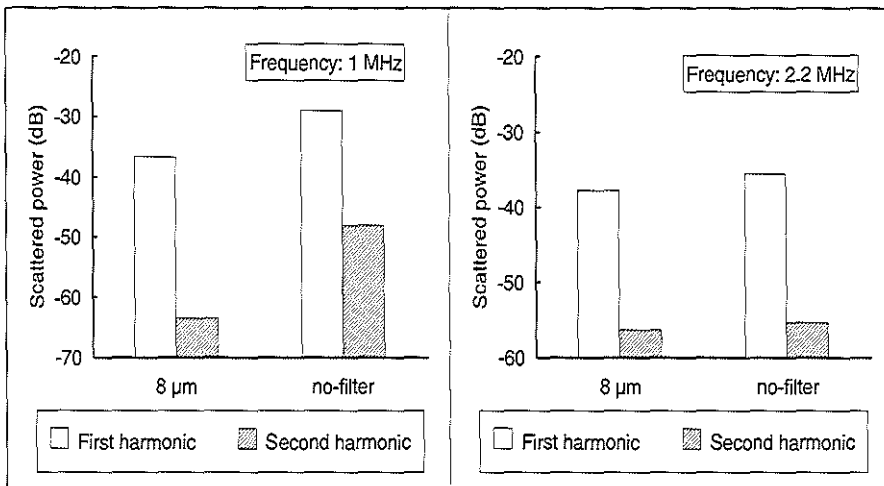


Figure 5-10 Measured scattering response with the 3.5 MHz transducer as receiver at a pressure amplitude of 25 kPascal for unfiltered Albunex® and Albunex® filtered with a 8 μ m filter. Left panel: driving frequency 1 MHz, right panel: driving frequency 2.2 MHz.

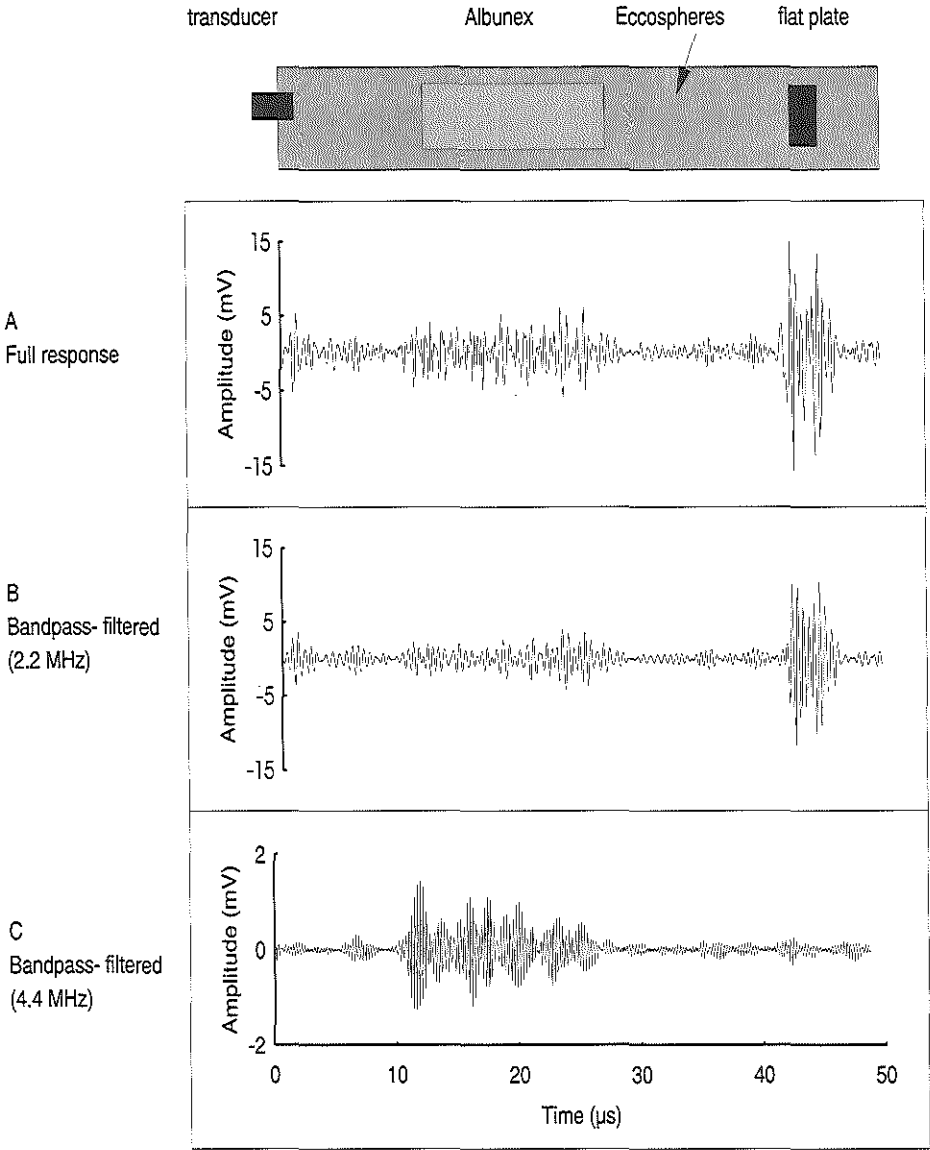


Figure 5-11 Time signal as received by the 3.5 MHz transducer. Top panel: Time signal as received by the transducer. Middle panel: Time signal after bandpass filtering at 2.2 MHz. Bottom panel: Time signal after bandpass filtering at 4.4 MHz.

Discussion

Simulations of the bubble behaviour by solving the RPNNP equation [V-1] for all the possible variables results in large volume of computational data. We have restricted ourselves to a specific driving frequency of 2 MHz, specially chosen diameters of the bubble at which resonance occurs, a fixed acoustic pressure amplitude of 50 kPascal and as a medium water at 20° C. The 2 MHz driving frequency is realistic in the field of medical diagnosis, both resolution and the attenuation for the first as well for the second harmonic is acceptable. The bubble diameters vary in our simulations between 2, 3.4 and 6 μm and the driving frequency is then above resonance, at resonance, and half the linear resonance frequency of the bubble. Eatock¹⁰ concluded that with a moderate acoustic amplitude of 50 kPascal the behaviour of bubbles is essentially linear, unless the driving frequency matches one of the following conditions: it is within 10% of the resonance frequency of the bubble, or it is a low integer fraction (1/2, 1/3,...) of the resonance frequency, or to a lesser extent, it is a low harmonic of the resonance frequency.

The simulation for air bubble and Albunex[®] microspheres in water illustrated in Figure 5-2 and Figure 5-3 show that the ratio of second and first harmonic has its greatest value when the driving frequency is at half resonance frequency, while the absolute value of the second harmonic is maximal when the driving frequency equals the resonance frequency. The magnitude of the scattering cross-section of the second harmonic for a resonant Albunex[®] microsphere is more than 20 dB lower than a resonant air bubble. Calculating the scattered power of the second harmonic of Albunex[®], taking into account its size distribution, shows a maximum value at a driving frequency of 1.5 MHz. At a driving frequency of 2 MHz the difference between first and second harmonic is 25 dB. Comparing an air bubble with an Albunex[®] microsphere, both driven at a frequency of 2 MHz, being half the resonance frequency (see Figure 5-2 and Figure 5-3, bottom panels), delivers a remarkable difference in the magnitude of the second harmonic compared to the first harmonic. The friction inside the shell, which dominates for small microspheres is responsible for this effect.

Measurements demonstrate that a second harmonic response occurs for Albunex[®], which is 20-30 dB lower than the first harmonic for acoustic pressures up to 50 kPascal. Comparison of Albunex[®] with Eccospheres, as shown in Figure 5-9 and in the "imaging" experiment as shown in Figure 5-11, reveal significant differences in the second harmonic magnitude. In both experiments it is important to minimize the

acoustic travelling path in the Isoton[®] in order to avoid any misinterpretation. Comparison of the scattering measurements for 1 and 2.2 MHz driving frequency is difficult for technical reasons. The acoustic pressures have been measured with a calibrated sensor of limited accuracy (10 %). Furthermore, the beams of the two transducers have different profiles, and the pressure is not constant in the region of scattering. The results of such comparative measurements should therefore be interpreted with caution.

There is an apparent increase in the nonlinearity in the medium when adding Albunex[®]. The value of B/A increases by a factor of 100 for a dilution of 1:40,000 of Albunex[®] as shown in Figure 5-8. For biological tissue at diagnostic frequencies values of B/A vary between 10 and 15 (water, $B/A=5$)^{18,19}.

Small rigid spheres are used in our experiments, which, like the Albunex microsphere, approximate an omnidirectional scattering for long wavelengths^{20,21}. Therefore any misinterpretation, resulting from a combination of the nonlinear propagation in water and the omnidirectionality of the scattering of Albunex[®] microspheres is avoided.

The scattered power at a frequency of 2.2 MHz indicates a difference between first and second harmonic of 16-20 dB as shown in Figure 5-10 for both filtered and unfiltered Albunex[®]. A difference of 25 dB is predicted in Figure 5-6, which is lower than the measured values, and may be due to a pressure dependency of the two model parameters S_r and S_p . Another possible explanation is the fact that the acoustic wave is not a plane wave with a constant pressure amplitude at the place of measurement. Furthermore, it is noted that the pressure dependency is not a simple quadratic function of the driving pressure amplitude. This is a subject for further study.

Measurements reported here are performed at acoustic pressure amplitude between 25 and 50 kPascal with a sine burst consisting of 10 periods. Under these conditions rectified diffusion can be neglected¹⁷.

Exploitation of the second harmonic component opens new perspectives for 2D echocardiography. For example, simultaneous images can be made using two transducers: one providing a normal 2D image with all heart structures including the contrast agent; the other providing an image of only the contrast agent. In the "imaging" experiments reported here one transducer is used as transmitter and receiver. It is unavoidable that significant second harmonic components are still present in the transmitted signal when the transducer is used below its center frequency (in our experiment the 4.4 MHz component is 25 dB below the 2.2 MHz).

As this can totally obscure the effect for strong reflectors, it is better to construct a special "second harmonic transducer". Such a transducer would consist of a small circular transducer and a ring-shape transducer designed to operate at the double frequency. Both transducers should be mounted in the same plane, but with a low mechanical coupling. Another possibility is to construct a combination ferro-electric ceramic with polymer piëzo-electric material. The ceramic disc can generate the transmitting acoustic signal and the polymer material, which is mounted on top of the ceramic disc can act as receiver. Two special properties of the polymer material can be exploited: it is a relatively good receiver and, because of its low acoustic impedance, and it also acts as an acoustic matching layer between ceramic and the medium. The latter solution has the advantage of a better acoustic beam definition.

Conclusion

The presence of second harmonic scattering component of Alburnex[®] has been demonstrated. This opens new perspectives for echocardiographic imaging technology and one possible use in 2D echocardiography is outlined. Further studies need to focus on a possible pressure dependency of the two model parameters S_r and S_p and an improved definition of the transmitted acoustic field.

References

1. Gramiak R., Shah P.M. Echocardiography of the aortic root. *Invest Radiol* 3 356-366 1968
2. Kremkau F.W., Shah R., Kramer D.H. Ultrasound cardiography contrast studies in anatomy and function. *Radiology* 92 939-948 1969
3. Noltingk, B.E. & Neppiras, E.A., Cavitation produced by ultrasonics, *Proc. Phys. Soc. B* 63 (1950), 674-685.
4. Devin, C., Survey of thermal, radiation, and viscous damping of pulsating air bubbles in water, *J. Acoust. Soc. Am.* 31 (1959), 1654-1667.
5. Medwin, H. Counting bubbles acoustically: a review. *Ultrasonics* (1977) 15(1) 7-13
6. Tucker, D.G. & Welsby, V.G., Ultrasonic monitoring of decompression, *Lancet* I (1968), 1253.
7. Welsby, V.G. & Safar, M.H., Acoustic non-linearity due to micro-bubbles in water, *Acustica* 22 177-182 (1969),
8. Lauterborn, W., Numerical investigation of nonlinear oscillations of gas bubbles in liquids, *J. Acoust. Soc. Am.* 59 (1976), 283-293.
9. Miller D.L. Ultrasonic detection of resonant cavitation bubbles in a flow tube by their second-harmonic emissions. *Ultrasonics* september 1981
10. Eatock, B.C., e.a., Numerical studies of the spectrum of low-intensity ultrasound scattered by bubbles, *J. Acoust. Soc. Am.* 77 (1985), 1692-1701.

11. Schrope, B. Newhouse, V.L. and Uhlendorf, V. Simulated capillary blood flow measurements using a nonlinear ultrasonic contrast agent. *Ultrasonic Imaging* 14(2) april 1992
12. De Jong N, Hoff L. Ultrasound scatter properties of Albunex[®] microspheres. *Ultrasonics* 1993 31(3) 175-181
13. De Jong N, Hoff L, Skotland T. and Bom N. Absorption and scatter of encapsulated gas filled microspheres: theoretical considerations and some measurements. *Ultrasonics* 1992 30(2) 95-103
14. Coackly, W.T. and Nyborg, L.N. Cavitation: Dynamics of gas bubbles: Applications in: *Ultrasound: It's applications in medicine and biology: part one* (ed Frey, F.J.) Elsevier Scientific Publishing Company, New York-Oxford-Amsterdam (1978) Ch II 77-159
15. Adler L. and Hiedemann E.A. Determination of the nonlinearity parameter B/A for water and m-Xylene. *J. Acoust. Soc. Am.* 34 (1962), 410-412
16. Bacon D.R. Finite amplitude distortion of the pulsed fields used in diagnostic ultrasound. *Ultrasound in Med. & Biol.* 1984 189-195
17. Flynn H.G. Physics of acoustics cavitation in liquids. in: *Physical acoustics, principles and methods*. ed. Mason W.P. vol 1 part B Academic Press New York and London 1964
18. Law W.K., Frizell L.A. and Dunn F. Ultrasonic determination of the nonlinearity parameter B/A for biological media. *J. Acoust. Soc. Am.* 69 (1981), 1210-1212.
19. Cartensen E.L., Law W.K., McKay N.D. and Muir T.G. Demonstration of nonlinear acoustical effects at biomedical frequencies and intensities. *Ultrasound in Med. & Biol.* 1980 359-368
20. Morse, P.M. and Ingard, K.U. *Theoretical acoustics*. McGraw Hill, New York (1968) p 436-441
21. Kroon de M.G.M., Wal vander L.F., Gussenhoven W.J. and Bom N. Angle-dependent backscatter from the arterial wall. *Ultrasound in Med. & Biol.* Vol 17 No 2 1991 121-126.

VI

TRANSPULMONARY ECHOCONTRAST EFFECTS

Abstract

The contrast effect in the right and left ventricle after intravenous injection of Albunex^R in healthy volunteers is reported. The observed effects, especially the difference in contrast enhancement between the right and left ventricle are explained based on in-vitro experiments. Albunex^R is administrated intravenously in three dosages; 0.01, 0.02 and 0.04 ml per kg body weight in 10 healthy volunteers. Echocardiographic studies are performed using the apical four chamber view. Off line analysis of the video density for different regions are carried out for all dosages. In all the subjects a density increase in the left ventricle could be observed after intravenous injection. Albunex^R, exposed to a range of overpressures, are studied under the microscope. A model of the Albunex^R microspheres together with a model of the sieving action of the lung capillaries, is used to calculate the expected backscattered power. In vitro testing of Albunex^R diluted in 5% human serum albumin at an overpressure of 160 mmHg reveal disappearance of the microspheres. The expected calculated decrease in backscattered power before and after lung passage of the contrast agent is 10 dB for 2.5 MHz.

This chapter is based on a manuscript, which has been published:

Title :Quantification of transpulmonary echocontrast effects

Authors :N. de Jong, F.J. ten Cate, W.B. Vletter, J.R.T.C. Roelandt

In :Ultrasound in Medicine and Biology 1993 19(4)

INTRODUCTION

Contrast echocardiography has been evolving since 1968 when Gramiak and Shah¹ observed a contrast effect following indocyanine dye injection on M-mode echocardiograms. Since that time the clinical application of contrast echocardiography has been largely replaced by colour Doppler flow imaging. More recently, contrast echocardiography gained renewed interest when experimental studies indicated it's potential to assess myocardial perfusion. Using intracoronary or intra-aortic injections, contrast agents have been used to identify myocardial perfusion defects² and areas at risk³, and to indicate coronary blood flow^{4,5} or flow reserve^{6,7}. However, in order to accurately measure perfusion, a contrast agent must satisfy several criteria. The agent should be inert, that is without systemic hemodynamic effects, and should not alter coronary blood flow⁸. The microspheres which provide backscatter for echocardiographic imaging should not be larger than red blood cells, and should have identical velocity flow profiles and physiologic transit times without impeding flow. The microspheres must persist long enough to perfuse the tissue to be imaged, and provide adequate ultrasound backscatter to be detected with available equipment. For purposes of quantification the ultrasound properties of the agent have to be known together with the concentration and size distribution in the area of interest. Agents which have been used in the past have failed to meet one or more of these criteria. Many are hyperosmolar and therefore alter coronary blood flow and/or systemic blood pressure^{9,10,11}, while others alter left ventricular contractility. Hand agitated solutions and hydrogen peroxide contain relatively large microspheres providing good backscatter, but impede capillary flow and have prolonged transit times^{12,13}. Also, microspheres used in early studies are neither small nor stable enough to pass through the pulmonary circulation in sufficient quantities to opacify the left ventricle following an intravenous injection¹⁴.

Experimental studies with sonicated albumin microspheres have shown that these are sufficiently small and stable, with satisfactory longevity and capable of passing through the pulmonary circulation in experimental animals, and that they do not alter hemodynamics, coronary blood flow, or left ventricular contractility¹⁵. Furthermore, sonicated albumin microspheres can be generated in high concentrations, thus providing an intense backscatter despite their small size. Sonicated albumin therefore appears to fulfil all the criteria set forth for an "ideal" myocardial contrast echo agent.

Recently, clinical experience using intravenous Albunex[®], a sonicated albumin solution containing stable microspheres of known size and concentration, has been reported.

The agent is safe and causes left heart opacification after intravenous injection¹⁶. We studied the in-vitro behaviour of Albunex^R in order to explain the observed contrast effects in the right and left ventricle after intravenous injection of increasing dosages of Albunex^R in humans.

Table VI-a Dosage regimen for the 10 volunteers participating in the study. Low concentration = 4.7×10^8 , high concentration = 8.3×10^8 microspheres/ml.

Injection no	Material	Dosage (ml kg ⁻¹)	Concentration (microspheres/ml)
0	Human serum Albumin	1 ml	5%
1	Albunex ^R	.01	4.7×10^8
2	Albunex ^R	.01	8.3×10^8
3	Albunex ^R	.02	4.7×10^8
4	Albunex ^R	.02	8.3×10^8
5	Albunex ^R	.04	4.7×10^8
6	Albunex ^R	.04	8.3×10^8

METHODS AND MATERIALS

The studies are performed in ten healthy male volunteers, age 20-25 years after giving written informed consent. All underwent a complete history and physical examination, electrocardiogram, and laboratory evaluation including glucose, serum electrolytes, urea, creatinine, calcium, phosphate, uric acid, cholesterol, liverprofile, complete blood count, thrombin time, and urinalysis. All subjects are required to be within 10% of their ideal body weight, with blood pressure between 100-140 / 70-90 mmHg, heart rate between 50-90 beats/min, temperature less than 37.1 centigrade, normal electrocardiogram, and normal laboratory data. Exclusion criteria included previous neurologic, cardiac or lung disease, known right to left heart shunts, blood product allergies, drug or alcohol dependence, or women of child bearing potential. No echocardiographic abnormalities are noted. These volunteers can be defined as normal in so far as this can be established by complete medical examination. The protocol is approved by the Medical Ethics Committee of the hospital. The safety aspects have been reported recently¹⁶.

Two-dimensional echocardiographic examination.

The volunteers are examined in the left lateral decubitus position using a Toshiba SSH/160A apparatus with a 3.75 MHz phased array transducer. As all volunteers are

healthy and young, they are able to breathe as superficially as possible. This is done to keep the 2D echo image as stable as possible during the injection of Albunex[®] and to minimize the effects of venous return on the echocontrast images. Apical four-chamber views are obtained, and gain settings and density are optimized at the beginning of the examination. These settings are not changed during the examination. Images are recorded on VHS 1/2 inch videotape.

Albunex[®] administration protocol

A 20 gauge intravenous catheter is placed in a large forearm vein of the subject and a maintenance infusion of normal saline is initiated. The contrast agent used (Albunex[®], Molecular Biosystems, San Diego CA, USA) is a stable, prepared albumin-based agent consisting of microspheres with a mean diameter between 3-5 μm . Two solutions of different microsphere concentration are administered, 4.7×10^8 microspheres/ml (low concentration) and 8.3×10^8 microspheres/ml (high concentration). Three different dosages are used; 0.01, 0.02 and 0.04 ml per kg body weight. Prior to the first Albunex[®] injection, subjects received a 1 ml dose of 5% human albumin as control. The complete dosage regimen is given in Table VI-a. Injections are administered through a three-way stopcock connected to the intravenous catheter, and following each injection, the saline is allowed to run wide-open for 30 seconds to flush the injection. After the injections, the heart rate, blood pressure, respiratory rate and electrocardiogram (via the single lead electrocardiogram displayed on the echo apparatus) are recorded and a neurologic evaluation is made.

Two-dimensional echo imaging is performed just prior to each injection and continued for 3 minutes following each injection or until contrast is no longer visible. A final four-chamber image is recorded following the last injection. An example of a video recording just before injection and at its peak density after the injection is shown in Figure 6-1.

Videodensitometry

The video recorded images are digitized via an IBM AT computer, connected to a high resolution frame grabber which allows acquisition of 52 frames. Image resolution is 512 x 512 pixels. The video gray scale values are expressed in 256 (8 bit resolution) levels, where the value 0 means black (no echo) and 256 white (maximum echo). The video gray scale value is referred to as density throughout this manuscript and is expressed in arbitrary units.

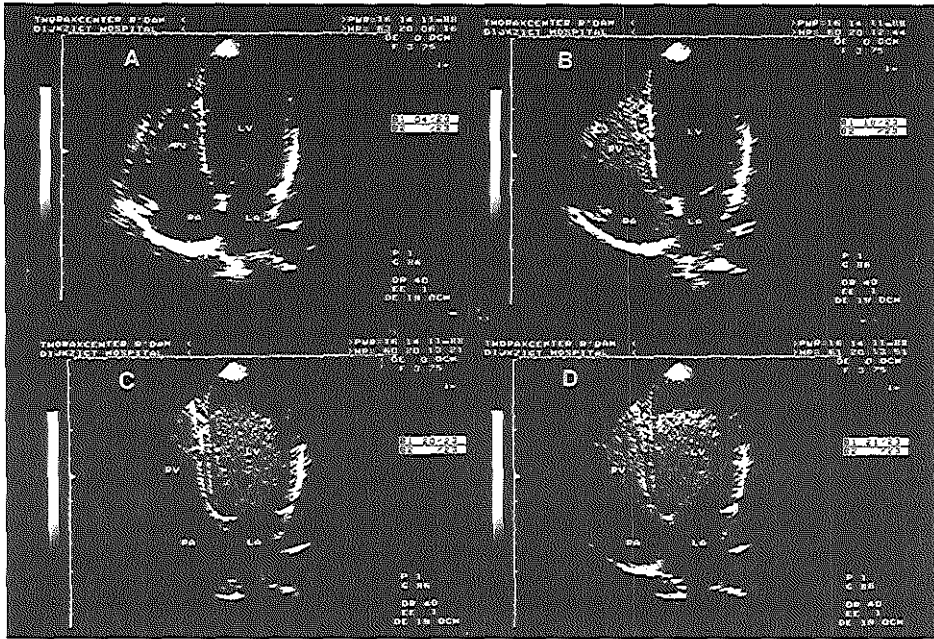


Figure 6-1 Four-chamber view of a normal heart. Panel A, prior to contrast injection; Panel B, contrast in the right ventricle; Panel C, contrast in both left and right ventricle; Panel D, after 30 s the contrast in the right ventricle starts to diminish.

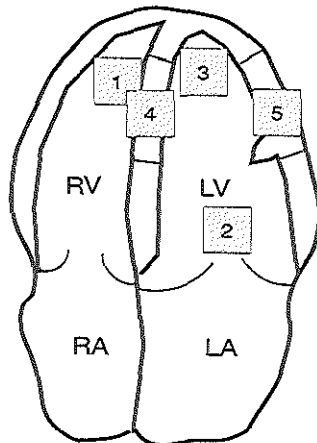


Figure 6-2 Schematic illustrations of the five regions of interest. 1, right ventricular cavity; 2, the inflow part of the left ventricular cavity; 3, the apex of the left ventricular cavity; 4, the middle of the interventricular septal myocardium; 5, and the myocardium of the lateral wall of the left ventricle.

Five regions of interest for each of the 52 acquired video images are identified. Position and orientation of each region can be adjusted independently in all images. It is also possible to change the preset regions of interest in particular images as all information is stored on disk and is always available for re-processing. Measurements are carried out automatically once all regions are defined. Analysis includes measurements of the mean density and deviation in each region as well the corresponding time density curve. All parameters of this curve can be calculated, including the maximum density, density increase and decrease, and area under the curve. The regions of interest are placed in the right ventricular cavity (1), the inflow part of the left ventricular cavity(2), the apex of the left ventricular cavity (3), the middle of the interventricular septal myocardium (4) and the myocardium of the lateral wall of the left ventricle (5) (see Figure 6-2).

When contrast is visually detected, five enddiastolic frames prior to contrast appearance is taken as the start frame. Fifty-two successive enddiastolic frames are then grabbed into the computer for analysis of the time course of contrast appearance and disappearance. Enddiastolic frames are chosen because these images are the most stable and most clearly show the effects of the contrast agent. The computer stores all the measured intensities and constructs a time-density curve of echo contrast appearance and disappearance for the different regions. For each region the mean density is also determined.

The final time-density curve is constructed by subtracting the baseline density. Low pass filtering is performed to smooth the curve. Furthermore, two beats are selected for a frame by frame videodensity analysis in both the left as well as the right ventricle in order to register cyclic variations. For the right ventricle the beats are taken sufficiently long time after injection so that attenuation is minimal. For the left ventricle beats are taken around the time at which peak density occurs.

In vitro studies

Microscopic investigations are performed on Albunex[®] (concentration of the batch used: 3.72 microspheres/ml). Albunex[®] is diluted 1:200 in 5% human serum albumin and placed in a cavity which can be viewed under a microscope. The human serum albumin is air saturated at atmospheric pressure. The pressure inside the cavity can be controlled between 0 and 200 mmHg. A camera is mounted on the microscope to record the images. After placing the cavity with diluted Albunex[®] under the

microscope first recordings are made under ambient pressure, in order to check that the initial conditions of the human serum albumin do not influence the microspheres. After 1 minute a static overpressure of 160 mmHg is applied and the microspheres number and shape are studied visually.

To calculate the influence on the backscatter power of Albunex[®] caused by the sieving action of the lungs the size distribution of the pulmonary capillaries, as described by Hogg¹⁷, is used. Before passing the lungs a typical size distribution of Albunex is assumed, afterwards it is assumed that the larger microspheres have been sieved according to the size distribution of the pulmonary capillaries. The calculated backscatter power is based on the expected size distribution and the theoretical model of an Albunex[®] microsphere. This model theoretically describes the attenuation and scatter properties of a microsphere as described in chapter III and IV and reported by De Jong^{18,19}.

RESULTS

Safety

Two different concentrations of Albunex[®] are used in this study. No abnormalities are detected in the laboratory, electrophysiologic, general physical or neurologic examinations either before, immediately after or three days after the study related to the injection of Albunex[®] or human serum albumin¹⁶.

Videodensitometry

The control injections of 5 % human serum albumin do not show an enhancement of the video density in any region. The contrast effect in all patients as measured in the left and right ventricle cavity is shown in Figure 6-3. The density increases for low doses (injection 2) and for high doses (injection 6) are given. The measurements show that the contrast effect in the right ventricle is always higher than in the left ventricle. Furthermore, Albunex[®] appears in the left ventricle of all subjects at the highest dose, but a positive indication is also apparent at lower dosages. For example, at the lowest dosages with a high concentration of Albunex[®] (injection 2), eight out of ten subjects have a increased density in the left ventricle, although nothing could be detected for two subjects (no's 2 and 9). The negative result in patient no. 9 can be explained by the administration procedure during which a mechanical obstruction occurred in the venous drainage from the left arm.

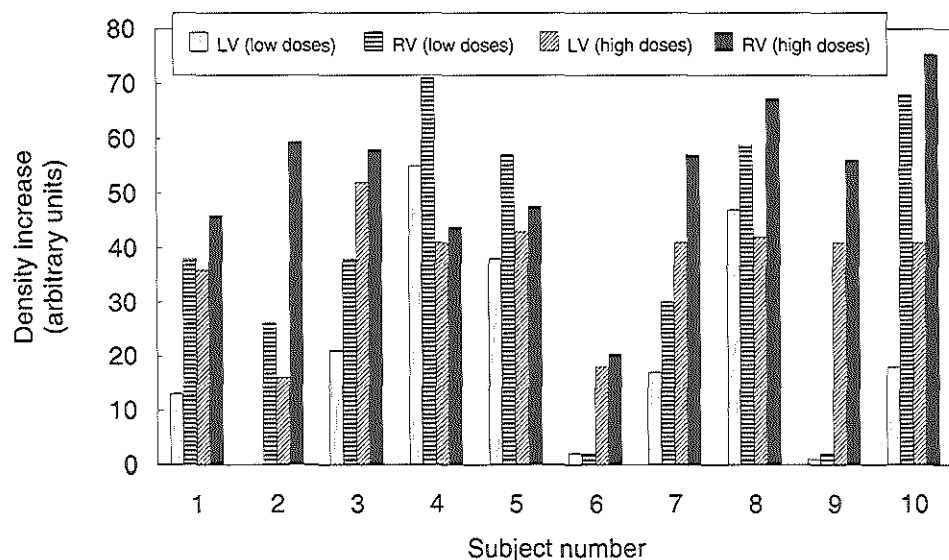


Figure 6-3 The measured density increase in the left and right ventricle after an intravenous injection of Albunex[®] for the 10 subjects studied and for high concentration of Albunex[®] (8.3×10^8 microspheres/ml). □ density increase in the left ventricle after intravenous injection of 0.01 ml Albunex[®]/Kg; ▨ density increase in the right ventricle after intravenous injection of 0.01 ml Albunex[®]/Kg; ▩, density increase in the right ventricle after intravenous injection of 0.04 ml Albunex[®]/Kg; ■, density increase in the right ventricle after intravenous injection of 0.04 ml Albunex[®]/Kg.

An example of the contrast effects as observed in one patient is shown in Figure 6-4. The measured time-density curve is displayed in each box and corresponds to 45 seconds of contrast effect. The different injections are ordered by column while the different regions are ordered sequentially by row. A variety of parameters can be calculated from these recordings such as: time of arrival of contrast area under the curve, peak density, etc.

The density curves from the mid-interventricular septum are difficult to interpret because of "shadowing" by the contrast effect from the left ventricle apex. A small increase in density at the highest dosage is seen in the lateral wall of two subjects, one of which is shown in Figure 6-4.

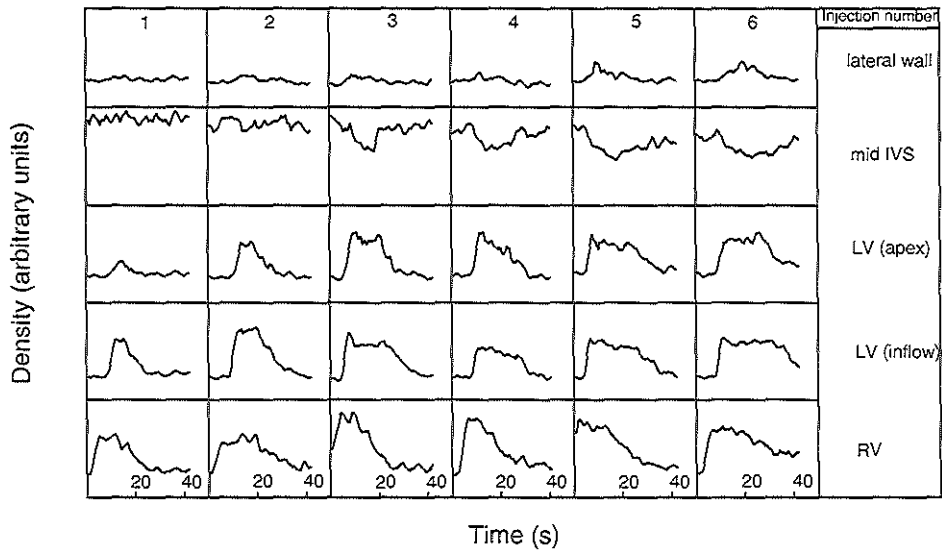


Figure 6-4 Example of measured videodensity curves of one of the subjects for the injections provided (1-6) at the regions of interest studied. Horizontally the injection number is denoted, vertically the region of interest.

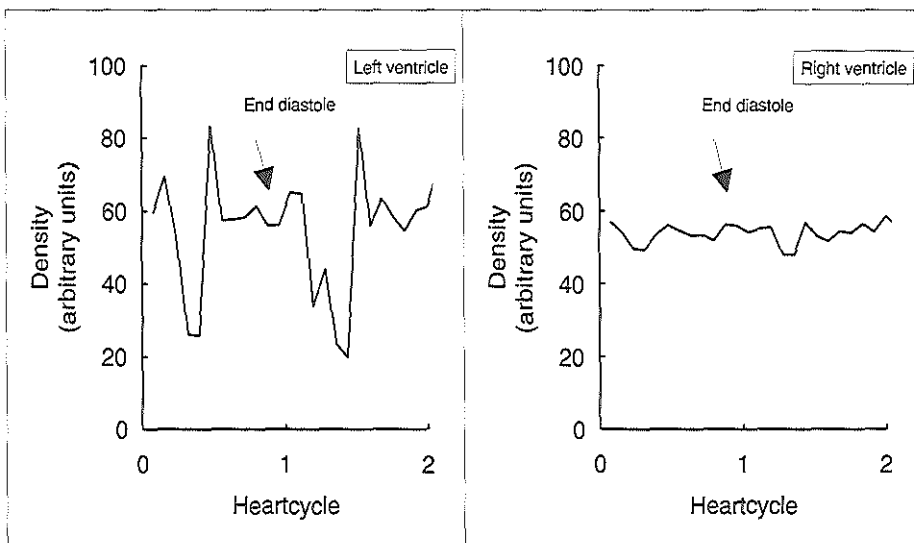


Figure 6-5 Measured videodensity of one of the subjects represented over two entire heart cycles. The left panel shows the videodensity in the left ventricle 20 seconds after injection, the right panel shows the videodensity in the right ventricle 40 seconds after the same injection.

Table VI-b Mean density increase and standard deviation for the 5 region of interest and 6 injections

Region	injection number					
	1	2	3	4	5	6
1	29±17	35± 22	46 ± 23	47 ± 17	47 ± 18	53 ± 15
2	13 ± 14	18 ± 18	24 ± 18	24 ± 14	25 ± 16	33 ± 16
3	7 ± 5	16 ± 14	28 ± 22	25 ± 16	31 ± 19	44 ± 16
4	13 ± 10	8 ± 8	13 ± 5	12 ± 6	13 ± 7	14 ± 8
5	5 ± 4	5 ± 3	7 ± 6	10 ± 13	8 ± 5	11 ± 8

The mean density increase together with their standard deviations for all objects are listed in Table VI-b. The different regions are shown vertically and the injection numbers horizontally. There is an increase in density in regions 1, 2, 3 for nearly all injections, but no significant increase in the measured density in regions 4 and 5. The average density in the right ventricle is higher than that in the left ventricle as already shown in Figure 6-3.

The measured density variation in the left ventricle and right ventricle during two heart cycles of one patient is shown in Figure 6-5. The sampling rate permitted twelve measurements per cardiac cycle. The right ventricle density variation is about five units and is lowest at end-systole. This may indicate that total backscatter is pressure dependent. The same pattern is apparent for the left ventricle density measurements (range 60 units), although the variation is much larger and consistent with the higher pressure variations in the left ventricle.

There is generally a very high attenuation due to the contrast in the right ventricle and this is most apparent at the highest dosages. As a result only a very small band along the edge of the right ventricle could be seen interfering with the visualisation of more distant structures. Attenuation in the right ventricle as high as 60 dB cm⁻¹ is noticed, while in the left ventricle it is generally much less, 1 to 3 dB cm⁻¹. The difference in density increase ranges between 3 and 45 "grey scale" values. This suggests a loss of microspheres during transit between the right and the left ventricles. Furthermore, there is an unexpectedly large variation in the increase in density. This apparent variation among normal subjects might have several causes, including: different Albunex^R characteristics; different physical situation, i.e. subject

dependency; and procedural dependency. The fact that a smaller variability in density values is observed in the left ventricle suggests that the microspheres appearing in the left ventricle are less sensitive to these causative factors. This can be due to the larger microspheres, which would only appear in the right ventricle. Since Albutex[®] requires careful handling, large variations through handling of the product might also occur.

In vitro results

The in vitro studies involve Albutex[®] microspheres diluted 1:200 in 5% human serum

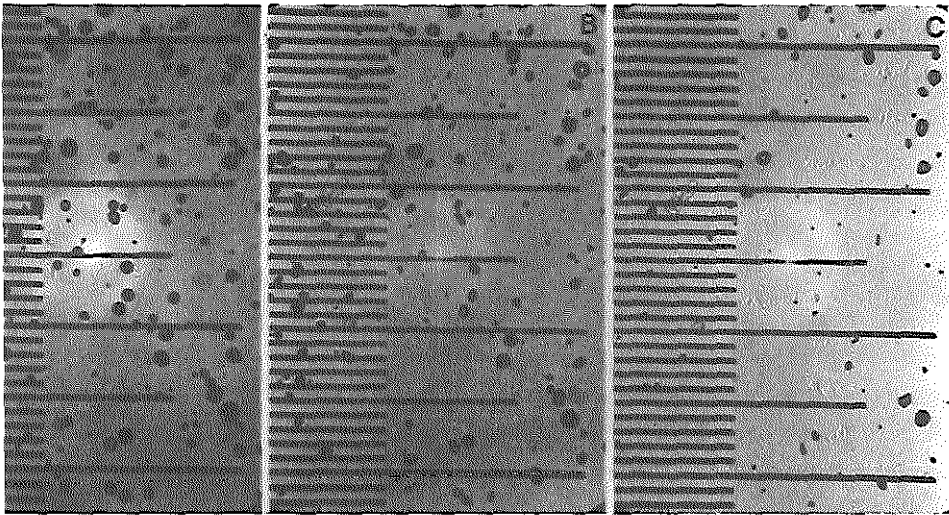


Figure 6-6 Microscopic view of diluted Albutex[®]. A. just before overpressure; B. 1 second after applying an overpressure of 160 mmHg; C. 5 seconds after applying an overpressure of 160 mmHg.

albumin, exposed to overpressures of 160 mmHg. Figure 6-6 shows recordings of the Albutex[®] microspheres just before, 1 and 5 seconds after applying an overpressure of 160 mmHg. Photograph A shows a variety of microspheres sizes, all the microspheres appear more or less spherical. Note that the scale is 10 μ m between the bars and that the larger microspheres are over-represented due to flotation. After 1 second of overpressure photograph B shows that some microspheres have disappeared and that the shape of all the microspheres has changed. This effect is caused by diffusion of the gas inside the microsphere to the surrounding medium.

The overpressure is responsible for an undersaturation of the gas concentration in the fluid and therefore a difference in concentration of gas between the inside and outside of the microspheres. Photograph C shows an almost complete disappearance of the microspheres. The remainder of the microspheres are non-spherical and have a decreased gas content. After approximately 20 seconds all the microspheres have disappeared.

DISCUSSION

A detailed report on the safety and efficacy of Albunex[®] after intravenous injection, in which our center participated, has recently appeared¹⁶.

It is shown that the quantitative analysis of the contrast effect at the left side of the heart after an intravenous injection of Albunex[®] has limitations relating to the stability of the microspheres and the filtering action of the lung capillaries.

An attenuation of the acoustic power of approximately 2 to 3 dB cm⁻¹ at 3.75 MHz due to the microspheres is noted in the left ventricle. In chapter III it is shown that this degree of attenuation occurs for an Albunex[®] dilution of 1:10,000. In the worst case, the 2.5 ml injectate diluted in the blood volume of the human (5 litres) results in a dilution of 1:2,000. According to the known relationship between attenuation and concentration, it can therefore be reasoned that the concentration in the left ventricle is much less than expected. This indicates a loss of microspheres between the right ventricle and left ventricle which may be explained by 3 factors:

- a) Pressure dependency/diffusion of microspheres.
- b) Filtering action of the lungs.
- c) Dilution effect.

The influence of the static ambient pressure on diluted Albunex[®] is examined in the in vitro study, while the in-vivo situation involves a pulsatile system. Cyclic variation in intensities have been reported using sonicated human serum albumin²⁰. The videodensity variation during a cardiac cycle in both the ventricle and especially in the left ventricle indicates a large pressure dependency. The effect of the sieving action of the lungs can be demonstrated with a simulation of the expected backscatter intensity. When Albunex[®] is intravenously injected the lung capillaries will sieve the larger microspheres. The normalised size distribution of the lung capillaries¹⁷ is shown Figure 6-7; capillaries between 4.5 and 5.5 μm are the most prevalent. The mean diameter is around 6 μm . The shaded area in the figure denotes the probability for a particle with a given diameter will pass through these capillaries. For small particles

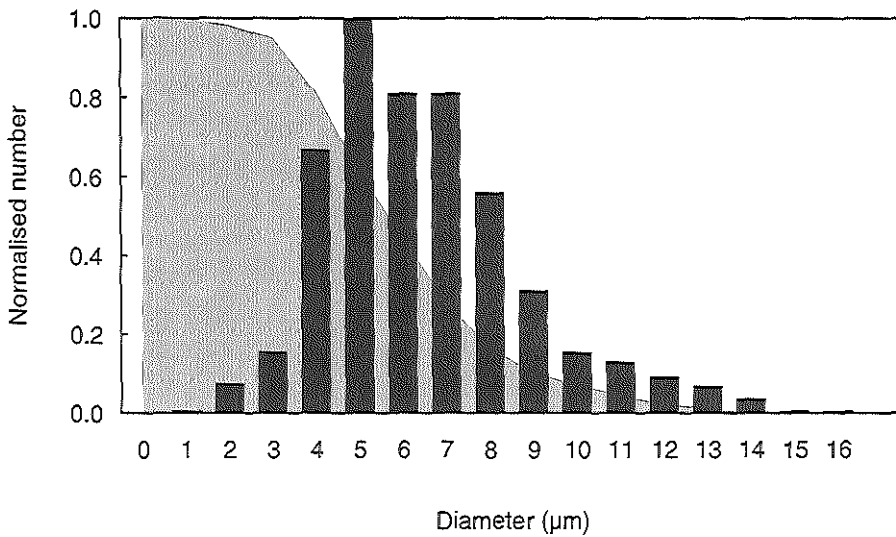


Figure 6-7 Normalised size distribution of lung capillaries¹⁸(bars) and the probability (shaded area) that a microsphere of particular size will pass these capillaries.

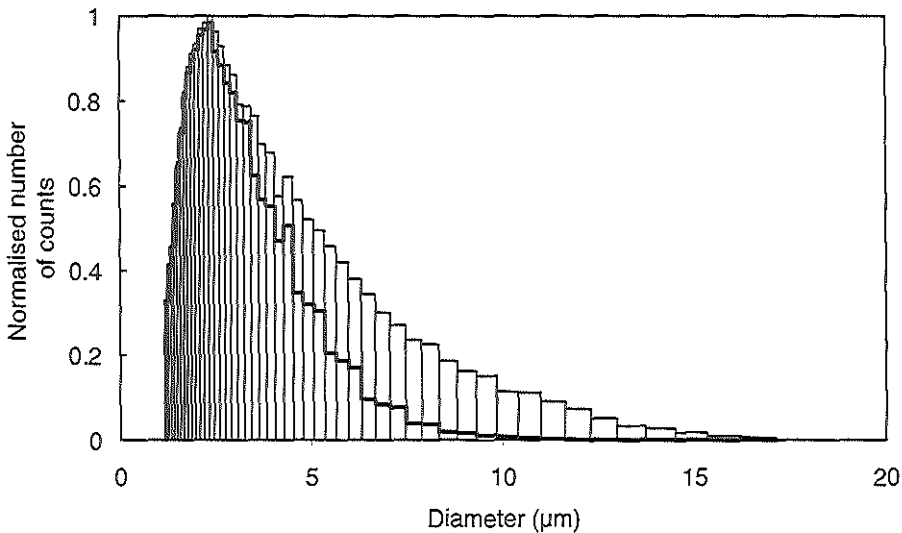


Figure 6-8 Normalised size distributions of Albunex^R as measured with the Coulter counter²⁰ (thin curve) and the calculated size distribution after lung passage assuming the capillary distribution of Figure 6-7 (thick curve).

this probability is equal to 1, for 6 μm about 0.5 and for 10 μm about 0.1. The resulting effect on the size distribution of Albunex[®] is shown in Figure 6-8. The bar diagram gives the normalised number of counts as function of the channel diameter as measured with a Coulter Multisizer II¹⁸. The Multisizer has an aperture of 50 μm employing 64 channels with diameters ranging from 1 to 35 μm . The width of each channel increases for larger channel diameters as indicated in the figure. The thick curve in the figure is calculated assuming a filtering with the properties shown in Figure 6-7 to simulate the sieving action of the lung. The larger microspheres disappear while the number of smaller microspheres remain unaffected. The consequence of this effect on backscattering capacity can be calculated for clinically used frequencies based on the model developed in chapter IV, describing the acoustic properties of Albunex[®] microspheres. The model predicts a 10 dB difference at 2.5 MHz, while for 5 MHz the calculated difference in backscattered power is 5 dB.

Albunex[®] is injected undiluted intravenously. When the microspheres arrive in the heart, the solution is diluted and consequently a decrease in the peak concentration and an increase in contrast duration is measured.

The Albunex[®] microspheres are filled with air which is capable of diffusing through the encapsulation. Venous blood is not saturated for air and furthermore, the gas content changes when flowing towards the heart. Differences in gas concentrations between the microspheres and the surrounding blood will cause diffusion and consequently will change the size of the microspheres.

CONCLUSION

This study shows that an intravenous injection of Albunex[®] results in an echo-density increase in the left ventricle in all subjects at the highest dosages used. In general, there is a major difference between the contrast effect in the left ventricle as compared to the right ventricle. This is due to the disappearance of microspheres, for which the lung filtration effects and the pressure dependency effects of the microspheres are considered to be the most important. This explanation is supported by in vitro experiments and computations based on the known properties of Albunex[®].

References

1. Gramiak R, Shah PM. Echocardiography of the aortic root. *Invest Radiol* 1968;3:356-8
2. Armstrong WF, Mueller TM, Kinney EL, Tickner EG, Dillon JC, Feigenbaum H. Assessment of myocardial perfusion abnormalities with contrast enhanced two-dimensional echocardiography. *Circulation* 1982;66:166-73
3. Kaul S, Pandian NG, Okada RD, Pohost GM, Weyman AE. Contrast echocardiography in acute myocardial ischemia: I. In vivo determination of total left ventricular "area at risk". *J Am Coll Cardiol* 1984;4:1272-82
4. Ten Cate FJ, Drury JK, Meerbaum S, Noordsy J, Feinstein S, Shah PM. Myocardial contrast two-dimensional echocardiography: Experimental examination at different coronary flow levels. *J Am Coll Cardiol* 1984;3:1214-26
5. Tei C, Kondo S, Meerbaum S, Ong K, Maurer G, Wood F, Sakamaki T, Shimoura K, Corday E, Shah PM. Correlation of myocardial echo contrast disappearance rate ("wash-out") and severity of experimental coronary stenosis. *J Am Coll Cardiol* 1984;3:39-46.
6. Keller MW, Glasheen W, Smucker ML, Burwell LR, Watson DD, Kaul S. Myocardial contrast echocardiography in humans II. Assessment of coronary blood flow reserve. *J Am Coll Cardiol* 1988;12:925-34.
7. Cheirif J, Zoghbi WA, Raizner AE, Minor ST, Winters WL, Klein MS, De Bauche TL, Lewis JM, Roberts R, Quinones MA. Assessment of myocardial perfusion in humans by contrast echocardiography. I. Evaluation of regional coronary reserve by peak contrast intensity. *J Am Coll Cardiol* 1988;11:735-43.
8. Keller MW, Glasheen W, Teja K, Gear A, Kaul S. Myocardial contrast echocardiography without significant hemodynamic effect or reactive hyperemia: A major advantage in the imaging of regional myocardial perfusion. *J Am Coll Cardiol* 1988;12:1-39-47
9. Hajducski K, Rajagopalan RE, Meerbaum S, Drury JK, Corday E. Effects of intracoronary administered echo contrast agents on epicardial coronary flow, ecg, and global and regional hemodynamics. *J Cardiovasc Ultrasonogr* 1987;6:84-93
10. Kondo S, Tei C, Meerbaum S, Corday E, Shah PM. Hyperaemic response of intracoronary contrast agents during two-dimensional echographic delineation of regional myocardium. *J Am Coll Cardiol* 1984;149-56
11. Kloster FE, Friesen WG, Green GS, Swan HJC. Effects of coronary arteriography on myocardial blood flow. *Circulation* 1972;46:438-444
12. Feinstein SB, Shah PM, Bing RJ. Microbubble dynamics visualized in the intact capillary circulation. *J Am Coll Cardiol* 1984;4:595-600
13. Ten Cate FJ, Feinstein S, Zwehl W, Meerbaum S, Fishbein S, Shah PM, Corday E. Two-dimensional contrast echocardiography. II Transpulmonary studies. *J Am Coll Cardiol* 1984;3:21-7
14. Meltzer RS, Serruys PW, McGhie J, Roelandt J. Pulmonary wedge injection yielding left sided echocardiographic contrast. *Br Heart J* 1980;44:390-4
15. Keller MW, Feinstein SB, Watson DD. Successful left ventricular opacification following a peripheral injection of a sonicated contrast agent: an experimental evaluation. *Am Heart J* 1987;114:570-5
16. Feinstein SB, Cheirif J, Ten Cate FJ, Silverman PR, Heidenreich P, Dick C, Desir RM, Armstrong WF, Quinones MA, Shah PM. Safety and efficacy of a new transpulmonary ultrasound contrast agent: Initial multicenter clinical results. *J Am Coll Cardiol* 1990;16:316-24
17. Hogg JC. Neutrophil Kinetics and Lung Injury. *Physiological review* 1987; 67; 4

18. De Jong N, Hoff L, Skotland T. and Bom N. Absorption and scatter of encapsulated gas filled microspheres: theoretical considerations and some measurements. *Ultrasonics* 1992; 30; 95-103
19. De Jong N, Hoff L. Ultrasound scatter properties of Albunex[®] microspheres. *Ultrasonics* 1993 31(3) 175-181
20. Shapiro JS, Reisner SA, Lichtenberg GS, Meltzer RS. Intravenous contrast echocardiography with use of sonicated albumin in humans: Systolic disappearance of left ventricular contrast after transpulmonary transmission. *J Am Coll Cardiol* 1990,7 1603-1607

VII

Discussion and conclusions

Abstract

Conventional two-dimensional echographic instrumentation is poorly suited for processing the acoustic scattering signals of echo contrast agents. The special properties of the echo-contrast agents, such as phase information, frequency shifts and second harmonic response require special signal processing in order to optimally visualize the contrast agent. The characteristics of such special 2D contrast echographic instrumentation is described. Furthermore, some proposals are made in order to improve the contrast agent Albunex[®]. Briefly, some of the acoustic properties of two other commercial echo contrast agents, Levovist/Echovist and Ultravue, are described. Finally the state of the art of the video-densitometry is summarized.

The 2D echographic contrast instrument

Clinical contrast echocardiography has been performed hitherto with conventional echographic instrumentation used for cardiac diagnosis in the out-patient clinic, catheterization lab or operating room. These 2D instruments have been considerably improved over the last two decades generating well defined ultrasound scanning planes, with very sensitive transducers and advanced signal processing. The final result is optimally presented on a video monitor in order to obtain images which can be used for clinical decision making. Recent developments in the low diagnostic frequency range from 2-10 MHz, such as Color Coded Doppler and transesophageal echocardiography (TEE) have not changed the essence of 2D echocardiography. Color Doppler is an extension of the already well established single Doppler methodology and it has turned out to be very useful to display the blood velocity information in a more easily interpretable way, i.e. in color mixed with the 2d grey-scale information. The main effort went into the software development, while the hardware could remain unchanged. The introduction of the TEE technique required no adaption or improvement in the echo apparatus itself at that time. It was only the front end, the transducer, which needed to be redesigned in order to make it possible to introduce the transducer into the esophagus to image the heart from the posterior side.

However, intravascular imaging, intracardial and intravascular Doppler, developed only over the last decade and operating in the high diagnostic frequency range, did require completely new developments in both instrumentation and software. Here the principal property of the contrast agent, visualisation of the blood stream, is less important because the high frequency used made it possible already to visualize the blood.

It is believed that contrast agents will be useful especially for the low diagnostic frequency range, e.g. out-patient clinic diagnostic, surgery and catheterization lab where relatively simple methods can deliver much information. Although some experimental echo equipment have been designed¹ to perform rf measurements, and some special purpose software for automatic delineation of the contours of the left ventricle cavity and on-line grey value determination has been developed in the last few years, it is necessary to develop special 2D echographic contrast instrumentation in order to exploit the full range of possibilities of the contrast agents. These possibilities include enhancement of the backscatter, change in frequency content, acoustic velocity change, generation of a second harmonic and omnidirectional scattering.

Design

New 2D echographic contrast instrumentation will consist of three main parts, which is shown schematically in Figure 7-1: 1) the front-end or the acoustic transducer; 2) the hardware; 3) the software or control and signal processing. The transducer generates the acoustic waves and converts the received acoustic energy into electrical signals. The hardware produces the electrical signals for the transducer, amplifies and stores the received echo's. The software controls the hardware and processes the received data. It also controls the format of the displayed image.



Figure 7-1 Schematic drawing of a 2D echographic contrast instrument

1) The acoustic transducer.

The transducer for a two-dimensional system can be either a mechanical or a phased array transducer. A mechanical system consists in principle of only one circular transducer with beam steering performed by a mechanical rotating system. A phased array transducer contains many small elements which are individually connected electrically to, and controlled by, the hardware in order to achieve beam steering. Phased array systems are far more popular than mechanical ones in the field of cardiology. For the sake of simplicity, a mechanical transducer is considered here, but the principle can be easily applied to a phased array system.

The transducer must be sensitive to both the first harmonic as well as the second harmonic frequency. This can be achieved by a combination of two different materials: PZT and PVDF. PZT is the classical Piëzo-electric material and PVDF is a thin plastic. The transducer design is conventional, i.e. the front of the transducer (patient-side) consists of an acoustic lens formed by a material with the same acoustic impedance as water but with a lower velocity. This lens is curved and focuses the ultrasound beam at 5-6 cm axial distance. The PVDF material is mounted adjacent to the lens. Commercially available PVDF has an acoustic impedance of about 3.5 MRays. By choosing the right thickness, this layer can act as 1/4 wavelength matching layer between the PZT material and the medium. The PZT Piëzo material is backed with light, dispersive material to ensure a high sensitivity and a minimum

of false echo's within the transducer. The PZT will be used as both a transmitter and receiver, while the PVDF transducer will act only as a receiver, taking advantage of the good receiving capabilities of the PVDF material. In such a design the PZT ceramic will generate the ultrasonic wave and receive the first harmonic, while the PVDF part will be sensitive for the second harmonic.

Another possible design for such a dual-frequency transducer would be to use two pieces of Piëzo material: one with a conventional resonant frequency and the other twice that. The high frequency transducer would have a circular shape, while the low frequency transducer a ring shape with a inner diameter slightly larger than the high frequency transducer. Each transducer would have its own matching layer, differing only in thickness, and it's own backing which would consist of the same material. The transducers would be mounted such that the front of the matching layers are in one plane and an acoustic lens would cover both transducers. The outer transducer would transmit the acoustic signal and receive the first harmonic, while the inner transducer would receive only the second harmonic. This design has the advantage of lower mechanical coupling between the high and low frequency transducers. The beam profile in this design, however, will be compromised, especially for the low frequency transducer.

2) Hardware

The hardware must generate a high voltage double or triple pulse in order to produce a sinus burst of two or three periods. Two receiving circuits are required; one for the first harmonic and the other for the second harmonic transducer. Due to the complex signal processing requirements, it will be necessary to digitize the received signals at the very front-end. For a mechanical 2D contrast system analog to digital conversion for only 2 receiving channels is necessary but for a phased array system this clearly represents an increase in complexity².

It will be necessary that the demodulated signal be compressed in order to render the 60-80 dB dynamic range of the acoustic signal into the 20-30 dB range of the videoscanned memory and monitor. The raw acoustic lines, digitised in 16 bits words, are corrected for transducer characteristics and applied acoustic energy. This correction would be built into the echoapparatus and determined at fabrication e.g. by a flat plate reference measurement. The received signals can be stored in two different ways for later analysis.

a) Demodulated data of all the acoustic lines.

Considering a scanning depth of 200 μ s (15 cm) and a resolution of 400 points per acoustic line, the data rate will be 2 Mwords per second. This yields 60 Mwords for

a recording of 30 s, which could be stored in RAM memory with a capacity of 120 Mbyte (low-cost, access time 500 ns). Advanced data compression techniques (50% compression) would be applied to each recording and the results transferred to a rewritable optical disk of 600 Mbyte capacity. About 10 half-minute recordings can be stored in this way. Off-line processing can then restore the data and display it in the desired format. The grey scale information with 16 bits resolution is linear and independent of the instrumentation. All the information is available for e.g. background subtraction to be done in the correct way.

b) RF data is stored.

The operator selects a region of interest for recording each frame or ECG triggering is used for storing the whole 2D image. The maximum temporal data rate is 25 M words per second, while the averaged data rate is 1 Mbyte per second after selection has been made. The data is stored in fast RAM (40 ns access time) with a capacity of 1Mbyte. During the interval that no rf data is gathered, the data is transferred to slower RAM to make the faster RAM available for the next cycle. The data is subsequently stored on an rewritable optical disc for later analysis.

3) Software

In principle, the software should be included in the 2D echographic contrast instrument. Nevertheless it may be desirable to perform some time consuming processing off-line. The processing software can be split into four main categories.

- a) Aligning all the images of interest by cross-correlation of the subsequent images. There are two degrees of freedom while working with the acoustic lines; rotation around the insertion point and a translation along the acoustic line.
- b) The conventional gray scale analysis as a function of time. The region of interest can be identified in the first image and the time-density curve calculated over the images of interest with the original dynamic range of 60-80 dB which will be completely linear. The resulting data is independent of the echo apparatus and is directly related to the scattering/reflecting properties of region under consideration.
- c) Fourier transformation of the rf signal. The mean frequency in a region of interest can be calculated from the Fourier data and different regions can be compared in order to determine the frequency dependent attenuation or pressure influences. Phase information from the Fourier transform reveals the acoustic velocity.
- d) Auto-correlation techniques or other special tissue identification software can be implemented. In this case the contrast agent will be used mostly for backscatter enhancement.

Albunex[®]

In this thesis the acoustic properties of Albunex[®] are described together with some clinical experiments. The agent is able to pass the lung capillaries after intravenous injection and gives a good contrast effect in the left ventricle cavity. It will be probably the first on the market with these capabilities. However, Albunex[®] diluted in a saturated liquid and exposed to an overpressure of 160 mm Hg, which can occur in the left ventricle or in the coronary system, has a dramatic effect on the existence of the microspheres. The stability of diluted Albunex[®] under ambient pressure, however, is satisfactory and has been independently confirmed³. The mechanism for the loss of microspheres in vitro is the diffusion of the gas inside the microsphere to the surrounding fluid. Gas concentration differences determine such diffusion rates. In the circulation the gas concentration also varies from the venous site of injection to the left ventricle. The most important components which change are carbondioxide and oxygen. In venous blood the relative contributions are 6 and 5 percent respectively, in the left ventricle cavity 5 and 13 percent⁴. The gas content of the Albunex[®] microsphere is assumed to be that of air, which means ~0% carbondioxide and 21% oxygen. When injected intravenously there is a diffusion gradient for both CO₂ and O₂; the CO₂ will diffuse quickly into the microsphere and O₂ relatively slowly outwards. This results in an increase in the net gas content and thereby an increase in the diameter of the microsphere.

Diffusion of a gas in a liquid is dependent on the velocity of the molecules and the viscosity of the liquid. The velocity of the gas depends on the size of the gas molecules and the temperature. The disappearance of gas bubbles in a saturated liquid is due to the surface tension causing a permanent overpressure inside the bubble, which results in a permanent concentration difference between the inside and outside of the bubble. The shell around the Albunex[®] microsphere however greatly improves longevity by eliminating this surface tension. Also, the shell itself constitutes an additional barrier for the diffusion process. Nevertheless, concentration differences between the inside and outside of the microsphere will eventually destroy the microsphere as the surrounding shell is permeable to air. Nitrogen and oxygen molecules both have a size of about 0.36 nm and are apparently small enough to diffuse through the shell. Replacing the nitrogen and oxygen with another gas of larger molecules should improve the persistence. Possible candidates include inert gasses such as Xenon, which is 50% larger or Sulphur hexafluoride which is about 2 times larger. Exchanging the gas content of existing Albunex[®] requires an accurate control of the gas content of the surrounding liquid. Saturation of the raw product

before manufacturing is only possible with gases which can withstand high temperatures. The gas used will not affect the acoustic properties of the microspheres as long as the gas behaviour can be approximated by an ideal gas.

Ultravue^R

Ultravue^R is a registered trade mark of Delta Biotechnology limited, Nottingham, England. The raw product is recombinant albumin. The product is delivered in a powder form, containing 3×10^8 microcapsules which must be suspended in water. These microcapsules have a diameter range of 3-10 μm and are gas filled. The shell encapsulating the gas has a thickness of 100-200 nm. The product is currently undergoing testing in animal experiments.

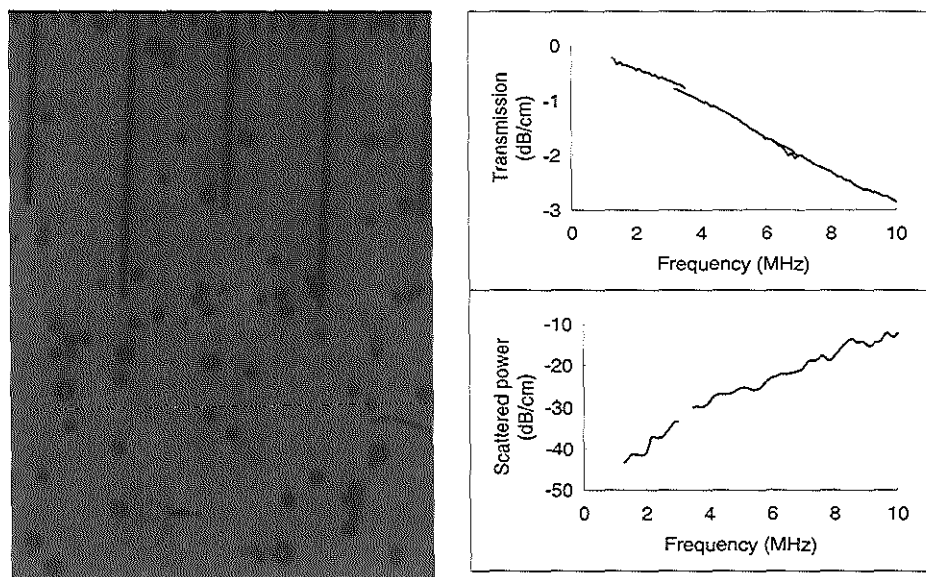


Figure 7-2 Some characteristics of Ultravue^R, 3×10^8 microcapsules are diluted in 600 ml water. Left panel, microscopic view, grid equals 10 μm . Right panel, acoustic transmission and scattered power as function of frequency.

A microscopic view of the microcapsules diluted into 600 ml water is shown in Figure 7-2. It can be appreciated that the average size is below 8 μm . The photograph also shows a certain clustering, but no coagulation is noticed. An undersaturation of the gas concentration in the fluid does not influence the visual appearance of these microcapsules, such as shape and size. Some acoustic

measurements, carried out in the frequency range from 1 to 10 MHz are shown in the right panel of the figure. The transmission measurements demonstrate an increasing attenuation with increasing frequency, indicating that no resonance phenomenon occurs for this frequency range. Any possible resonant frequency will have a relatively high value due to the rigid shell of these microcapsules. The scatter magnitude shows an increasing value for higher frequency, characteristic for particles responding below their resonance frequency.

Echovist^R and Levovist^R

Echovist^R and Levovist^R are registered trademarks of the Schering product SH U 454 and SH U 508A respectively. Levovist^R is the transpulmonary derivative of Echovist^R and is chemically identical to it, apart from a minor galenic modification⁵. The acoustic properties of Levovist^R are described by Schrope⁶ and Schlie⁷. The latter reports only a slight change in acoustic velocity for solutions as concentrated as 200 mg/ml and a peak attenuation at 2.5 MHz. The size distribution of the bubbles is calculated from the attenuation curves, making some simplifying assumptions. This distribution has a maximum value at a diameter of 2.7 μm . In vitro measurements further show a good pressure stability. The echogenicity of Levovist^R decreases only 1 dB per minute under a elevated pressure of 100 mmHg. Schrope reports the presence of a second harmonic for Levovist^R. Echovist^R is a non-transpulmonary agent, which became commercially available in Germany in October 1991. Levovist is now under evaluation in clinical trials.

An in-vitro measurements carried out on Echovist^R is shown in Figure 7-3. The transmission through Echovist^R, after the prescribed preparation of 850 mg in 8.5 ml, is given, as a function of the frequency. Undiluted, it provides an attenuation as high as 100 dB cm⁻¹ at a frequency of 3 MHz. The transmission increases as a function of the frequency, indicating that the dominant bubble sizes have their resonance phenomenon below 1 MHz.

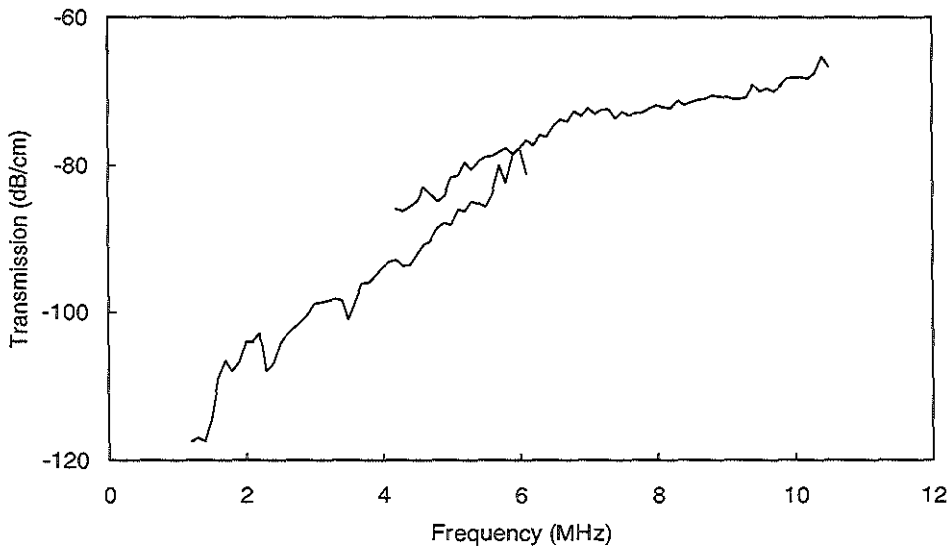


Figure 7-3 *Transmission as a function of frequency for Echovist with a concentration of 100 mg/ml.*

Videodensitometry

Echocardiographic contrast studies of the myocardium should easily detect a regional perfusion deficit. The absence of contrast will be noticeable in the underperfused area when the injected contrast agent provides an enhancement of the backscatter in other areas of the myocardium. In less explicit cases, when less than expected backscatter enhancement occurs or when the contrast washout time is prolonged, no easy diagnosis can be made and there is a need for a more quantitative approach in order to judge the perfusion of the specific area under consideration.

With videodensitometry a time-intensity curve can be constructed in several regions of interest of the myocardium. Such curves show an initial buildup (wash-in), then the backscatter intensity reaches a maximum, and subsequently the contrast is washed out and the backscatter decreases until it reaches its initial value again. In general, these gray-scale values are fitted to an analytical gamma curve of the form $y = A_t(t-t_{in})^s \exp(-\xi(t-t_{in}))$ for $t > t_{in}$, where t denotes the time, t_{in} the time of the start

of appearance of the contrast, and A_t , ζ and ξ the parameters to be estimated. Many clinical studies have been published in the last decade which try to correlate parameters of the measured time-intensity curves with angiographic determined severity of stenosis, pressure drop across a lesion and myocardial bloodflow⁸⁻¹¹. The parameters used in the time intensity curves include: Peak intensity, wash-in time, wash-out time, area under the curve, etc.. These clinical studies are mostly pragmatical; modelling and application of existing indicator dilution theory has only recently been reported^{12,13}.

The principle of the indicator dilution theory, original developed by Stewart and Hamilton, can be described as follows: if the concentration of a uniformly dispersed indicator in an unknown volume is determined, and the total volume of the indicator is also known, then the unknown volume can be determined. This principle results in the following two equation, of which the second can be derived from the first one¹⁴:

$$F = \frac{M_{tot}}{\int_0^{\infty} C(t) dt} \quad \text{[VII-1]}$$

and

$$V = F \bar{t} \quad \text{[VII-2]}$$

F = flow
 M_{tot} = injected indicator
 $C(t)$ = concentration of the contrast as function of time
 V = volume
 \bar{t} = mean transit time

An extensive discussion of these equations is outside the scope of this paragraph, but some remarks need to be made in order to stress the importance of these basic equations for interpretation of the video contrast time-intensity curves.

For a one-input multiple-output system, it can be shown that the time integral of the concentration of each output is equal and equal to the quotient of input flow and total injected indicator¹⁴ according to equation [VII-1]. For contrast echocardiography which receives the backscatter of a certain volume of tissue containing multiple channels with blood containing the contrast, that this integral denotes the blood volume. In this way the blood volume of different parts of the tissue can be compared.

Equation [VII-2] represent the relationship between flow, volume of a tract and the mean transit time of the tracer through the tract. When the contrast is injected as a bolus, \bar{t} can be calculated from the contrast-time curve measured at the end of the tract. When the blood volume is known flow can be calculated according to equation [VII-2]. When the injection can not be considered as a bolus, the input time-concentration curve has to be determined and a deconvolution of the output time-concentration curve has to be performed. No information is necessary about the absolute concentration of the tracer.

The real situation is much more complicated. The blood volume is not easy to determine, and it changes during the cardiac cycle. It is necessary to make certain assumption about stagnant volumes, and the determination of \bar{t} is affected by noise especially at low flow values. Deconvolution with the input signal is also noise sensitive and besides, it is necessary to measure this input function. The application of equation [VII-1] requires that the amount of injected contrast is known and that it remain stable during the measurement. Furthermore, the received acoustic signal from the contrast agent has to be recalculated in terms of the concentration of the agent.

Videodensitometry also has a number of pitfalls, but these can be easily resolved. First, until now it has been difficult, if not impossible, to compare data from one center with another. The measured gray-scale values are equipment dependent and non-linear with respect to the backscatter properties of the medium of interest. This can be easily overcome by storing the data in a linear format and correcting for transducer characteristics and electronics, as described in the first paragraph of this chapter. The data can be stored on small removable optical discs. Second, the analysis is hampered by the motion of the heart. The specification of the regions of interest must be monitored possibly repositioning for each frame to be analysed. This can be automated by image processing techniques or by contour detection. In general, the motion of the heart can be eliminated by aligning the images. Cross-correlation of sequential images for establishing the optimal alignment is time consuming, but can be optimised by using special processors and by developing a good search strategy.

It has already been shown that the current contrast agents can serve as a blood tracer¹⁵. With an improved 2D echomachine capable of measuring the scattered power of the contrast agent and with the known acoustic properties of the agent, fundamental approach to these time intensity-curves in order to determine regional perfusion of the myocardium.

Final Conclusion

Contrast echography will play an increasingly important role in the near future, both within the field of cardiology as well as other areas of medicine. The understanding and exploitation of the characteristics of the echo contrast agents will be essential to this process. At the moment no commercial contrast agent fulfils the ultimate goal: detection in the myocardium after intravenous injection. This thesis describes the acoustic properties of several contrast agents, especially Albunex[®], which are important for further improving and exploiting the unique properties of gas bubbles or encapsulated gas filled microspheres. A whole generation of 2D echographic instrumentation is necessary to exploit these unique properties and will open the possibility of obtaining new and clinically significant information.

References

1. Monaghan, M.J. Metcalfe, J.M. Baker, J.H. Jewitt, D.E. Detection of myocardial contrast using backscatter spectral frequency analysis. *Eur Heart J* 1990; 11; 113
2. De Jong, N. Mittertreiner, W.H., Ligtoet, K.M. and Ten Cate, F.J. A computerized system that uses high-frequency data for analysis of myocardial contrast echocardiograms. *J Am Soc Echo* 3 1990 99-105
3. Bleeker H.J., Shung K.K. and Barnhart J.L. Ultrasonic characterization of Albunex[®], a new contrast agent. *J. Acoust. Soc. Am.* 87(4) 1990
4. Despopoulos, A. and Silbernagl, S. Color atlas of physiology. 1986 Thieme Verlag Stuttgart-New York
5. Schlieff, R. Ultrasound contrast agents. *Current Opinion in Radiology* 3 1991 198-207
6. Schroepe, B. Newhouse, V.L. and Uhlendorf, V. Simulated capillary blood flow measurements using a nonlinear ultrasonic contrast agent. *Ultrasonic Imaging* 14(2) april 1992
7. Schlieff, R. Schürmann, R. Balzer, T. Zomack, M. and Niendorf, H.P. Saccharide based contrast agents. In: *Advances in echo imaging using contrast enhancement*. Nanda, N. and Schlieff, R. (eds.) 1993 Kluwer Academic Publishers Dordrecht, The Netherlands
8. Ten Cate F.J., Serruys P.W., Huang H, de Jong N, Roelandt J. Is the rate of disappearance of echo contrast from the interventricular septum a measure of left anterior descending coronary artery stenosis? *European Heart Journal* 1988;9:728-833
9. Reisner, S.A. Ong, L.S. Lichtenberg, G.S. et al. Quantitative assessment of the immediate results of coronary angioplasty by myocardial contrast echocardiography. *J Am Coll Cardiol* 13 1989 852-56
10. Cheiriff J, Zoghbi W.A., Raizner A.E., et al. Assessment of myocardial perfusion in humans by contrast echocardiography, I: Evaluation of regional coronary reserve by peak contrast intensity. *J Am Coll Cardiol* 1988;11:735-743

11. Kaul, S. Kelly, P. Oliner, J.D. Glaseen, W.P. Keller, M.W. and Watson, D.D. Assessment of regional myocardial blood flow with myocardial contrast two-dimensional echocardiography. *J Am Coll Cardiol* 1989 13 468-82
12. Heidenreich, P.A. Wiencek, J.G. Zaroff, J.G. Aronson, S. Segil, L.J. Harper, P.V. and Feinstein, S.B. In vitro calculation of flow by use of contrast ultrasonography. *J. Am. Soc. Echocardiography* 1993 (1) 51-61
13. Kessler, A.C. Toepasbaarheid van 2D-echocardiografie voor het schatten van lokale flowwaarden. Thesis Technical University Delft 1992 (In Dutch)
14. Trautman, E.D. and Newbower, R.S. The development of indicator-dilution techniques. *IEEE Transactions on Biomedical Engineering* 1984 (12) 800-807
15. Keller MW, Glasheen W, Teja K, Gear A, Kaul S. Myocardial contrast echocardiography without significant hemodynamic effect or reactive hyperemia: A major advantage in the imaging of regional myocardial perfusion. *J Am Coll Cardiol* 1988;12:1-39-47

Summary

The diagnostic applications of ultrasound have soared during the last 20 years. Significant improvements in equipment, as well as advancements in knowledge, have been achieved further confirming the inherent merits of echo-diagnostic techniques. Although different structures in the body can be imaged in a non-invasive way, blood itself remains very difficult to detect by ultrasound; the red blood cells although large in number, scatter very little ultrasonic energy. While blood flow in the large vessels (e.g. aorta, and left and right ventricle) can be visualized with the aid of the Doppler effect, the blood flow in the coronary system of the heart can be barely discerned. If this could become possible, for example through the administration of an echo-contrast agent, a considerable extension of the field of diagnostic ultrasound could be achieved. The acoustic properties of echo-contrast agents in this context are further explored in this thesis.

A review of the historical development of cavitation effects and negative pressures in fluids is presented in chapter I, for which the mathematical development serves as a basis for the current understanding of echo-contrast materials. Furthermore, several potential clinical applications in the field of cardiology are presented. The determination of myocardial perfusion after intravenous injection of the contrast agent is the most important of these. A number of commercially available materials are described as well as some more prosaic home-made echo-contrast agents.

The potential possibilities of contrast agents are examined in greater detail in chapter II. First, the acoustic backscatter properties of small gas bubbles is compared with those of solid particles of the same dimensions. The properties of gas bubbles in solution are then investigated. The specific properties of gas bubbles which influence transmission velocity, resonance behaviour, emission of higher harmonics and an increase of the backscattered energy is described. These characteristics, for instance, open the possibility of non-invasive determination of local pressures in the heart and the construction of two-dimensional echo-images for which the area containing only the contrast agent is visualized.

The ultrasonic attenuation and scattering of Albunex[®] is described in chapter III. Albunex[®] is a commercial contrast agent which is marketed in Europe by Nycomed, Norway. This agent consists of encapsulated air bubbles with a mean diameter of 3-4 μm , of which 95% are smaller than 10 μm in diameter. A theoretical model for this contrast agent is developed and tested experimentally by attenuation studies in the frequency range 700 kHz to 8.5 MHz.

The model is further developed in chapter IV, in order to also describe the backscatter properties of this contrast agent. The upper frequency range is extended from 8.5 to

12.5 MHz and the scatter and attenuation properties determined as a function of the size of these encapsulated air bubbles. This section is concluded with a determination of the ideal size of an Albunex[®] microsphere, based on minimal attenuation and maximal scattering.

Theoretical aspects of the nonlinear acoustic behaviour of air bubbles and encapsulated air bubbles are described in chapter V. The nonlinear effects of gas bubbles, at an acoustic pressure of 50 kPascal, is 100 times greater than that of encapsulated gas bubbles such as Albunex[®]. Nevertheless, it is shown experimentally that higher harmonic components, which originate in the scattered signal of Albunex[®], can be easily measured. Furthermore, a one-dimensional experiment is performed in which the backscattered acoustic energy from a medium with contrast agent, solid particles and a plate reflector is analyzed. Two A-modes are calculated; a conventional one with all objects in the medium, and a "second harmonic" signal in which only the contrast agent is visible.

Chapter VI contains results of a clinical study using the contrast agent Albunex[®] administered intravenously in which it is shown that this contrast agent has no apparent side effects. The measurements indicate that the contrast effect is smaller than would be expected from in-vitro measurements, and that there is a considerable difference between the effects observed in left and right ventricle. Possible explanations such as diffusion, lung filtration, and pressure differences between left and right ventricle are examined and tested by in-vitro experiments.

A general discussion, reviewing the current state of development and the major conclusions is presented in chapter VII. A description of what a 2D echo contrast apparatus should look like is given. Among other possibilities, such a machine could provide instantaneous pressure measurements, simultaneous conventional and contrast images, and linear grey scale measurements. Furthermore, suggestions are made for improving the properties of Albunex[®]. The merits of other commercial contrast agents, for example Lechovist[®]/Levovist[®] and Ultravue[®], are briefly described in this context. Finally the value of the presently known parameter set used for quantifying the contrast effect, i.e the time-intensity curve are discussed and suggestions are made for a more fundamental approach.

Samenvatting

De diagnostische toepassingen van ultrageluid hebben de laatste 20 jaren een enorme vlucht genomen. Apparatuur en kennis zijn, door de grote waarde die aan echo-diagnostiek wordt gegeven, sterk verbeterd. Met behulp van ultrageluid kunnen verschillende structuren in het lichaam niet invasief worden weergegeven. Bloed echter is met ultrageluid heel moeilijk te detecteren omdat de bloedplaatjes, alhoewel groot in aantal, weinig scatteren. Met behulp van het Doppler effect kan alleen maar de bloedstroming in de grote bloedvaten worden weergegeven, bijvoorbeeld in de aorta en linker- en rechter ventrikel. De bloedvoorziening in het coronaire stelsel van het hart kan niet of nauwelijks zichtbaar worden gemaakt. Toediening van een echocontrastmiddel, dat dit wel mogelijk maakt, zou een aanzienlijke uitbreiding betekenen van de diagnostische ultrageluids toepassingen. In dit proefschrift worden de akoestische eigenschappen van echocontrastmiddelen onderzocht.

In hoofdstuk I wordt eerst een historisch overzicht gegeven over cavitatie effecten en negatieve drukken in vloeistoffen, waarvan de mathematische beschrijving als grondslag dient voor de huidige echocontrast vloeistoffen. Verder worden de potentiële klinische toepassingsmogelijkheden binnen de cardiologie gegeven, waarvan bepaling van myocardial perfusie na intraveneuze injectie van het contrastmiddel de belangrijkste is. Een aantal commerciële middelen wordt kort beschreven, naast een aantal home-made echocontrastmiddelen.

In hoofdstuk II wordt ingegaan op potentiële mogelijkheden van contrastmiddelen. Eerst worden de akoestische backscatter eigenschappen van kleine gasbellen vergeleken met die van vaste deeltjes van dezelfde afmeting. Vervolgens wordt van gasbellen het oplossen in een vloeistof onderzocht. De voor gasbellen specifieke kenmerken zoals beïnvloeding van de ultrageluidssnelheid, resonantiegedrag, emissie van hogere harmonische en verhoging van de backscatter worden beschreven. Deze kenmerken openen bijvoorbeeld de mogelijkheid van het niet-invasieve bepalen van lokale drukken in het hart en constructie van 2-dimensionale echobeelden waarin alleen de aanwezigheid van het contrastmiddel wordt weergegeven.

In hoofdstuk III worden ultrageluidsverzwakking en scattering van Albunex^R behandeld. Albunex^R is een commercieel contrastmiddel dat in Europa op de markt wordt gebracht door Nycomed, Noorwegen. Dit contrastmiddel bestaat uit ingekapselde luchtbelletjes met een gemiddelde diameter van 3-4 μm en waarvan 95% kleiner is dan 10 μm . Een theoretisch model voor dit contrastmiddel wordt opgezet en getoetst aan experimenteel verkregen resultaten van de ultrageluidsverzwakking in het frequentie bereik van 700 kHz tot 8.5 MHz.

In hoofdstuk IV wordt het model verder uitgebreid om ook de scatter eigenschappen van dit contrastmiddel adequaat te kunnen beschrijven. Het frequentiebereik is uitgebreid van 8.5 naar 12.5 MHz. De scatter en verzwakkingsmetingen zijn uitgevoerd als functie van de grootte van deze ingekapselde luchtbelletjes. Conclusie wordt getrokken met betrekking tot de ideale grootte van een Albunex^R microsphere uitgaande van een minimale verzwakking en een maximale scattering.

In hoofdstuk V wordt het niet lineaire akoestische gedrag van luchtbell en ingekapselde luchtbell en eerst theoretisch beschreven. Het niet lineaire effect van gasbell en is bij akoestische drukken van 50 kPascal een factor 100 groter dan van ingekapselde gasbell en, zoals bijvoorbeeld Albunex^R. Experimenteel wordt aangetoond dat hogere harmonische componenten, die ontstaan in het gescatterde signaal van Albunex^R, meetbaar zijn. Verder wordt een 1-dimensionaal experiment uitgevoerd waarin de terug-gescatterde akoestische energie uit een medium met contrastmiddel, vaste deeltjes en een plaatreflector wordt geanalyseerd. Twee A-modes worden berekend; een conventionele met alle objecten in het medium, en een "tweede harmonische" waarin alleen het contrastmiddel zichtbaar is.

In hoofdstuk VI wordt een klinische studie beschreven met het contrastmiddel Albunex^R, dat intravenous wordt toegediend. Deze studie laat zien dat dit contrastmiddel geen bijwerkingen heeft. Metingen tonen verder aan, dat het contrast effect kleiner is dan verwacht mag worden uit in-vitro metingen en dat er een aanzienlijk verschil is tussen de effecten in linker- en rechterventrikel. Mogelijke verklaringen zoals diffusie, longfiltratie en drukverschillen tussen linker- en rechterventrikel worden aangegeven en gestaafd met in-vitro experimenten.

In hoofdstuk VII wordt beschreven hoe een 2D echocontrast-machine er uit dient te zien. Met zo'n machine kunnen o.a instantane drukmetingen worden uitgevoerd, simultaan conventionele en contrastbeelden worden gemaakt en lineaire grijswaarde metingen worden uitgevoerd. Verder worden er suggesties gedaan voor verbetering van Albunex^R en worden kort de merites van andere commerciële contrastmiddelen, Lechovist^R/Levovist^R en Ultravue^R, beschreven. Tenslotte wordt de waarde van de huidige parameters die gebruikt worden bij het quantificeren van het contrast effect, in casu de tijd-intensiteits curve, beschreven en worden er suggesties gedaan voor een fundamenteelere aanpak.

List of symbols

A	radius of the transducer	m
A(t)	amplitude of the time domain signal	
A _{corr} (t)	corrected amplitude of the time domain signal	
A _L (f)	attenuation in lossless medium	m ⁻¹
A _R	amplitude term	m ²
b	1/Γ, Γ polytropic coefficient	
B/A	nonlinear parameter of the medium	
c	acoustic velocity	m s ⁻¹
C ₀	saturation concentration of gas in a liquid	mol m ⁻³
C _g	thermal conductivity	W m ⁻¹ K ⁻¹
C _i	dissolved gas concentration in a liquid	mol m ⁻³
C _{pg}	specific heat of a gas at constant pressure	J kg ⁻¹ K ⁻¹
C _p	specific heat at constant pressure	J kg ⁻¹ K ⁻¹
C _v	specific heat at constant volume	J kg ⁻¹ K ⁻¹
d	distance	m
D	diffusion constant air-water	m ² s ⁻¹
dS	cross-sectional area of volume element	m ²
d _T	(R _g T C ₀)/P _h	
dx,dz	length of a volume element	m
E	Young's modulus	N m ⁻²
F _{fric}	frictional force	N
f	frequency	s ⁻¹
f _r	resonant frequency	s ⁻¹
G	shear modulus	N m ⁻²
I	intensity of acoustic field	W m ⁻²
I ₀	incident intensity of acoustic field	W m ⁻²
I _s	backscattered intensity	W m ⁻²
k	angular wave number	m ⁻¹
K	bulk modulus	N m ⁻²
k ₁ ,k ₂	constants	
m	effective mass of bubble-liquid system	kg
n	concentration of scatterers	m ⁻³
N	number of scatterers	
P	pressure	N m ⁻²
P _a	pressure inside the bubble	N m ⁻²
p _b	pressure outside the bubble	N m ⁻²
p _{ac}	applied acoustic pressure	N m ⁻²

p_{go}	initial gas pressure inside the bubble	$N\ m^{-2}$
P_h	ambient pressure	$N\ m^{-2}$
p_{lo}	atmospheric pressure	$N\ m^{-2}$
P_R	power received by the transducer	W
P_s	scattered power	W
P_T	total transmitted power	W
p_v	vapour pressure	$N\ m^{-2}$
ΔP	pressure change	$N\ m^{-2}$
r	distance	m
R	instantaneous bubble radius	m
R_0	initial radius of bubble	m
R_a	internal radius of bubble	m
R_b	external radius of bubble	m
R_g	universal gas constant	$J\ K^{-1}\ mol^{-1}$
R_{max}	maximum radius	m
R_{min}	minimum radius	m
S_a	stiffness of the bubble-liquid system	$N\ m^{-1}$
S_f	shell friction parameter	$N\ m^{-1}$
S_p	shell elasticity parameter	$kg\ s^{-1}$
t	time	s
T	temperature	K
t_w	wall thickness	m
u	radial displacement of the bubble	m
v_m	volume concentration of the mixed component	
v_g	volume concentration of the gas	
V	volume	m^3
ΔV	volume change	m^3
z	distance to transducer	m
\dot{R}	first time derivative of the radius	$m\ s^{-1}$
\ddot{R}	second time derivative of the radius	$m\ s^{-2}$
Σ_a	absorption cross-section	m^2
Σ_e	extinction cross-section	m^2
Σ_s	scattering cross section	m^2

α	attenuation coefficient	dB cm^{-1}
β	surface tension coefficient	
γ	C_p/C_v	
Γ	polytropic exponent of the gas	
γ_κ	compressibility term	
γ_ρ	density term	
δ_f	damping coefficient due to the friction inside the shell	
δ_{rad}	damping coefficient due to re-radiation	
δ_t	total damping coefficient coefficient	
δ_{th}	damping coefficient due to heat conduction	
δ_{vis}	damping coefficient due to viscosity of the liquid	
η	viscosity	N s m^{-2}
κ	compressibility of medium	$\text{m}^2 \text{N}^{-1}$
κ_d	compressibility of a scattering particle	$\text{m}^2 \text{N}^{-1}$
κ_g	the compressibility of the gas	$\text{m}^2 \text{N}^{-1}$
κ_m	compressibility of the mixed component	$\text{m}^2 \text{N}^{-1}$
κ_w	compressibility of the original component	$\text{m}^2 \text{N}^{-1}$
λ	wavelength	m
ν	Poisson ratio	
ρ	density	kg m^{-3}
ρ_d	density of a scattering particle	kg m^{-3}
ρ_g	density of a gas	kg m^{-3}
ρ_m	density of the mixed component	kg m^{-3}
ρ_w	density of the liquid	kg m^{-3}
σ	surface tension	N m^{-1}
ω	angular frequency	s^{-1}
ω_r	angular resonant frequency	s^{-1}

Acknowledgements

Contrast echocardiography started as a project sponsored by the Dutch Heart Foundation at the Erasmus University in Rotterdam in 1986. The project was initiated by Folkert ten Cate who had earlier worked closely together with Steve Feinstein in the USA. Cees Ligtoet was initially responsible for the technical development. After he left, I became involved and fundamental research was carried out in close cooperation with Wim Mittertreiner, while clinical experiments were done by Folkert Ten Cate assisted by Jan Hein Cornel. In 1988 the first contact were made with Karin Frislid and Thor Arne Gronnerod from Nycomed Imaging, Norway. They sponsored most of the fundamental research on contrast agent from the beginning of 1990. My stay at the research and development department at Nycomed in the summer of 1990 and the winter of 1991 was very pleasant and fruitful. The discussion with Cath Cristiaansen, Lars Hoff and Tore Skotland resulted in a more profound knowledge of the material.

From the Erasmus University, I want to acknowledge Klaas Bom for his never ending enthusiasm for new innovating developments, Charles Lancée for his criticism, Ronald Cornet for his contribution to understand the acoustic behaviour of the contrast agent, Leo Bekkering for his ability to convert vague ideas into useful mechanical measurement modules, Frits Mastik, who accompanied me partly in 1990 during my stay in Norway, for his computer assistance and Wim Vletter for his skill at making magnificent echocontrast images.

Further, I want to thank Corrie Eefting and Yvonne van der Steen for solving all kinds of problems, Ria Eldering for her assistance and for offering coffee every time I entered her office, Elma Gussenhoven, Meindert Taams and Hongkie The, with whom I closely worked together in early days, Jan Honkoop, Kie Djoa, Pieter Brommersma, Harm ten Hoff, Hans Rijsterborgh, Li Wenguang and Frans van Egmond for their general presence, which made the time at the department challenging and the work interesting. Finally, I want to thank Ron Brower for his suggestions and Jos Roelandt and Piet Verdouw for their contribution to the contrast project.

Publikations of the author

1. **De Jong N**, Klumper JW, Groen FCA, Verbeek PW. The smallest box around a package. *Pattern Recognition* 14: 173-178, 1981.
2. Lancée CT, Ligtoet CM, **De Jong N**. On the design and construction of a transesophageal scanner, In: Hanrath P, Bleifeld W, Souquet J (eds) Cardiovascular diagnosis by ultrasound. Transesophageal, computerized, contrast, Doppler echocardiography. Martinus Nijhoff Publishers, The Hague/Boston/London: 260-269, 1982.
3. **De Jong N**, Souquet J, Faber G, Bom N. Transducers in medical ultrasound: part two. Vibration modes, matching layers and grating lobes, *Ultrasonics* 23: 176-182, 1985.
4. Wells PNT, **De Jong N**, Bom N, Somer J. Transducers in medical ultrasound. Part 4: transducer safety, *Ultrasonics* 24: 230-232, 1986.
5. Gussenhoven EJ, Van Herwerden LA, Roelandt J, Bos E, **De Jong N**. Detailed analysis of aortic valve endocarditis: comparison of precordial, esophageal and epicardial two-dimensional echocardiography with surgical findings, *J Clin Ultrasound* 14: 209-211, 1986.
6. Gussenhoven WJ, Bos E, Roelandt J, Van Herwerden L, Haalebos M, **De Jong N**, Ligtoet CM. Transösophageale und intraoperative zweidimensionale Echokardiographie, In: Erbel R, Meyer J, Brennecke R (eds) Fortschritte der Echokardiographie. Springer-Verlag, Berlin/Heidelberg/New York/Tokyo: 231-237, 1985.
7. Bom N, Lancée CT, **De Jong N**, Ligtoet CM. Diagnostic ultrasound: history, transducers, artefacts and new applications, In: Berkhout AJ, Ridder J, Van der Wal LF (eds) Acoustical imaging, volume 14. Plenum Press, New York/London: 397-403, 1985.
8. **De Jong N**, Lancée CT, Gussenhoven WJ, Bom N, Ligtoet CM. Trans-esophageal echocardiography, *Med Biol Engng Comp* 23, Suppl Part 1. Proc of the XIV Int Conf on Med and Biol Engng and VII Int Conf on Med Phys, Aug 11-16, 1985, Espoo, Finland: 204-205, 1985.

9. **De Jong N**, Lancée CT, Gussenhoven WJ, Bom N, Ligetvoet CM. Transoesofagale echocardiografie, *Ultrasonoor Bull* 2: 28-31, 1985.
10. **De Jong N**, Bom N, Lancée CT. Esophageal echocardiography, IEEE, Eighth Annual Conference of the Engineering in Medicine and Biology Society CH2368-9: 3-6, 1986.
11. **De Jong N**, Den Ouden A, Brinkman JF, Niesing R, Lancée CT, Bom N. A multiwire saw for the production of ultrasound transducers, *J Phys E Sci Instrum* 20: 1457-1461, 1987.
12. Lancée CT, **De Jong N**, Bom N. Design and construction of an esophageal phased array probe, *Med Progr Technol* 13: 139-148, 1988.
13. Gussenhoven EJ, Taams MA, Roelandt J, Bom N, Honkoop J, **De Jong N**, Ligetvoet CM. Oesophageal echocardiography, *Int J Cardiac Imag* 2: 231-239, 1987.
14. Bom N, Lancée CT, **De Jong N**, Slager CJ. Special transducers, *Chinese Journal of Ultrasound in Medicine* (1988) 4: supp. 12-5.
15. Bom N, Lancée CT, Slager CJ, **De Jong N**. Ein Weg zur intraluminären Echoarteriographie, *Ultraschall* 8: 233-236, 1987.
16. **De Jong N**, Den Ouden A, Brinkman JF, Niesing R, Lancée CT, Bom N. Een draadzaag voor het produceren van ultrageluidstransducenten, *Mikroniek* 27: 135-139, 1987.
17. Bom N, **De Jong N**, Gussenhoven WJ, Lancée CT. A transesophageal probe for cardiac imaging, In: Bondestam S, Alanen A, Jouppila P (eds) EUROSON '87. Proc Sixth Congr Eur Fed Soc Ultrasound Med Biol. Finnish Society for Ultrasound in Medicine and Biology, Helsinki: 287, 1987 (Abstr).
18. Gussenhoven WJ, Taams MA, **De Jong N**, Roelandt J, Bom N, The SHK. Transoesofagale echocardiografie, *Gamma* 38: 344-348, 1988.

19. Gussenhoven EJ, Taams MA, Roelandt J, **De Jong N**, Bom N. Transesophageal echocardiography in the outpatient clinic, *J Echocard Ultrason Med (JEMU)* 9: 247-254, 1988.
20. Taams MA, Gussenhoven WJ, Schippers LA, Roelandt J, Van Herwerden LA, Bos E, **De Jong N**, Bom N. The value of transoesophageal echocardiography for diagnosis of thoracic aorta pathology. *Eur Heart J* 9: 1308-1316, 1988.
21. Ten Cate FJ, Widimsky P, Serruys PW, **De Jong N**, Mittertreiner WH, Roelandt JRTC. Myocardial contrast two-dimensional echocardiography: initial observations during cardiac catheterization. *Am J Noninvasive Cardiol* 2: 238-243, 1988.
22. Taams MA, Gussenhoven EJ, Cahalan MK, Roelandt JRTC, Van Herwerden LA, The HK, Bom N, **De Jong N**. Transesophageal Doppler color flow imaging in the detection of native and Björk-Shiley mitral regurgitation. *J Am Coll Cardiol* 13: 95-99, 1989.
23. Lancée CT, **De Jong N**, Gussenhoven WJ, Taams M, Bom N, Brommersma P, Roelandt JRTC. Technological developments of transesophageal echocardiography in a historical perspective, In: Erbel R, et al. (eds) *Transesophageal echocardiography*, Springer Verlag, Berlin/Heidelberg: 3-12, 1989.
24. Ten Cate FJ, **De Jong N**, Mittertreiner W, Serruys PW, Roelandt J. Myocardial contrast two-dimensional echocardiography. *Int J Cardiac Imag* 4: 53-56, 1989.
25. Gussenhoven WJ, Taams MA, **De Jong N**. Transoesofageale echocardiografie. *Ultrasonoor Bull* 1-89:39-40, 1989.
26. Ten Cate FJ, Serruys PW, Silverman PR, Verdouw PD, **De Jong N**. Current myocardial perfusion echo methodology precludes an accurate assessment of coronary vascular reserve. *J Am Coll Cardiol* 13 No. 2: 116 A, 1989 (abstr.)
27. Ten Cate FJ, Silverman PR, Vletter WB, Mittertreiner W, **De Jong N**, Frisliid K. Dose-echo intensity relations of right and left cardiac chambers after intravenous use of Albunex. *Eur Heart J Supp* September 1989 (abstr.)

28. Ten Cate FJ, Silverman PR, Vletter WB, **De Jong N**, Frislid K, Sutherland G. Safety and efficacy of intravenous albunex[†] injections in humans. Abstracts of the 8th Symposium on Echocardiology, Erasmus University Rotterdam 1989: 87-88.
29. **De Jong N**, Ten Cate FJ, Mittertreiner W. In vitro acoustical behaviour of microparticles used for myocardial echo perfusion. Abstracts of the 8th Symposium on Echocardiology, Erasmus University Rotterdam 1989: 97-98.
30. Erbel R, Engerding R, Daniel W, Mohr-Kahaly S, Rennollet H, Gussenhoven WJ, Sutherland G, Taams M, Visser C, Koolen J, Jaarsma W, **De Jong N**, Roelandt JRTC, Meyer J. Follow-up of aortic dissection by TEE. Abstracts of the 8th Symposium on Echocardiology, Erasmus University Rotterdam 1989: 111.
31. Ten Cate FJ, Cornel JH, Serruys PW, Vletter WB, **De Jong N**, Mittertreiner WH. Drainage of Myocardium by Thebesian Veins: Clinical Visualization by Myocardial Contrast Echo-cardiography. *Circulation* Vol 80 No 4 Suppl.II; II-369 (abstr.)
32. Silverman PR, Ten Cate FJ, **De Jong N**, Mittertreiner W, Vletter WB, Frislid K. Intravenous Albunex[†] injections increase intramyocardial Backscatter. *Circulation* Vol 80 No 4 Suppl.II; II-369 (abstr.)
33. **De Jong N**, Ten Cate FJ, Mittertreiner W. In vitro acoustical behaviour of microparticles used for myocardial echo perfusion. In syllabus "Advances in echocardiography: contrast echocardiography perfusion imaging, transesophageal echo". September 21-22, 1989.
34. **De Jong N**, Mittertreiner WH, Ligtvoet KM, Ten Cate FJ. A computerized system that uses high-frequency data for analysis of myocardial contrast echocardiograms. *J Am Soc Echocardiogr* 3: 99-105, 1990.

35. **De Jong N**, Ten Cate FJ, Lancée CT, Roelandt JRTC, Bom N. Principles and recent developments in ultrasound contrast agents. *Ultrasonics* 29: 324-330, 1991.
36. Smyllie JH, Van Herwerden LA, Brommersma PD, **De Jong N**, Bom N, Bos E, Gussenhoven WJ, Roelandt J, Sutherland GR. Intra-operative epicardial echocardiography: early experience using a newly developed small surgical transducer. *Am J Soc Echo* 4: 147-154, 1991.
37. Brommersma P, Smyllie JH, Van Herwerden LA, **De Jong N**, Bom N, Bos E, Gussenhoven WJ, Roelandt J, Sutherland GR. The design, construction and clinical evaluation of a small phased array transducer for intra-operative echocardiography. *Med Prog Technol* 16: 213-218, 1990.
38. **De Jong N**, Hoff L, Skotland T, Bom N. Absorption and scatter of encapsulated gas filled microspheres: theoretical considerations and some measurements. *Ultrasonics* 30(2) 95-103, 1992.
39. **De Jong N**, Lancée CT: Physics and developments of ultrasound contrast agents. *Ultrasonoor Bulletin* 20: 5-14, 1992.
40. **De Jong N**, Hoff L. Ultrasound scatter properties of Albunex[®] microspheres. *Ultrasonics* 31(3) 175-181, 1993
41. **De Jong N**, Ten Cate F.J., Vletter W.B., Roelandt J.R.T.C. Quantification of transpulmonary echocontrast effects. *Ultrasound in Medicine and Biology* 19 (4) 279-288, 1993

Curriculum vitae

De schrijver van dit proefschrift is op 4 november 1954 in Nieuwerkerk a/d IJssel geboren. Hij volgde het lager onderwijs in Reeuwijk en het middelbaar onderwijs op het Antonius College te Gouda. In 1972 behaalde hij hier het HBS-b diploma. Met de studie Natuurkunde aan de Technische Hogeschool Delft begon hij in dat zelfde jaar en na de Propaedeuse in 1974 legde hij het kandidaats-examen in 1977 met goed gevolg af. Zowel het kandidaats onderzoek als later het afstudeer onderzoek werd gedaan in de vakgroep Patroon Herkennen van Prof. dr. ir. Verhagen. In dit onderzoek werkte hij aan de besturing en ontwikkeling van een "flying spot scanner" voor het scannen/belichten van negatieven ten behoeve van onder andere automatische herkenning van handgeschreven letters, chromosoom classificatie en beeldbewerking. Het ingenieurs diploma behaalde hij in 1978.

In 1978 trad hij in tijdelijke dienst bij TNO/TPD. Ten behoeve van tarifiering en automatische afhandeling van colliës bij van Gend en Loos, ontwikkelde hij een computer/transport systeem, dat automatisch de kleinste rechthoekige box om een willekeurig voorwerp kon bepalen.

Van mei 1979 tot mei 1980 werkte hij als agrarisch medewerker op de boerderij van zijn ouders in Reeuwijk. Het doel hiervan was het eventueel overnemen van de boerderij en beroepsmatig veehouder te worden. Na een jaar werd hiervan afgezien.

In 1980 kwam hij in tijdelijke dienst van de Erasmus Universiteit in Rotterdam. Op de afdeling Echocardiografie, onder leiding van Prof. dr. ir. Bom en dr. ir. Lancée, werkte hij aan de ontwikkeling van ultrasonoor transducenten voor echocardiografische apparatuur. Van 1982 tot 1986 ontwikkelde hij een slokdarmscanner, waardoor echo-diagnostiek van het hart wezenlijk kon worden verbeterd. Dit project werd gesponsord door Delft Instruments.

Gesponsord door de Nederlandse Hartstichting, startte hij in 1987 met het onderzoek naar echocontrast middelen en werd de basis gelegd voor dit proefschrift. In 1989 volgde een tijdelijke aanstelling bij het ICIN (later is dit KNAW geworden) en werd dit onderzoek gecontinueerd. Sinds begin 1990 wordt het echocontrast project financieel ondersteund door Nycomed, Noorwegen.
